METATHESIS OF BUTENE TO PRODUCE PROPYLENE OVER MESOPOROUS TUNGSTEN OXIDE CATALYST: SYNTHESIS, CHARACTERIZATION AND KINETIC MODELING

BY

TAZUL ISLAM BHUIYAN

A Thesis Presented to the
DEANSHIP OF GRADUATE STUDIES

KING FAHD UNIVERSITY OF PETROLEUM & MINERALS

DHAHRAN, SAUDI ARABIA

In Partial Fulfillment of the
Requirements for the Degree of

MASTER OF SCIENCE

In

CHEMICAL ENGINEERING

JUNE 2013

KING FAHD UNIVERSITY OF PETROLEUM & MINERALS

DHAHRAN- 31261, SAUDI ARABIA

DEANSHIP OF GRADUATE STUDIES

This thesis, written by **Tazul Islam Bhuiyan** under the direction his thesis advisor and approved by his thesis committee, has been presented and accepted by the Dean of Graduate Studies, in partial fulfillment of the requirements for the degree of **MASTER OF SCIENCE IN CHEMICAL ENGINEERING.**

Dr. Sulaiman Al-Khattaf
(Advisor)

Dr. Usamah Al-Mubaiyedh
Department Chairman

Dr. M. Mozahar Hossain
(Member)

Dr. Salam A. Zummo
Dean of Graduate Studies

17/6/13
Date

Dr. Abdallah Al-Shammari
(Member)

DEDICATION

This work is dedicated to my father, Muhammad Abdur Rafique Bhuiyan and to my mother, Begum Rokeya, for their immeasurable love and support.

ACKNOWLEDGEMENT

All praise is to Allah (SWT) the lord of the worlds. And may the peace and blessings of Allah be upon the Holy Prophet Muhammed, the leader of mankind (SAW).

I would first like to extend the warmest appreciation to my supervisor, Dr. Sulaiman Al-Khattaf, for his mentorship, valued guidance and critical supervision throughout the planning, execution, and communication of my thesis work. I am extremely thankful to the time devoted by supervisor to critically review and constructively criticize my written materials. My appreciation also goes to my other thesis committee members; Dr. Mohammad Mozahar Hossain and Dr. Abdallah Al-Shammari for their immense assistance throughout this work. Never would I forget the contributions of Dr. Mozahar Hossain particularly in the area of modeling and Dr. Palani Arudra in the area of catalyst synthesis and performance evaluation.

To my parents, my wife (Tameema Hossain), brother (Mazharul Islam), and sisters (Rafia Sultana and Zakia Sultana)), I am deeply appreciative of your patience, encouragement and love throughout the study.

I also want to offer my regards and appreciation to all of those who supported me in any respect during the completion of the thesis work.

I would like to acknowledge the support provided by Saudi Aramco for funding the project. The supports from Chemical Engineering Department and Center for Refining and Petrochemicals (CRP) of KFUPM are highly appreciated. The support from the Ministry of Higher Education, Saudi Arabia, in establishment of the Center of Research Excellence in Petroleum Refining & Petrochemicals at King Fahd University of Petroleum & Minerals (KFUPM) is also appreciated.

TABLE OF CONTENTS

Contents

LIST OF TABLES

LIST OF FIGURES

LIST OF SCHEMES

THESIS ABSTRACT

Full Name : **TAZUL ISLAM BHUIYAN**

Thesis Title : **METATHESIS OF BUTENE TO PRODUCE PROPYLENE OVER MESOPOROUS TUNGSTEN OXIDE CATALYST: SYNTHESIS, CHARACTERIZATION AND KINETIC MODELING**

Degree : **MASTER OF SCIENCE**

Major Field : **CHEMICAL ENGINEERING**

Date of Degree : **June, 2013**

Metathesis of 2-Butene to produce propylene over tungsten oxide contained on mesoporous catalyst was studied. Mesoporous silica (MCM-41 and SBA-15) having tungsten oxide in the framework was synthesized by hydrothermal crystallization process using CTAB and P123 as structure directing agents, respectively. Tungsten oxide was supported on the MCM-41 and SBA-15 by wet impregnation method for a comparative study. The synthesized materials were characterized by XRD, N_2 adsorption isotherm, NH_3-TPD, Pyridine-FT-IR, UV-vis DRS, Raman spectroscopy, H_2-TPR and SEM techniques. The catalysts were used to perform metathesis reaction of 2-butene in a fixed-bed reactor at different temperatures, different residence time and under atmospheric pressure. This research work also reports the reaction mechanism and reaction kinetics of 2-butene metathesis over tungsten oxide containing mesoporous silica (SBA-15) catalyst. Physicochemical characterization of the catalyst indicates that the dispersion and nature of tungsten oxide species on the catalyst are mainly responsible for the metathesis activity. The estimated apparent activation energy of 2-butene isomerization reaction

found to be the lowest (39.4 kJ/mol) among the competing reactions. The activation energy of cross metathesis of 2-butene and 1- butene, self-metathesis of 1-butene and 2-butene cracking are 71.3, 176.9 and 73.1 kJ/mol, respectively. These results are consistent to the product selectivity and the proposed reaction scheme, which suggests that the isomerization of 2-butene gives 1-butene and it further reacts (cross metathesis) with 2-butene to produce propylene.

THESIS ABSTRACT (ARABIC)

ملخص الرسالة

الاسم الكامل : تاج الإسلام بوحيان

عنوان الرسالة : تفاعل الإحلال و الإبدال للبيوتين لإنتاج البروبلين على حفاز أوكسيد التنجستون المسامي

الدرجة العلمية : الماجستير

التخصص : الهندسة الكيميائية

تاريخ الدرجة : حزيران 2013

تمت دراسة تفاعل الإحلال و الإبدال للمركب 2-بيوتين لإنتاج البروبلين على أوكسيد التنجستون المدعم على حفّاز مسامي. تم تركيب و إنتاج السيلكا المسامية (SBA-15, MCM-41) التي تحتوي على أوكسيد التنجستون في إطارها التكويني عن طريق عملية البلورة الحرارية باستخدام CTAB و P123 كعوامل موجه للتركيب. تم تركيب و إنتاج أوكسيد التنجستون المدعم على حفازات السيلكا المسامية (MCM-41,SBA-15) باتباع طريقة التلقيح المبلل و ذلك من أجل المقارنة . تم فحص خصائص الحفازات المنتجة من خلال اختبارات عدة :انكسار الأشعة السينية XRD ، و امتصاص و طرح النيتروجين N_2 adsorption-desorption ، و الطرح لدى درجة الحرارة المبرمجة للأمونيا NH_3-TPD و تقنيات ريمان للتحليل الطيفي. تم استخدام مفاعل أنبوبي ثابت الحشوة لإجراء كافة التجارب عند درجات حرارة مختلفة ، و أوقات مكوث متعددة و تحت تأثير الضغط الجوي. يضيف هذا البحث تقنية و ميكانيكية تفاعل الإحلال و الإبدال لـ 2-بيوتين على حفاز السيليكا المسامية (SBA-15) المحتوي على أوكسيد التنجستون. تشير الخصائص الكيميفيزيائية للحفاز إلى أن طبيعة التوزيع و طبيعة دقائق أوكسيد التنجستون على الحفاز المسؤول الرئيس عن نشاط تفاعل الإحلال و الإبدال. يشير تحليل

المنتجات إلى أن درجات الحرارة المنخفضة تفضل أرمتة البيوتين بينما درجات الحرارة المرتفعة كانت متطلبًا لتفاعل الإحلال و الإبدال . تم إيجاد طاقة التنشيط الظاهرية لتفاعل أرمتة 2-بيوتين و التي كانت الأقل بين التفاعلات المتنافسة بمقدار 39.4 كيلوجول / مول. طاقة التنشيط لتفاعل الإحلال و الإبدال المهجن من 2-بيوتين و 1-بيوتين ، إحلالًا و إبدالًا ذاتيًا من 1-بيوتين و تكسير 2-بيوتين هي 71.3 و 176.9 و 73.1 كيلو جول / مول بالترتيب النتائج كانت متوافقة مع اختيارية المنتج و مخطط التفاعل المقترح و الذي يقترح أن أرمتة 2-بيوتين تعطي بيوتين و تتفاعل أيضا (إحلال و إبدال مهجن) مع 2-بيوتين لإنتاج البروبلين.

CHAPTER 1

INTRODUCTION

1.1 Background

Propylene is one of the key "building block" petrochemical used as feedstock for large no of polymers and chemical intermediates. Global propylene demand grew from 37.2 million tons in 1995 to approximately 67 million tons in 2006. Demand for propylene is expected to grow at almost 5 percent growth rate annually for the period of 2007-2015 which will rise over 100 million tons by 2015 [1]. Major propylene derivatives are polypropylene, acrylonitrile, cumene, oxo-alchohols, propylene oxide, acrylic acid, isopropyl alchohol and polygas chemicals. However, the demand for propylene is mainly increasing for the high consumption of polypropelyne [2]. Figure 1.1 shows how propylene demand was increased from 1970 to 2004 for the high consumption of polypropylene [3]. Propylene derivatives are mostly turn into a wide range of end-use applications including automotive, construction, consumer durable and non-consumer durable, packaging and electronics [1]. Figure 1.2 shows overall propylene value chain-starting from source refinery crude oil to the consumer end use of propylene. Ethane, propane, butane, naphtha and gas oil are the petrochemical feedstock of a petrochemical industry. Main petrochemicals intermediates are ethylene, propylene, butadiene and BTX

(benzene, toluene and xylene). Main propylene derivative polypropylene produces mechanical parts, containers, fibers, films, woven bag, food storage, bucket, kitchen appliance, carpet, lawn furniture etc. [15].

Current global production of propylene stands at about 75 million tons per year. This propylene is manufactured commercially from two sources- ethylene steam cracker plants and refinery fluid catalytic cracking (FCC) [2]. Currently, in most of the steam cracking units, ethylene and propylene are produced in a typical ratio of 1:0.65 based upon on its feedstock [3, 4]. In a report, it found that 25% of the new ethylene crackers planned for startup in the 2003-2006 timeframe are based on ethane, which yields little propylene [1]. Thus the amount of propylene are able to be produced from steam cracker is almost fixed. In FCC units, propylene is produced as co-product of gasoline with very low yield and increasing the yield is not economical and limited due to priority of gasoline [5]. However, to make up the gap in between the supply and demand of propylene, refineries are able to capture more propylene from fluid catalytic crackers (FCC) and purify refinery grade propylene to either chemical grade or polymer grade propylene, but this solution has limits [3].

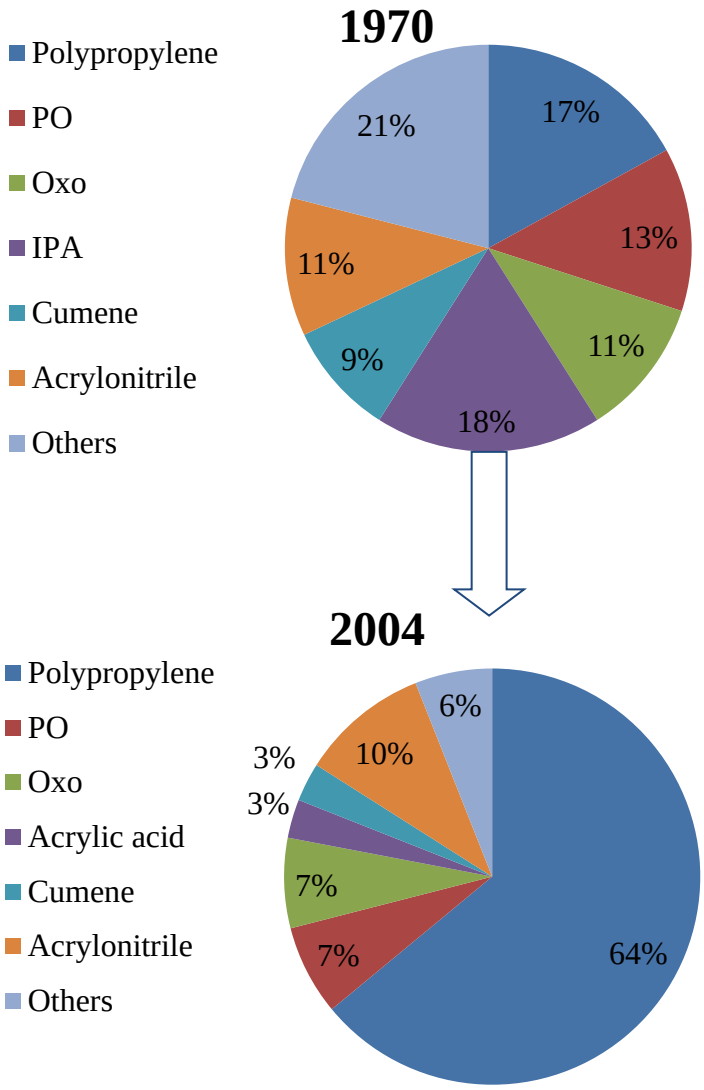

Figure 1.1 Global Propylene demand pattern, 1970-2004 [3]

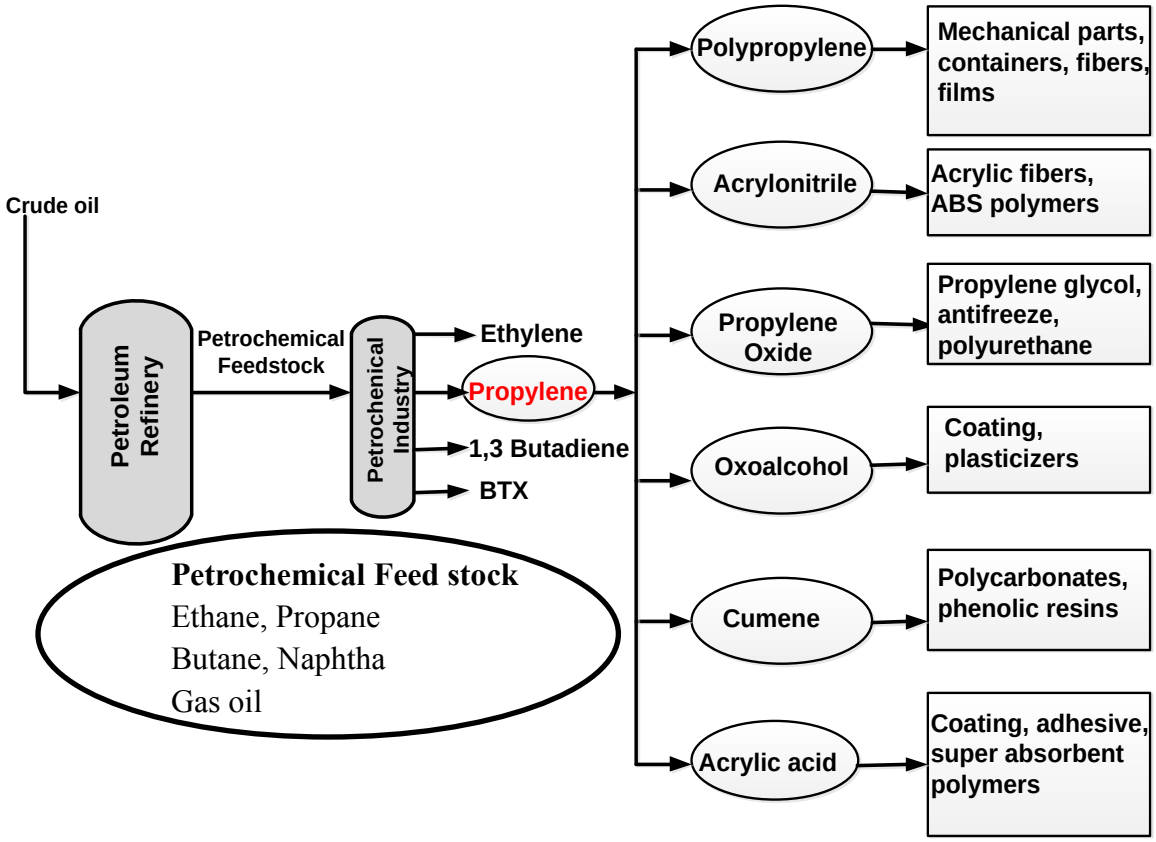

Figure 1.2 Crude oil to propylene consumer end product [15]

So, other technologies like propane dehydrogenation [7, 8], catalytic cracking of $C4^+$ olefins [9, 10], olefin metathesis [11] and methanol to olefin [12] are focused more for the production of propylene. On the other hand, with the increasing capability of petroleum refining and ethylene production, large amounts of C4 resources are produced. In the effluents from a steam cracking units, the C4 output is 30-40% of the ethylene yield which is higher than 90% is alkenes and dienes. In the FCC units, C4 output is 10-13% of the feeds, of which higher than 50% is alkenes, as shown in Table 1.1 [5]. From Fisher-Tropsch syntheses, a large amount of low value C4 olefins also produce [13]. So, it is becoming an important issue to upgrade low value C4 resources from the steam cracker and FCC units and to convert into valuable propylene product and this is one of the main focus areas of my thesis.

Table 1.1 Components of the steam cracker from FCC and steam crackers

Component	FCC unit	Steam cracker
iC_4H_{10}	34	1
C_4H_{10}	10	2
iC_4H_8	15	22
1-C_4H_8	13	14
2-C_4H_8	28	11
Diene		48
C4 alkyne		2
Total	100	100

1.2 Main Industrial Technologies for Propylene Production

Over 88 percent of propylene produced in the world is either as a byproduct of ethylene in a steam cracking unit or byproduct of gasoline via FCC. Some on purposes propylene production technologies are emerged such a propane dehydrogenation, catalytic cracking of C4 or higher olefins, olefin metathesis, methanol to olefin (including methanol to propylene), enhanced FCC. All of these routes are soon exploiting commercially to verify degrees. Figure 1.3 shows a breakdown of propylene capacity according to technology [14].

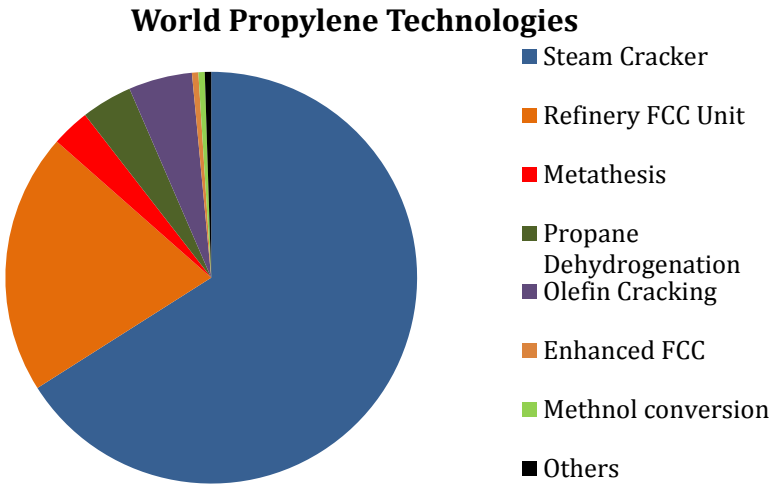

Figure 1.3 Distribution of Propylene capacities [14]

1.2.1 Steam Cracking

In a steam cracking unit feedstocks include a variety of hydrocarbons such as natural gas liquids (e.g. ethane, propane, and butane) and petroleum liquids (e.g. naphtha and gas oils). Ethylene is the main product of the process and propylene is formed as a co-product of ethylene during this process which is presented in Figure 1.4. When the feedstock are fed to steam cracking furnace at a temperature of 790-870 °C, the feedstock molecules "crack" to produce methane, hydrogen, ethylene, propylene, butadiene, benzene, toluene, and other co-products [14]. Two variable effects the distribution of co-products: type of feedstocks and severity of operation. In a market limited ethylene production, the feed stocks could be changed by naphthenic naphtha and gas oil so that ethylene production could be minimized [1]. Table 1.2 shows steam cracking feedstock's versus yields of intermediate petrochemical products. From a ethane based steam cracker, ethylene is produced 76% while propylene yield 3%. On the other hand, from naphtha based steam cracker, propylene yield 16% compare with 31% ethylene.

Still now the demand of ethylene is higher than propylene. It varies on region to region and feedstock of steam cracker. But from the above discussion it is defined that due to smooth flow of ethylene, from steam cracker it will not be possible to fill up the gap of propylene supply and demand.

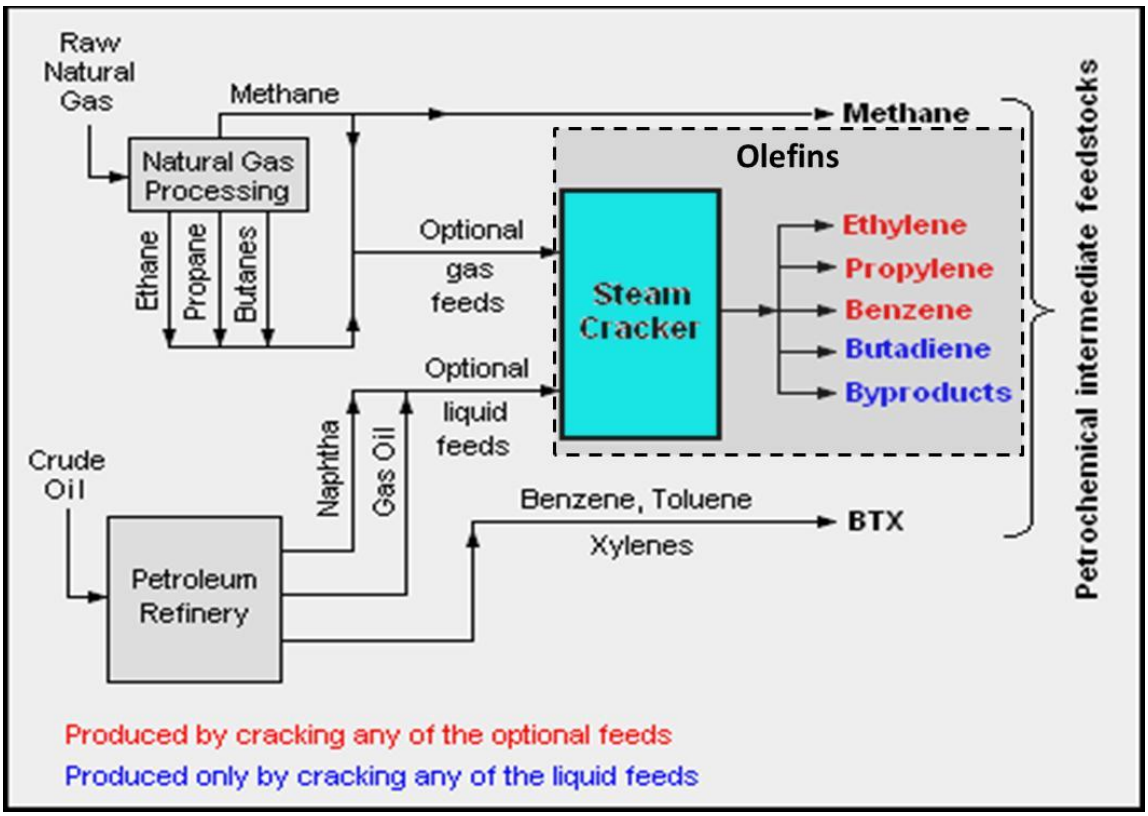

Figure 1.4. Flowchart of propylene production as a byproduct of ethylene in a steam cracker unit.

Table 1.2 Steam cracking feedstock's versus yields of intermediate petrochemical products

	Feed			
Yield %	Ethane	Propane	Naphtha	Gas Oil
Ethylene	76	42	31	23
Propylene	3	16	16	14
Butadiene	2	5	9	9

1.2.2 Recovery from Refinery streams and high severity FCC

Propylene is produced as dilute stream of propane from the three main refinery processes: fluid catalytic cracking, thermal cracking and coking [1]. Refiners use catalytic cracking to produce gasoline from heavy gas oils. The cracking process converts a significant portion of the feed to C_1 - C_4 products, including propylene. Propylene produced from catalytic cracking typically varies from 5 -19% in volume of the fresh feed charge. Figure 1.5 presents a flowchart of LPG propylene production from a refinery FCC unit. The actual percentage of propylene in the off-gases from any particular refinery depends on several variables, such as type of reactor, feedstock composition and type of catalyst, as well as on operating conditions (reaction temperature or recycle ratio). Over the years, significant development in catalyst side, zeolite based catalyst has improved the yield of propylene as well as octane content of gasoline [14].

To achieve higher outputs of light olefins, particularly propylene, the hydrogen content of the feedstock must be increased and the sulfur content reduced. This can be achieved by the utilization of low sulfur crude oils or using a higher performance feed hydrotreater

upstream of the FCC unit. There are several commercial FCC processes currently employed with major differences in the method of catalyst handling. Table 1.3 presents a comparison of the yield structure of conventional FCC and selected high-olefin technologies [2].

In a FCC, due to high demand of motor gasoline most of the countries are not interested to increase the capacity of propylene production. So, we need to focus of the on purpose propylene production technologies to increase the capacity.

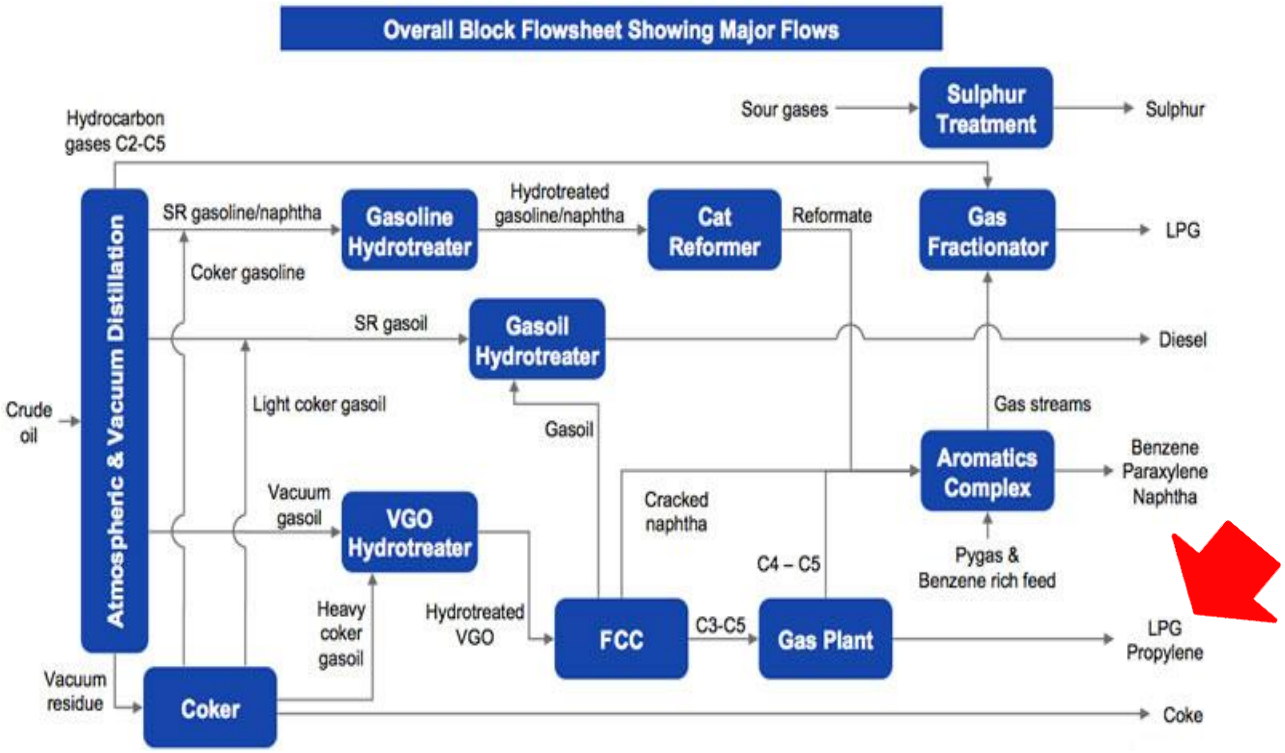

Figure 1.5 Flowchart of LPG propylene production from a refinery FCC unit.

Table 1.3 Product yields of conventional and emerging FCC process

Parameter	**FCC**	**DCC**	**PetroFCC**	**HS-FCC**
Reaction Temperature	500	530	590	600
Product yield%				
Ethylene	1.5	5.4	6.0	2.3
Propylene	4.8	14.3	22.0	15.9
Mixed butanes	6.9	14.7	22.0	17.4
Gasoline	51.5	39.0	28.0	37.8
Heavy & light oil	21.0	15.6	14.5	9.9
Coke	4.5	4.3	5.5	6.5

1.2.3 Propane dehydrogenation

Alkanes are typical feedstocks for transformation of alkenes, aromatics and other value added materials. Oxidative dehydrogenation of propane is another route to produce on purpose propylene production. ODH of paraffin's is an alternative to commercial methods of propylene production and due to exothermic reaction condition it is not limited by thermodynamic constraints. ODH is readily available to a number of licensors and used commercially. However, the process is economical in certain conditions and

certain regions. Current ODH catalysts also have limited activity and poor selectivity. So, it will be very difficult to improve the propylene supply by propane dehydrogenation [14].

1.2.4 Methanol to Olefins (MTO)

The availability of low priced methanol along with the rise of propylene demand makes the methanol to olefin or methanol to propylene technology viable. Low cost gas region normally focused on ethane cracking rather than heavy liquid cracking, for that these regions have sufficient ethylene than propylene [1]. This technology can applied only the regions where availability of gas supply is very high.

1.2.5 Motivation- Olefin Metathesis technology for propylene production

Commercially available metathesis technology (OCT-ABB Lumus) involves the reaction of ethylene and butene to produce propylene where ethylene used as major feedstocks. Olefin metathesis can be added to a steam cracking unit to boost up the propylene production by ethylene and by product butene reaction. This technology is used by various licensors [1]. Figure 1.6 shows flowchart of propylene production utilizing C4-fraction by-products of Chiba production base where Idemitsu, Sumitomo,and MCI each have facilities for the production of petrochemical products and derivatives from olefins and aromatics. The companies' ethylene crackers and a fluid catalytic cracker (FCC) are located close to one another. In addition, the complexes are connected with a pipeline network. The three companies strengthen their competitiveness by capitalizing on the strength of their close location to develop a high-efficiency production system for clean

fuel and propylene utilizing C4-fraction by-products from the refinery and petrochemical plants as well as ethylene as raw materials [16].

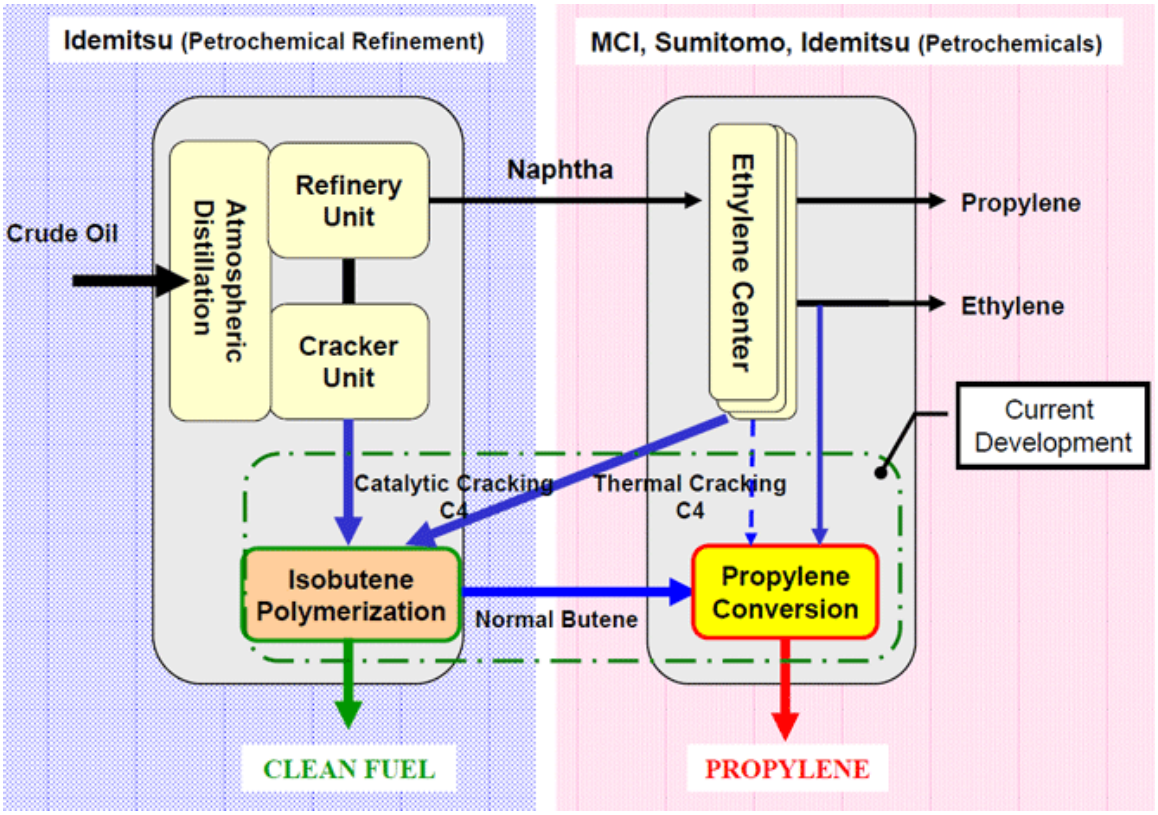

Figure 1.6 Flowchart of propylene production utilizing C4-fraction by-products.

There are currently 20 metathesis OCT Lummus plants in operation (2010). Two additional plants are planned to be built by the end of 2015. Most of the world's propylene via metathesis capacity is being added in the regions of the Middle East, driven by plans to upgrade low-cost natural resources, and in Asia, driven by strong demand growth in the region.

In 2003, a semi-commercial unit owned by Sinopec in Tianjin (China), was built to demonstrate auto-metathesis of butene and 1-hexene production. This facility maximizes the 1-butene/1-butene metathesis reaction to produce 3-hexene, and then isomerizes the 3-hexene to 1-hexene. The plant has a capacity of producing 2 kta of 1-hexene [15].

In this research work, it is one of the prime issues to avoid the high demandable ethylene as a feedstock and use only C4 olefins in the metathesis reaction. In literature review details about the olefin metathesis, catalysts used in metathesis, current commercial technologies used on this area and reaction mechanism will be discussed.

CHAPTER 2

LITERATURE REVIEW

2.1 Introduction

Olefin metathesis is one of the very few fundamentally novel organic reactions exposed in last few decades. It was discovered by Banks and Bailey 48 years ago at Phillips Petroleum Co. It made a new industrial route to important petrochemicals, polymers, oleochemicals and specialty chemicals. At that time, the scientists were seeking an effective heterogeneous catalyst to replace the HF acid catalyst for converting olefins into high-octane gasoline via olefin iso-paraffin alkylation. When using a supported molybdenum catalyst, they found that instead of alkylating the paraffin, the olefin molecules were split, and discovered that propylene can be catalytically converted into ethylene and butene. Since then, industrial applications of the olefin metathesis reaction are always focused by increasing interest, especially ring opening metathesis polymerization, in recent years [19].

The basic concept of olefin metathesis is it transforms less desired olefins to higher ones through rearrangement of pairs of C=C bonds of olefins [19]. The key step in this process is formation of unstable metallacyclobutane intermediate by the [2 + 2] cycloaddition reaction between an alkene and a transition metal alkylidene (carbene) complex. This intermediate can either revert to the starting material or generate a new metal-carbene and then produce a new alkene. When two different alkene molecules react with each other, then it is called as cross metathesis. If same molecule used then it called as self-metathesis [19]. Propylene could be produced by several ways of metathesis using different type of catalyst which will be discussed further.

2.2 Industrial applications of Olefin Metathesis to Propylene Production

2.2.1 The Phillips triolefin process

The Phillips Triolefin Process was developed at Phillips Petroleum in the 1960s. It used a in a process from 1966-1972 using heterogeneous WO_3/SiO_2 catalyst to convert propylene to ethylene and 2-butene, for which ethylene demand was then growing. But due to growth of polypropylene fueled increased demand for propylene and the process was shut down. But olefin metathesis is an equilibrium reaction. Once the price of propylene rose high enough, running the Triolefin Process in reverse became attractive. Lyondell Petrochemical in the USA was the first commissioned in 1985 a plant based on this process to produce propylene. In 1996, Lumus acquired the technology from Phillips and now, there is plant of BASF Fina in the USA who uses this Lumus technology [18].

The Olefin Conversion Technology (OCT) from ABB Lumus Global converts butene and ethylene to polymer grade propylene via metathesis. Two main equilibrium reactions take place metathesis and isomerization. Propylene is formed by cross metathesis of ethylene and 2-butene at over 260 ℃ and 30-35 bar pressure. 2-Butene isomerization also takes place here. Based on stoichiometry, three tons of propylene produces from two tons of butene and one ton of ethylene.

$$\underset{\text{Ethylene}}{CH_2=CH_2} + \underset{\text{2-Butene}}{H_3C-CH=CH-CH_3} \rightleftharpoons \underset{\text{2-Propylene}}{2\ H_3C-CH=CH_2} \quad \text{.....(2.1)}$$

Figure 2.1 shows simple process flow diagram of Lumus OCT process. Vapor phase fixed bed metathesis reactor is used for the cross metathesis reaction of ethylene and C4 feed where the equilibrium reaction takes place. The butene conversion is greater than 60% with overall propylene selectivity exceeds 90% per pass. 37 OCT units have been licensed with a total propylene production capacity of 7.6 million tons per year. Among these, 23 units are integrated with ethylene plants; rest of them is integrated with FCC unit's refineries.

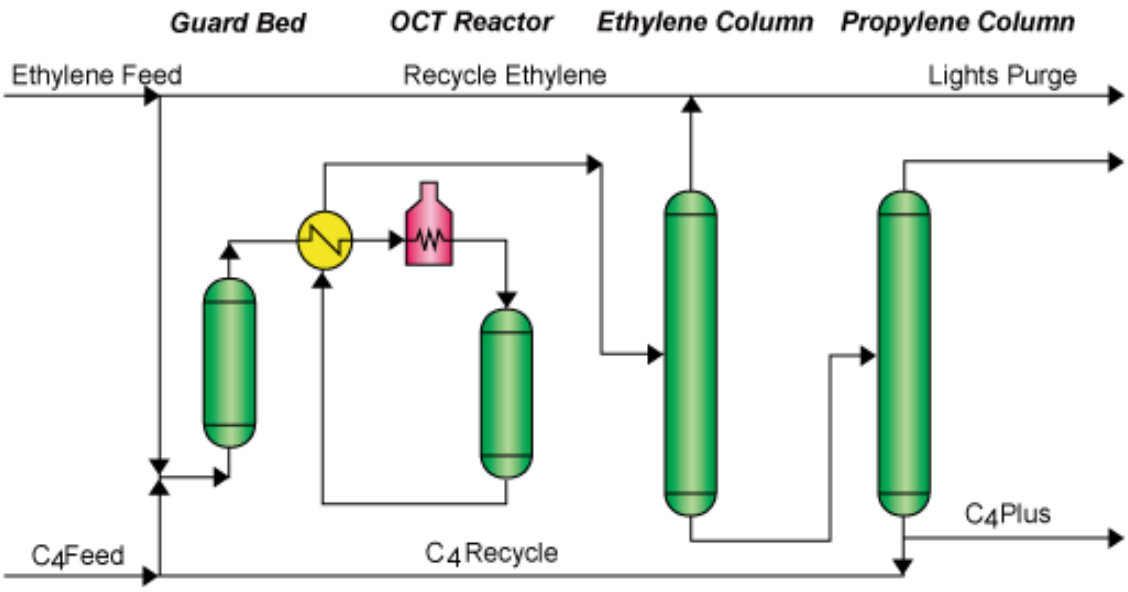

Figure 2.1 OCT Process flow schematic.

2.2.2 The Meta-4 process

The Institut Francais du Petrole (IFP) and the Chinese Petroleum Corporation (Kaoshiang, Taiwan) have jointly developed a process for the production of propene, called Meta-4. In their process, ethene and 2-butene react with each other in the liquid phase in the presence of a Re_2O_7/Al_2O_3 catalyst at 35 ◦C and 60 bars. The (equilibrium) conversion is 63% per pass. The process is not yet commercialized, mainly because of the cost of the catalyst and the requirement of a high purity of the feed stream [20, 21]. Table 2.1 shows overall comparison of Lumus OCT process and Axens Meta-4 process. Catalyst and operating conditions are totally different in these two processes.

Table 2.1 Comparison: Lumus OCT vs. Axens Meta-4

Parameter	**Lumus OCT**	**Axens Meta-4**
Catalyst	MgO and WO_3/SiO_2	Re_2O_7/Al_2O_3
Reaction temperature	280-320 ◦ C	30-40 °C
Reaction pressure	29 bar	60 bar (ensure liquid phase)
Reaction phase	gas	liquid

2.3 Basic Chemistry of Olefin Metathesis

Metathesis is a general term for a reversible reaction between two olefins, in which the double bonds are broken and then reformed to form new olefin products. In order to produce propylene by metathesis, a molecule of 2-butene and a molecule of ethylene are combined to form two molecules of propylene. This is a full productive and fast reaction. Some suitable catalysts enhance double bond isomerization of 1-butene to 2-butene or 2-butene to 1-butene inside the metathesis reactor further allows continued 1-butene and 2-butene cross metathesis reaction to produce propylene and 2-pentene. At the same time, 1-butene or 2-butene also undergoes isomerization reaction to produce isobutene. Cross metathesis of C4= alkenes produce propylene and C5= alkenes. On the other hand, self-metathesis of 1-butene or isobutene form ethylene and C6= alkenes. Due to the mechanism of olefin metathesis, there are some non-productive reactions such as 2-butene self-metathesis, ethylene self-metathesis and reaction of 1-butene or isobutene with ethylene. Table 2.2 summarizes the reactions that occur in the metathesis reactor. All the reactions are essentially isothermal. [15].

Table 2.2 Metathesis reactions of 1-butene, 2-butene, isobutene and ethylene

Reaction	Rate
(1) 1-butene + 2-butene → propylene + 2-pentene	Fast
(2) 1-butene + 1-butene → ethylene+ 3-hexene	Slow
(3) 1-butene+ isobutene → ethylene + 2 -methyl 2-pentene	Slow
(4) 1-butene + ethylene → no reaction	No reaction
(5) 2-butene + 2-butene → no reaction	No reaction
(6) 2-butene + isobutene →propylene + 2-methyl 2-butene	Fast
(7) 2-butene+ ethylene → 2 propylene	Fast
(8) isobutene + isobutene → ethylene+ isohexene	Slow
(9) isobutene + ethylene → no reaction	No reaction
(10) ethylene + ethylene → no reaction	No reaction

2.4 Advantage of auto metathesis of butene

The raw materials for conventional metathesis reaction are ethylene and 2-butene. In some cases, the supply of ethylene is tight and/or ethylene is expensive, making the building of a conventional metathesis unit unfeasible without subsidies.

Other disadvantages of conventional metathesis are:

I. **Intensive Use of Energy:** Conventional metathesis reactions take place with ethylene, which requires an intensive use of energy in the ethylene recirculation loop by using cryogenic refrigeration.

II. **Feedstock Loss:** Removing butadiene by hydrogenation from the butene feed before its use in a conventional metathesis results in the hydroisomerization of the butenes to paraffins, representing a feedstock loss more than 10%. Furthermore, removing isobutene by fractionation of the butenes feed before its use in a conventional metathesis results in an additional loss of butenes, since 1-butene is difficult to separate from isobutene without an expensive fractionation tower.

Although the yield of propylene is high in the conventional metathesis process, the aforementioned disadvantages motivated the development of a different process, in which a metathesis reaction occurs with butene as the only feedstock. This process is called butenes auto-metathesis [15]. Depending upon the catalyst, the overall product distribution varies. But ethylene, propylene, C_4=, C_5= and C_6= olefins are the products of tungsten, molybdenum or rhenium based catalyst.

In the process, a stream comprised of 1-butene plus 2-butene is mixed with recycled butenes and pentenes in the metathesis reactor. The exit stream leaving the reactor is sent to a separation unit, composed of distillation columns.

According to Gartside [22], the stream can contain C4 paraffins but the amount of isobutene should not exceed 2% of the feed mixture. Table 2.3 shows some reactions are also involved during the auto-metathesis of butene when 2-pentenes are recycled back to the reactor. The reactions (1) and (2) are the main auto-metathesis reactions. Reactions (3), (4) and (5) occur while the 2-pentenes formed through the main reaction are recycled back to the reactor.

Table 2.3 Auto metathesis reactions (Butenes to propylene)

Reaction
(1) 1-butene + 2-butene → propylene + 2-pentene
(2) 1-butene + 1-butene → ethylene+ 3-hexene
(3) 2-pentene + 1-butene → propylene + 3-hexene
(4) 2-pentene → 1-pentene
(5) 2-butene + 2-butene → no reaction
(6) 1-pentene +2-butene →propylene+ 3-hexene

The recycling of pentenes to the metathesis reactor has some advantages [15]:

I. Increase of selectivity to propylene.

II. Increase of hexene production, which is more valuable than pentene (as a comonomer for polyethylene production).

III. Hexene is a more valuable pyrolysis feed than pentene in a cracker, since it produces more ethylene and propylene than pentene or butene per unit of fuel.

IV. No need for further processing of pentenes to achieve higher propylene selectivity, such as reaction of pentene with ethylene to obtain propylene.

2.5 Catalyst used for Metathesis

2.5.1 Metals used for metathesis reaction

The metathesis reaction can be catalyzed by both heterogeneous and homogeneous catalyst systems that can form metal-carbene complex needed for the formation of the metallacyclobutane intermediate. Figure 2.2 shows metal used for metathesis reaction. A wide variety of transition metal compounds can catalyze the reaction mechanism; the most important are based on molybdenum, tungsten, ruthenium and rhenium for olefin metathesis. Table 2.4 indicates relative reactivity of metals with different types of groups. Ruthenium is highly reactive for olefin metathesis, then molybdenum and tungsten. Homogeneous catalysts consist of either a well characterized carbene complex of transition metal (e.g. Ru, Mo or W) or a combination of transition metal compound [usually an (oxo) chloride)] or an organometallic compound as co-catalyst. These homogeneous catalysts have a good perspective for polymerization. On the other hand, heterogeneous catalysts are more useful for petrochemical and organic synthesis [19].

Heterogeneous metathesis catalyst generally consists of a transition metal oxide [e.g. rhenium oxide, tungsten oxide or molybdenum oxide], or an organometallic precursor

deposited on a surface area. These solid catalysts are widely accepted for metathesis of lower alkenes due to the advantage of easy separation from the reaction products and regeneration after the reaction [20]. The most successful heterogeneous catalysis for olefin metathesis is based on rhenium, molybdenum and tungsten oxides [22]. Among them, rhenium oxide catalysts supported on alumina or silica-alumina are highly active and selective even at low temperatures (20-100°C), but the activities of catalysts with low loading (<10wt %) of Re are poor and the catalysts are easily deactivated [23-25]. The cost of rhenium compounds is also high [26]. Molybdenum oxide catalysts supported on alumina, siliceous material, silica alumina and zeolite alumina composite support have received much attention for their relatively low price and high activity at room temperature [27-32]. The main limitation of molybdenum catalysis is it requires comparatively pure feed stream [33].

The tungsten based catalysts shows good activity and selectivity for longer period of time. They are also resilience to frequent poisoning [34]. In additions, continuous regeneration without negative effects on catalyst structure makes the tungsten based catalysts most attractive for commercial use [34]. Usually the tungsten oxide catalysts require comparatively higher temperature (250-500 °C) to achieve appreciable activity and their catalytic activity widely depend on the oxidation state of tungsten species, the content of tungsten oxide, the properties of support and the pretreatment condition [35-38].

Periodic Table

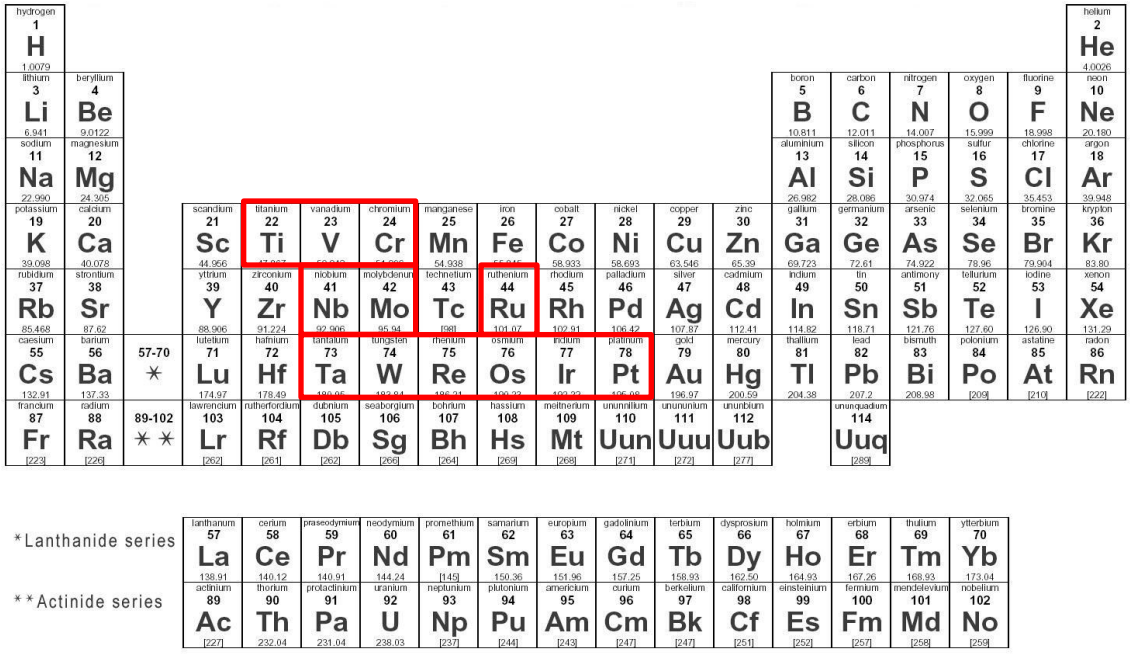

Figure 2.2 Metals used in metathesis reactions.

Table 2.4 Relative reactivity of metals with different groups.

Titanium	Tungsten	Molybdenum	Ruthenium
Acids	Acids	Acids	**Olefins**
Alcohols, Water	Alcohols, Water	Alcohols, Water	Acids
Aldehydes	Aldehydes	Aldehydes	Alcohols, Water
Ketones	Ketones	**Olefins**	Aldehydes
Esters, Amides	**Olefins**	Ketones	Ketones
Olefins	Esters, Amides	Esters, Amides	Esters, Amides

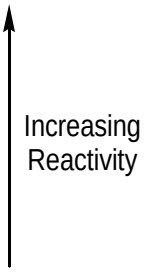

Support have a profound effect on the activity of catalyst, so many researchers used mesoporous materials with high surface area and tunable channel. According to previous studies, mesoporous silica based catalyst exhibited high activity in olefin metathesis, but operation a high temperature [39]. There are some deficiencies in microporous materials which can overcome in mesoporous materials. Figure 2.3 shows tungsten, molybdenum and rhenium based catalyst with different types of support described in open literature.

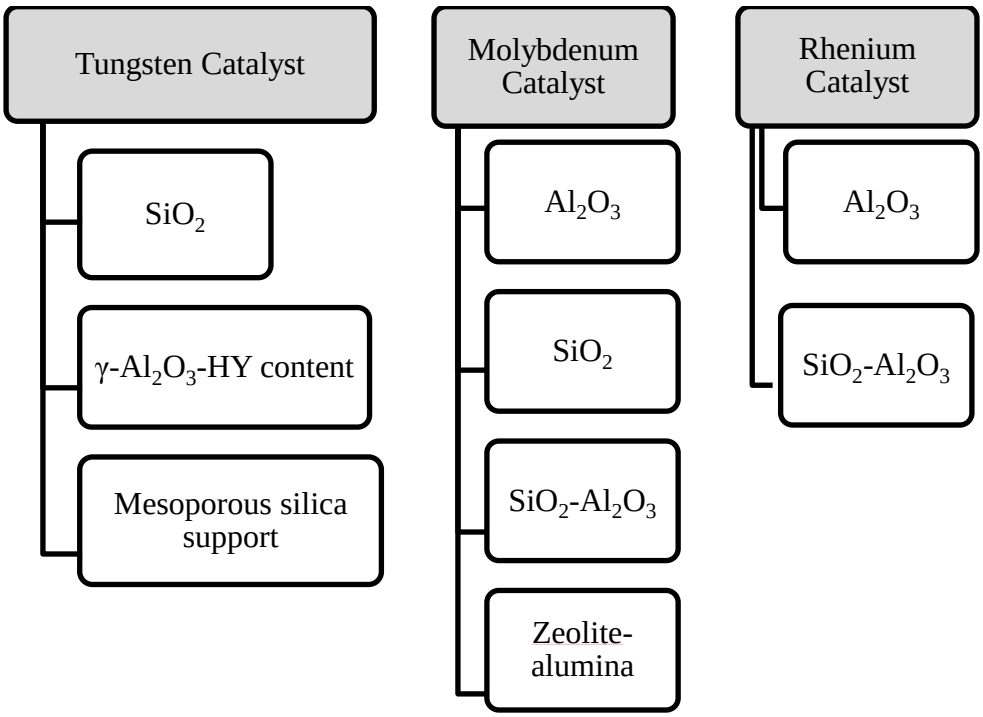

Figure 2.3 Tungsten, molybdenum and rhenium based catalyst with different types of support described in literature.

2.5.2 Mesoporos silica support

Porous materials have been intensively studied with regard to technical applications as catalysts and catalyst supports. According to the IUPAC definition, porous materials are divided into three classes; microporous (pore size < 2nm), mesoporous (2‑50nm), and macroporous (>50nm) materials [40]. In addition, also the term ‘nanoporous’ is increasingly being used. However, it is not clearly defined and loosely refers to pores in the nanometer size range. Many kinds of porous materials such as (pillared) clays, anodic alumina, carbon nanotubes and related porous carbons and so on, have been extensively described in the literature [40]. Among the family of microporous materials, the best known members are zeolites which have a narrow and uniform micropore size distribution due to their crystallographic ally defined pore system.

The first synthesis of an ordered mesoporous material was described in the patent literature in 1969. However, due to a lack of analysis, the remarkable features of this product were not recognized [41, 42]. In 1992, a similar material was obtained by scientist in Mobil Oil Corporation who discovered the remarkable features of this novel type of silica and opened up a whole field of research [43]. MCM-41, which stands for Mobil Composition of Matter No. 41, shows a highly ordered hexagonal array of one-dimensional pores with a very narrow pore size distribution [44, 45]. The walls, however, very much resemble amorphous silica. Other related phases such as MCM-48 and MCM-50, which have a cubic and lamellar mesostructure, respectively, shown in the Figure 2.4.

Figure 2.4 The M41S family of materials including MCM- 41, MCM-48 and MCM-50 [46].

2.5.3 MCM-41 and SBA-15

MCM-41 is a commonly used as mesoporous material. It is usually synthesized by a templating mechanism. Through phase separation, a continuous network surrounding template molecules is formed first. Then, by combustion and/or extraction, the template is removed, leaving the empty space inside the network material as mesopores [47]. Typical synthesis of mesoporous silica MCM-41 is presented in Figure 2.5. MCM-41 having well-defined structure symmetry are featured with tuneable pore diameters, high surface areas, and large pore volumes, enabling themselves to be promising candidates used in catalysis, separation, adsorption, sensing, nanostructure templating, and immobilization of biomolecules [46].

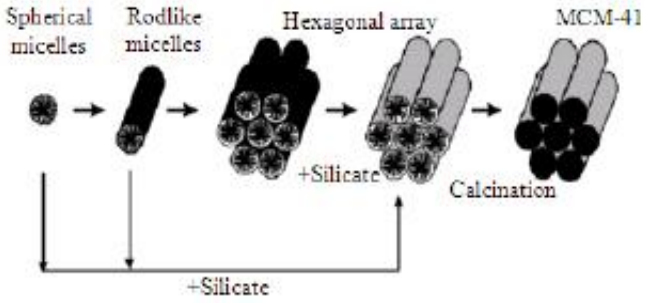

Figure 2.5 Liquid crystal templating mechanism of formation of the mesoporous silica material MCM-41 [46].

At recently, SBA-15 has become an important catalyst in many areas not only for its larger pores (5-30 nm) but also mechanically, thermally, hydro-thermally robust due to its thick framework walls (3-6 nm). The mesopore diameter of SBA-15 depends on the synthetic conditions: increasing the gel aging temperature leads to a larger pore diameter [40]. One interesting feature of SBA-15 is the microporosity which is present in its mesopore wall, by which the micropores connect neighboring mesopores. Figure 2.6 shows how micropores are connected with the neighboring mesopres. This mesoporous silica is highly ordered, large specific surface area, hexagonal array, uniform mesoporous channel and allows more diffusion and adsorption of larger molecules for wide applications compare to microstructure which only limits to separation and fine chemical catalysis [49]. The properties of siliceous SBA-15 are shown in Figure 2.7.

Figure 2.6 Network connectivity of pores in mesoporous SBA-15 [48].

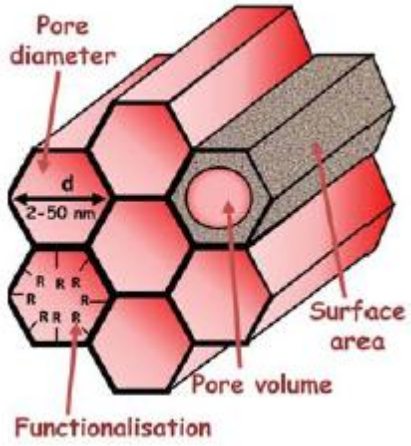

Figure 2.7 The properties of SBA-15 support: high pore volume, large surface area, well-ordered mesostructure and easy surface functionalization [49].

It has found that, deposition of heteroatom tungsten into the framework of SBA-15 increased metathesis activity significantly. Due to improve dispersion of tungsten species and presence of more active sites on the support, tungsten substitute SBA-15 materials exhibit best catalytic performance in metathesis of butene [50, 51].

In this research work, there will be detail overview of microporous and mesoporous catalyst activities in metathesis raection. In mesoporous support catalyst, tungsten substitute SBA-15 and MCM-41 will be discussed.

2.6 Reaction mechanism

In heterogeneous metathesis, the initial metal-carbene can be formed by a reaction between the catalyst and the promoter, if present, or by interaction of the substrate alkene with the transition metal center. In the latter case, more than one initiation mechanism has been devised on the basis of experimental evidence. The most widely accepted routes to the first metal-carbene include the formation of a π-complex between the reacting alkene and the transition metal, followed by either a 1,2-hydrogen shift mechanism or a hydride transfer to form successively a π-allyl complex, a metallacyclobutane and the metal-carbene [19] . Eqs (i) and (ii) are showing metal carbene complex formation from 1-butene and 1-butene.

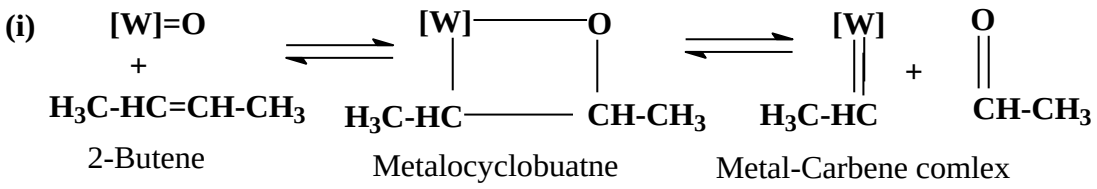

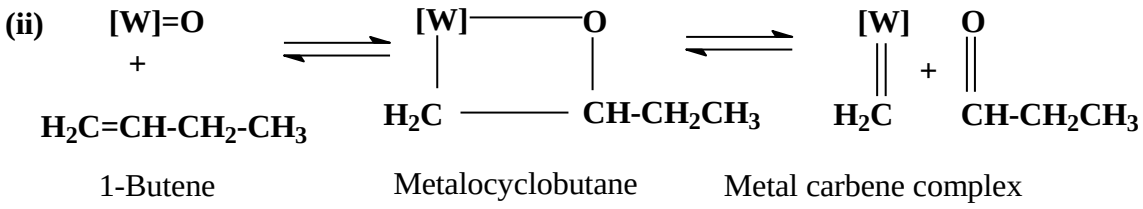

2.7 Propylene research: Kingdom perspective

Manufacturing costs, along with revenues and economic indicators, are determined as follows. Raw materials ethylene and butene account for more than 90% of the total manufacturing expenses. The values at which ethylene and butene feedstocks are acquired will consequently play a decisive role in the economic feasibility of a Lummus OCT unit. While ethylene prices are similar to those of propylene, namely between 961 and USD 1268/m ton, butene values, however, are typically much lower. Furthermore, the process is fed with a butene:ethylene mass ratio of approximately 3:1 (butene as raffinate-2). As a result, the valuation of butene becomes crucial in the overall economics of the process [15].

Ethylene feedstocks for metathesis can be supplied from either steam crackers or off-gas extraction from FCC units. Butene feedstocks may be supplied from either steam cracker crude C4 or refinery FCC mixed butenes. Butene availability as raffinate-2 in the Middle East tends to be reduced due to the growth of an ethylene industry almost completely based on ethane-based steam crackers that do not have raffinate-2 as a by-product but availability should increase with increased LPG cracking. The costs of chemicals, catalysts and main utilities, ranging from 28 to USD 77/m ton of propylene, represent from 4% to 8% of total manufacturing expenses, with regions with high energy product costs such as Europe and Southeast Asia occupying the high end of the scale. Lummus OCT by-products are basically fuels which may be used as an energy source for the process [15].

They represent a credit that ranges from 1% to 14% of the total manufacturing costs and, for similar reasons; Europe and Southeast Asia occupy the high end (at about 10% and 14% respectively). A plant's fixed costs, which include direct costs (e.g., labor, maintenance, and overhead) and indirect costs (e.g., insurance and property taxes), range from 16 to USD 29/m ton, or between 1.6% to 2.6% of the total manufacturing costs depending on the region for a plant with propylene capacity of 300 kta [15]. Figure 2.8 production costs of OCT Lummus Technology at different region. Middle East is showing the lowest manufacturing cost while West Europe shows highest manufacturing expense.

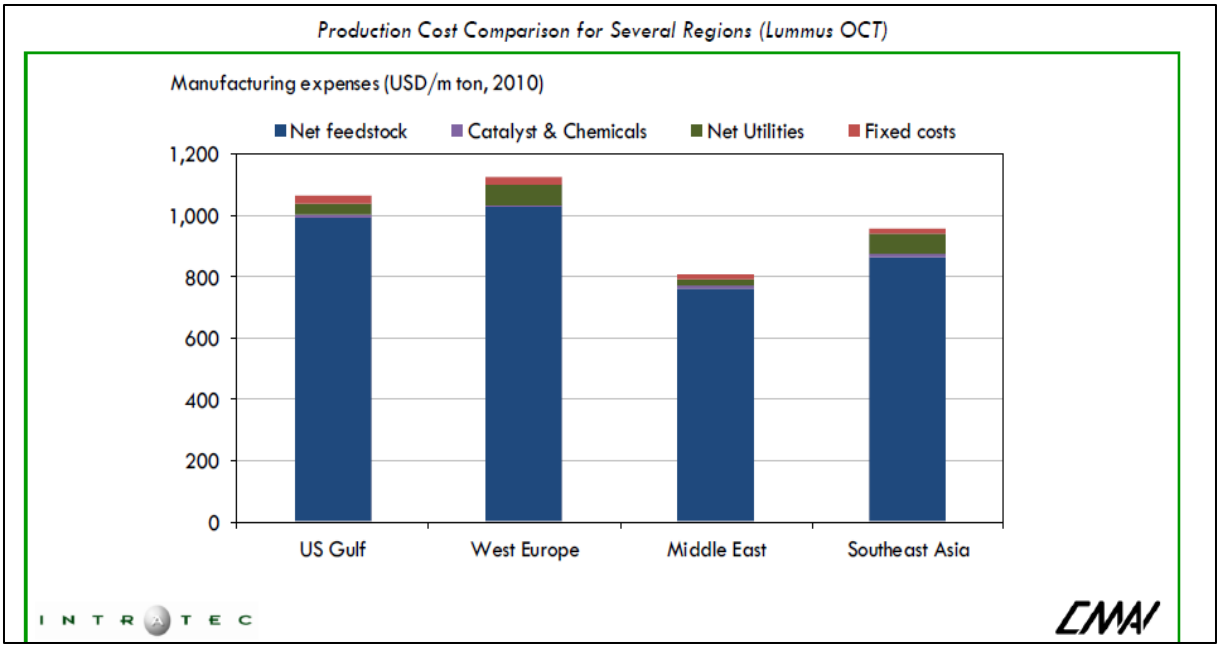

Figure 2.8 Production cost comparison several region.

2.8 Conclusion of literature review

After the thorough discussion in the introduction and literature review part, the significance of my thesis work is given below:

1. Product: Propylene is the raw material for a wide variety of products, and has established itself as the second major member of the global olefins business, only after ethylene.

2. Technology: Olefin metathesis can be added to a steam cracking unit or a refinery FCC unit to boost up the propylene production by ethylene and by product butene reaction. Middle East is the most cost effective place for the production of propylene using olefin metathesis.

3. Feed: Ethylene is expensive compare to C4 olefin stream. On the other hand, 1-butene is expensive as compared to 2-butene because 1-butene has huge demand as a monomer for the production of liner low density polyethylene (LLDPE) and polybutene. For that reason, 2-butene metathesis reaction is focused on this research work.

4. Catalyst: Metal tungsten has resistance to poisons and longer lime time compared to other metal used for olefin metathesis and for this, industrially it is more applicable. Mesoporous support SBA-15 and high surface area and large pore diameter which creates more active sites and increase the diffusion rate of reactant respectively.

5. Reaction mechanism and kinetic modeling: there is no work reported in the open literature studying the mechanism and kinetics modeling of butene metathesis to produce propylene.

CHAPTER 3

THESIS OBJECTIVE

The main objective of this thesis work to develop highly efficient catalyst for metathesis of C4 olefins to propylene and kinetics studies of the reaction. The effective catalyst will be selected on product propylene selectivity, feed 2-butene conversion and stability of the catalyst. To monitor progress of the overall objectives, activities have been categorized into the following four phases:

Phase I: Synthesis of tungsten oxide contained on mesoporous materials

This phase will be designed to synthesize of several WO_3 supported on mesporous silica catalyst. Tungsten oxide will be incorporated to the mesporous support SBA-15 and MCM-41 on both direct hydrothermal and impregnation method. Different amount tungsten oxide will be loaded into the support in both methods.

Phase II: Characterization of the supports and catalysts

The measurement of specific surface area and pore diameter will be carried out on AUTOSORB-1 (Quantachrome) and calculation will be done by Brunauer–Emmett–Teller (BET) method and the Barrett–Joyner–Halenda (BJH) method, respectively. The dispersion of WO_3 on the mesoporous support will be detected by X-ray powder diffraction (XRD) method. The tungsten oxide surface structure will be detected by

Raman Spectroscopy and UV-vis DRS method. The surface acidity of the different catalysts will be measured by and NH_3- TPD and FTIR pyridine adsorption method. The interaction between metal oxide and support will be analyzed by H_2 TPR method. SEM (Scanning Electron Microscopy) will be used to study catalysts, particularly to obtain data about shape, size, crystalline habit, homogeneity, contemporary presence of amorphous and crystalline (or different crystalline) compounds and their distribution, relative surface of different crystalline faces. The chemical compositions of synthesized catalysts will be determined by atomic absorption spectroscopy, using the Perkin-Elmer equipment (Model A Analyst 100).

Phase III: Catalysts test performances

The prepared catalysts' activity and selectivity will be determined for the metathesis of 2-butene process. A fixed bed tubular reactor was used for metathesis of 2-butene at reaction temperature (350 – 550 °C) and different (900-2700) GHSV. It is expected that the high GHSV will limit the tendencies of undesired reactions from taking place and the relatively low temperature will prevent the occurrence of metathesis reaction. The following areas will be studied to evaluate the performances of a catalyst on metathesis activity:

(i) Effect of synthesis method

(ii) Effect of tungsten oxide content in both impregnation and hydrothermal

(iii) Effect of temperature

(iv) Effect of residence time

(v) Stability of catalyst

Phase IV: Reaction mechanism, Model formulation, Parameter estimation and Model discrimination

Key to any process development is the availability of important design parameters such as the activation energy of the reaction, rate constants, etc. This will be involved the following:

(i) Proposing different possible reaction models.

(ii) Fitting experimental data into the proposed models to check the suitability of the models.

(iii) Determination of kinetic parameters; apparent activation energies, apparent reaction rate constants.

CHAPTER 4

EXPERIMENTAL

4.1 Experimental set up

4.1.1 Fixed bed tubular reactor system

The Micro Reactor System is a complete reaction system for vapor phase catalyst evaluation and continuous flow process analysis. The reactant preparation portion is capable of handling up to six inputs. Two inputs are high pressure liquid pumps and four inputs are mass flow controllers. The reactants are passed through a mixer/vaporizer assembly for blending and creation of a single homogeneous, non-pulsating stream to be fed to the reactor.

The feed controls include high pressure metering valves, in-line filters, reverse-flow check valves, Thermal Mass Flow Controller and a 2 or 3-way diverter valve. These valves permit on/off control and flow measurement of fluids prior to being directed into the system. These controls are mounted on the front panel of the reactor module. One thermostated, fixed bed tubular reactor is provided with a single-zone split tube furnace

heater controlled from furnace thermocouple along with the catalyst bed (process) thermocouple.

The reactor and heater are mounted within an isothermal oven. A forced convection blower assembly provides heating for the oven. This totally heated environment ensures that undesirable condensation is minimized. This adds significantly to the performance and reproducibility achievable in a Micro Scale Reactor. The multi-port reactor status valve can permit reactant bypass. This valve provides a convenient means of performing analytical sampling of the feed material. When the reactor is placed in the "by-pass" position, a high pressure, inert gas stream is activated to purge the reactor contents to a safe vent.

Pressure measurement at the inlet of the reactor is performed via a mechanical gauge assembly and digital pressure transducer. The gauge & transducer is isolated from the hostile reacting environment by a high pressure, silicone-filled isolator with a welded stainless steel diaphragm. Pressure is maintained by a manually-controlled, spring-loaded, back pressure regulator. Digital indication of pressure is offered herewith.

A heated multi-port, near zero dead-volume, sampling valve is provided for transfer of the vapor phase effluent from the system to a customer-supplied gas chromatograph. This

valve is also located in the isothermal oven. A heated transfer line and carrier gas controls are provided for sample transfer to a customer supplied gas chromatograph.

System control consists of three tunable PID controllers for temperature control of the reactor, oven, and transfer line. Also control system permits rotation of the multi-port reactor status and sampling valves. A rupture disc assembly is included as a standard feature to eliminate the risk of dangerous over pressurization. A multi-port reactor status valve allows purging of the reactor during a shutdown. Power is terminated to any heater station with a burned-out or open sensor via the individual temperature controller. A schematic diagram of experimental set-up is given in Figure 4.1.

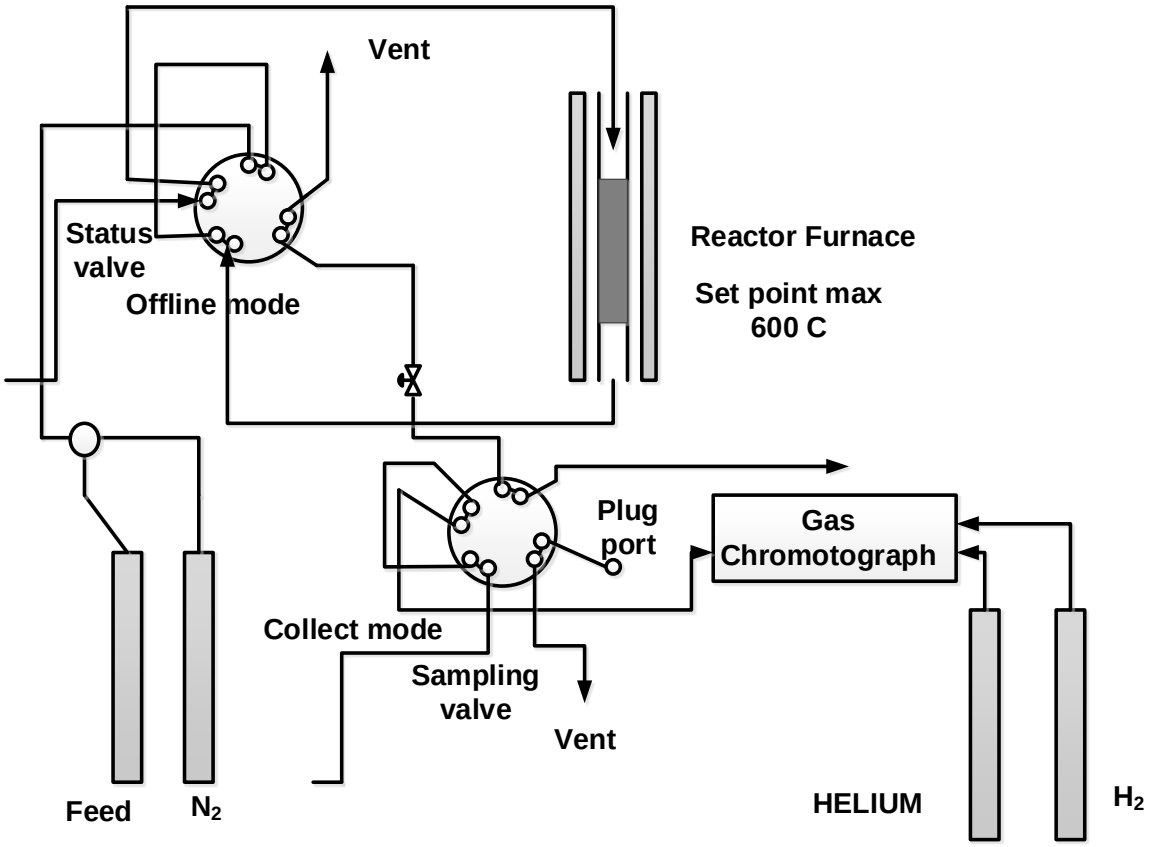

Figure 4.1 Schematic diagram of the fixed bed tubular reactor

4.1.2 Gas Chromatographic (GC) system

The quantitative analysis of the reaction products was carried out on line using Varian GC with FID (Varian 450-GC), equipped with a CP-Al_2O_3/Na_2SO_4 column (50 m length × 0.32 mm I.D. × df =5µm). The GC was programmed from 50 to 90 °C at a heating rate of 8 °C/min (hold it for 10 min at 90 °C) and 90 to 190 °C at a heating rate of 10 °C/min (hold it for 5 min at 190 °C). Helium is used as the carrier gas, while air and hydrogen gases are used for the FID detector. Furthermore, liquid nitrogen is used to facilitate the initial cryogenic operation of the GC temperature program. The liquid nitrogen cools the GC oven to -30 °C. The flow of liquid nitrogen is administered by a solenoid valve actuated from the GC's internal oven temperature controller. The integrator allows strip chart recording as well as integration of the GC detector signal. The integrator is connected to the GC via a HPIL instrument network cabling system.

4.2 Experimental

4.2.1 Materials

Pluronic 123($EO_{20}PO_{70}EO_{20}$), tetraethylorthosilicate (98%, TEOS), sodium tungstate (99.99%, $NaWO_4.2H_2O$), hydrochloric acid (36%), sodium metasilicate (98%, Na_2SiO_3), cetyltrimethyl-ammonium bromide (98%, CTAB), anhydrous ethyl acetate (99.8%) and ammonium metatungstate [99%, $(NH_4)_6H_2W_{12}O_{40}.xH_2O$] were purchased form Sigma-Aldrich and used without any further purification. 2-butene with 99.9% purity (50% Cis-

2-butene and 50% trans-2-butene) was purchased from Saudi Industrial Gas Company, Saudi Arabia.

4.2.2 Support Synthesis

Two types of mesoporous supports, SBA-15 and MCM-41were synthesized using the hydrothermal method.

4.2.2.1 Mesoporous SBA-15

Hexagonally ordered mesoporous SBA-15 was synthesized using triblock co-polymer P123 ($EO_{20}PO_{70}EO_{20}$) as structure directing agent and tetraethylorthosilicate (TEOS) as silica precursor. Synthesis of SBA-15 was performed according to the procedure reported in literature [50, 51]. In a typical synthesis, 6 g of Pluronic 123 was dissolved to 210 ml of 2M HCl and stirred at 40° C to achieve a transparent solution. After 3-4 h, 12.8 g TEOS was quickly added into the solution. The solution was stirred at 95 °C for 2 days. The solid products obtained were washed with water and dried at 80 °C overnight. The template was removed by calcination in air at 550 °C for 5h. The molar ratio of the gel composition is 1 SiO_2: 0.0167 P123: 5.82 HCl: 190 H_20.

4.2.2.1 Mesoporous MCM-41

Mesoporous support MCM-41 was synthesized by using the sodium metasilicate (Na_2SiO_3) and cetyltrimethyl-ammonium bromide (CTAB) as a source of silica and structure directing agent, respectively. Synthesis was performed according to the method described in literature [52]. 9.96 g of sodium metasilicate with 150 ml H_2O was stirred at 85° C for 30 minutes. Then, 9.8 g of CTAB was added to the solution and stirred for 10

minutes. 30 ml ethyl acetate was rapidly added into the solution under vigorous stirring. The stirring was continued for 24 h at 85° C. The solid products were recovered by filtration. After washing with deionized water several times, the solid was air-dried and then calcined in air at 600 °C for 4 h to remove the template. In this procedure, cheap and convenient sodium silicate was used as an inorganic silica precursor instead of expensive organic TEOS and ethyl acetate was employed as the acid producing precursor instead of a conventional strong acid, such as HCl or H_2SO4. The synthesis gel molar composition is 1 SiO_2: 0.335 CTAB: 3.8 EtOAc: 120H_2O.

4.2.3 Catalyst Synthesis

Several catalysts were synthesized by supporting tungsten on mesoporous silica SBA-15 & MCM-41 using hydrothermal crystallization and wet impregnation procedures (Table 1). The details of the synthesis procedure are given below:

4.2.3.1 W containing SBA-15 by direct hydrothermal method (WO_3-SBA-15)

Sodium tungstate ($NaWO_4.2H_2O$) was used as the source of tungsten ion for the synthesis of WO_3-SBA-15 by direct hydrothermal method. In a typical synthesis of WO_3-SBA-15, tungsten was incorporated into the framework of mesoporous support SBA-15 depending upon the Si/W molar ratio. Pluronic 123 was dissolved in HCl and TEOS was added with vigorous stirring. Then, calculated amount of sodium tungstate solution was added to the solution and stirred at 95 °C for 3 days under hydrothermal conditions. The resultant solid was filtered, dried and calcined at 550 °C for 5h. The catalysts obtained in this way were

identified as WO_3-SBA-15(x), where x represented the molar ratio of silicon to tungsten (Si/W). The molar ratio of the gel composition is SiO_2: (0.0166-0.033) WO_3: 0.0167 P123: 5.82 HCl: 190 H_20.

4.2.3.2 W containing MCM-41 by direct hydrothermal method (WO_3-MCM-41)

In a typical synthesis of WO_3-MCM-41, the solution of sodium tungstate was added into the solution of sodium metasilicate and CTAB, depending upon the Si/W molar ratio. Then ethyl acetate was added as an acid producing precursor and the solution was stirred for 24 hours at 85 ℃ under hydrothermal conditions. After filtration, the solid was air-dried and calcined at 600 ℃ for 4 h. The catalysts obtained in this way were identified as WO_3-MCM41(x), where x represents the molar ratio of silicon to tungsten (Si/W). The synthesis gel molar composition is SiO_2: (0.0166-0.033) WO_3: 0.335 CTAB: 3.8 EtOAc: 120 H_2O.

4.2.3.3 Impregnation method (WO_3/SBA-15 and WO_3/MCM-41)

WO_3/SBA-15 and WO_3/MCM-41 catalysts with different tungsten loading in the range of 5 and 10 wt% of WO_3 were prepared by wet impregnation method. Aqueous solution of ammonium metatungstate [$(NH4)_6H_2W_{12}O_{40}.xH_2O$] and the siliceous support SBA-15 or MCM-41 were mixed together and stirred for 3 h. Then the impregnated product was dried in an oven at 80°C for 12 h and calcined at 550 °C for 5 h. The catalysts obtained in this way were identified as WO_3/SBA-15(x) and WO_3/MCM-41(x) where x is the molar ratio of silicon to tungsten (Si/W).

4.2.4 Catalyst Characterization

4.2.4.1 X-ray powder diffraction

The samples were characterized by the X-ray powder diffraction (XRD) method, using a Rigaku Mini-flex II system using nickel filtered CuKα radiation (λ = 1.5406 Å) at a scanning rate of 1 ° min^{-1} in the 2θ range of 1.3-50°. The X-ray tube was operated at 40 kV and 30 mA.

4.2.4.2 N_2 adsorption isotherm

The surface areas of the samples were measured by nitrogen adsorption at −196 °C using AUTOSORB-1 (Quanta Chrome). Before adsorption measurements, samples (ca. 0.1 g) were heated at 220 °C for 2 h under nitrogen flow. The nitrogen adsorption isotherms of calcined materials were measured at liquid nitrogen temperature (−196 °C). The surface areas and pore diameters were calculated by the Brunauer Emmett-Teller (BET) method and the Barrett-Joyner-Halenda (BJH) method, respectively.

4.2.4.3 Scanning Electron Microscopy Analysis

SEM analysis has done by Gold Sputter Scanning electron microscope.

4.2.4.4 Inductively Coupled Plasma Analysis

The amounts of WO_3 present in the final samples were analyzed using ICP-AES (Ultima 2, Horiba scientific).

4.2.4.5 Raman Spectroscopy

Raman spectra were recorded at room temperature on Horiba Jobin Yvon in situ Raman, iHR 320 with synapse CCD detector (excitation line, 532.5 nm of an Ar+ ion laser; source power, 40-60mW; resolution, 4cm^{-1}).

4.2.4.6 UV vis DRS

UV vis DR spectra were recorded on a JASCO V-670 spectrophotometer at 200 nm per minute scan rate with $BaSO_4$ as reference.

4.2.4.7 Temperature programmed reduction

Temperature-programmed reduction (TPR) measurements were carried out using Micromeritics chemisorb 2750. Typically, about 100 mg of sample was pretreated at 300 °C for 2 h (ramping rate of 10 ºCmin^{-1}) under argon flow. After cooling the sample to 50 ºC in argon flow, the reduction was performed in a mixture of 5% H_2/Ar flowing at flow of 20 $mlmin^{-1}$ and heating rate of 10 °Cmin^{-1}, up to 1100 °C. Hydrogen consumed during TPR run was monitored by a thermal conductivity detector.

4.2.4.8 Temperature programmed desorption of ammonia

Temperature-programmed desorption of ammonia (TPD) was performed with BEL-CAT-A-200, chemisorption apparatus. This apparatus consists of a gas mixing unit, quartz micro reactor and a thermal conductivity detector (TCD). Samples were pretreated in a stream of He (50 ml/min) at 500 ◦C for 1 h. Then, NH_3 was adsorbed at 100◦C for 25 min. In order to remove loosely bounded ammonia, samples were purged with He stream

for 1 h at 100◦C. Then, the samples were heated again from 100 to 700 °C at a heating rate of 10° C/min in a flow of He (25ml/min) and the desorbed NH_3 was monitored by a TCD detector.

4.2.4.9 Pyridine adsorption by FT-IR

The acidity of synthesized material was analyzed by pyridine adsorption followed by FT-IR study. The catalyst sample was finely ground and pressed into a self-supporting wafer. The wafers were calcined under vacuum at 400 °C for 1 h, followed by exposure of pyridine vapour. The adsorbed pyridine was desorbed at various temperatures (150 to 350 °C). The thin wafer was placed in the FT-IR cell and the spectrum was recorded on a Nicolet FTIR spectrometer (Magna 500 model). The difference between the spectra of pyridine adsorbed on the samples and that of reference was obtained by subtraction. The amount of Bronsted acid sites (B) and Lewis acid sites (L) were calculated using the following equation as reported in literature [53].

C (pyridine on B sites) = 1.88 IA(B) R^2/W.

C (pyridine on L sites) = 1.42 IA(L) R^2/W.

Where, C = concentration (mmol/g catalyst); IA(B, L) = integrated absorbance of B or L band (cm^{-1}); R = radius of catalyst disk (cm); W = weight of disk (mg).

4.3 GC Calibration

The calibration of the gas chromatograph used in determining the product composition of reaction was done as explained in sections 4.3.1 and 4.3.2 below:

4.3.1 Determination of retention time for the different compounds

The retention times of all compounds of interest in this work were determined by analyzing pure samples of each of the compounds in the GC in turns. Table A4.1 shows the different hydrocarbons and their corresponding retention times and Table A4.2 shows the different aromatics retention times. These retention times were used to identify each component of the reaction products.

4.3.2 Correlating GC response and actual weight percentage of each compound

In calibrating the GC, standard samples of different compositions containing 2-butene and the main reaction products (ethylene, propylene, 1-butene, pentene, hexene) were prepared. The composition of the prepared samples were carefully chosen to reflect all the possible product compositions (obtained from preliminary experimental runs) under the different reaction conditions to be investigated. 0.2μl of the first sample was then injected into the GC and the GC responses (area %) for each of the components in sample were obtained.The sample procedure was repeated for all the other samples.

4.4 Catalyst Evaluation

4.4.1 Testing Procedure

The metathesis reaction of 2-butene (mixture of trans-2-butene & cis-2-butene 1:1) was performed in a fixed-bed tubular reactor (stainless steel tube grade 316 material , 0.312 inch ID × 0.562 inch OD × 8 inch length). A schematic diagram of the reactor is shown in Fig.1. In a typical experiment, the reactor was charged with 2 ml of catalyst previously sieved to a particle size of 0.5-1.0 mm diameter. The catalyst sample was first activated in a nitrogen stream at 550 °C for 1 h. The flow rates of feed (2-Butene) and N_2 were maintained at 5.0 ml/min and 25 ml/min, respectively, during the reaction. The metathesis reaction was carried out at different temperatures, ranging from 350-550 °C, GHSV (gas hourly space velocity) of 900-2700 h^{-1} and atmospheric pressure. To check the reproducibility of the experimental results, a number of runs were performed which were found to be excellent. Typical errors were in the range of ±1%.

The GC analyzed data were further processed to calculate the conversion and selectivity using the following equations according to Liu et al. (2013):

Conversion of 2-butene

$$X_{(2-C_4^=)} = \frac{\text{moles of 2butene converted}\left(\frac{W(2C_4^=)}{4}\right)}{\text{moles 2butene fed}} \times 100\ \% \qquad (1)$$

Yield

$$\text{Yield, } Y(C_n^{=}) = \frac{X_{(2-C_4^{=})} \times \frac{W(C_n^{=})}{n}}{\frac{W(C_2^{=})}{2} + \frac{W(C_3^{=})}{3} + \frac{W(1C_4^{=})}{4} + \frac{W(C_5^{=})}{5} + \frac{W(C_6^{=})}{6}} \times 100\ \% \quad (2)$$

Selectivity

$$S(C_n^{=}) = \frac{\text{Yield, } Y(C_n^{=})}{\text{Conversion of 2butene, } X_{(2-C_4^{=})}} \times 100\ \% \quad (3)$$

In the formula, $Y(C_n^{=})$ and $S(C_n^{=})$ is the yield and selectivity of alkene with carbon number *n*, and $W(C_n^{=})$ is the mass percent of alkene with different carbon number n.

CHAPTER 5

RESULTS AND DISCISSIONS

5.1 Metathesis of 2-butene over WO_3 contained on SBA-15

5.1.1 Physicochemical properties

5.1.1.1 X-ray powder diffraction

The X-ray diffraction patterns of the calcined SBA-15, WO_3-SBA-15 and WO_3/SBA-15 samples are shown in Figure 5.1 and d spacing values are given in Table 5.1. Two diffraction peaks in the region of 2θ = 1.5-2°, which can be indexed to the [1 1 0] and [2 0 0] diffractions characteristic of the *p6mm* hexagonal symmetry, were observed for the SBA-15 samples [54]. In all cases, 100 reflections were not observed due to limitation of XRD instrument. There is no significant difference in [1 1 0] and [2 0 0] diffractions for WO_3-SBA-15, whereas WO_3/SBA-15 samples shows decrease in peak intensity. The decrease in intensity shows the poor dispersion of tungsten oxide on impregnated SBA-15 samples. There were small peaks assigned to the crystalline phase of WO_3 as observed for WO_3-SBA-15 (30 and 60) samples. However, WO_3 impregnated on SBA-15 has

strong crystalline WO_3 peaks compared with hydrothermal synthesized WO_3-SBA-15 materials.

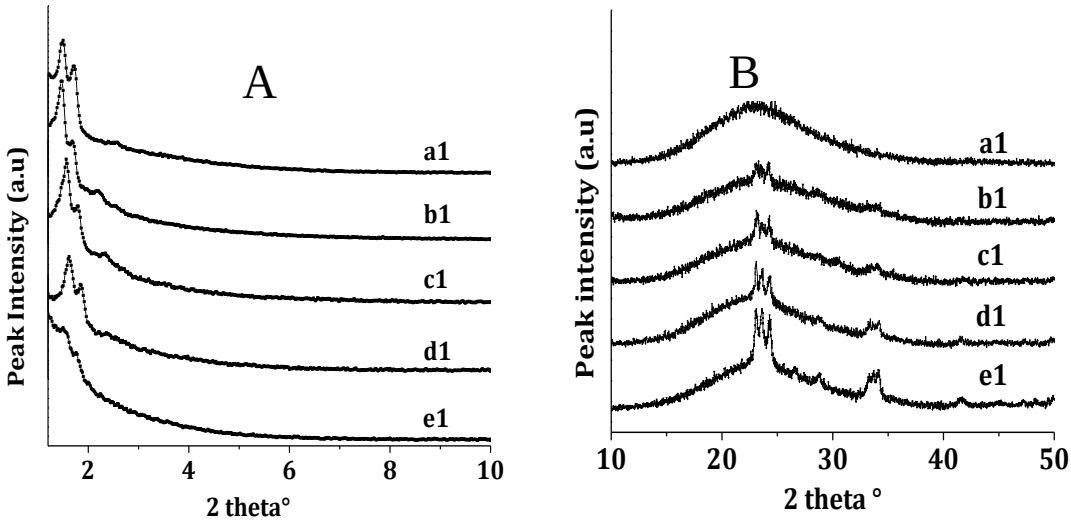

Figure 5.1 XRD patterns of different samples (a1) SBA-15, (b1) WO_3-SBA-15(60), (c1) WO_3-SBA-15(30), (d1) WO_3/SBA-15(73) and (e1) WO_3/SBA-15(35) at (A) low angle and (B) wide angle.

5.1.1.2 N_2 adsorption isotherm

The N_2 adsorption isotherms of SBA-15 samples are presented in Figure 5.2. These materials exhibit type IV classification, characteristic of mesoporous materials. According to the IUPAC classification, the hysteresis loops of the WO_3-SBA-15 can be classified as the H1 type, which shows two branches are almost vertical and nearly parallel over an appreciable range of relative pressure (P/P^0) [50]. H1 is associated with a more uniform pore distribution. A sharp increase in adsorbed volume at P/P^0 of approximately 0.70 arising from capillary condensation of nitrogen within the uniform mesoporous structures. The surface area and pore volume both shows a monotonic decrease with increasing concentration of tungsten (Table 5.1) compared with SBA-15 consistent with the formation of WO_3 within the mesoporous structure of SBA-15. As it is seen from Table 5.1, WO_3-SBA-15(30) and WO_3-SBA-15(60) materials have high surface area compared to impregnated WO_3/SBA-15(35).

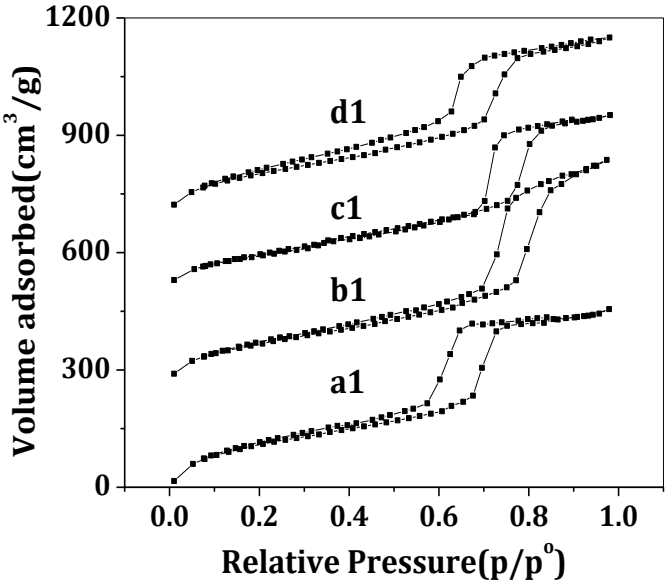

Figure 5.2 N_2 adsorption isotherm of different samples (a1) SBA-15, (b1) WO_3-SBA-15(60), (c1) WO_3-SBA-15(30) and (e1) WO_3/SBA-15(35).

Table 5.1 Physicochemical properties of WO_3 loaded SBA-15 catalysts

Samples	$d_{spacing}$ (nm)	% of WO_3 (ICP-AES)	Surface Area (m^2/g)	Pore Diameter (nm)	Total Pore Volume (cc/g)
SBA-15	5.53	-	833	4.4	0.939
WO_3/SBA-15(35)	5.69	10	468	4.3	0.636
WO_3-SBA-15(30)	5.597	9.19	501	6.9	0.777
WO_3-SBA-15(60)	5.974	4.92	571	6.2	0.988

5.1.1.3 Scanning Electron Microscopy

Figure 5.3 shows the SEM images of (A) SBA-15 and (B) WO_3/SBA-15 (35). SEM image (Figure. 5.3 (A)) shows that the SBA-15 sample has hexagonal array structure consist of mesoporous channel. Figure 5.3 (B) reveals after incorporation of WO_3 by impregnation method significant degradation of macroscopic structure. Figure 5.3 (C) and (D) are the images of WO_3-SBA-15 (30) at different resolution. Throughout the images well-defined rope-like domains with relatively uniform sizes of 1 μm largely maintained [50].

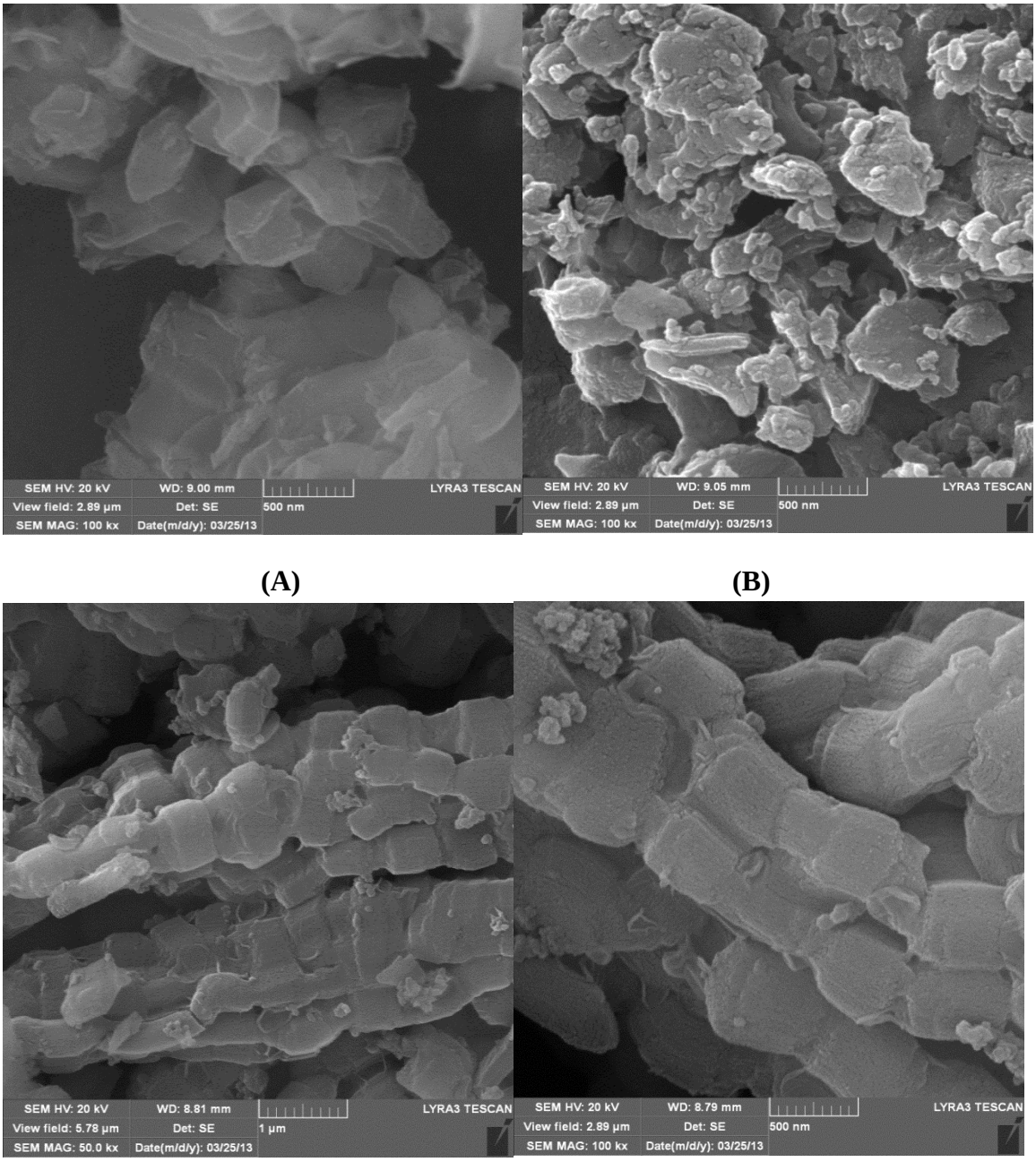

Figure 5.3 SEM images of (A) SBA-15, (B) WO_3/SBA-15 (35), (C) WO_3-SBA-15 (30) at 1µm and (D) WO_3-SBA-15(30) at 500 nm resolution.

5.1.1.4 Raman Spectroscopy

Raman spectra of the supports and catalysts are shown in Figure 5.4. For all the catalyst samples except the support materials, three strong peaks were observed at 265, 707 and 797 cm^{-1}. These crystalline WO_3 peaks were assigned to the symmetric stretching mode of W-O, bending mode of W-O and the deformation mode of W-O-W, respectively [55]. It is obvious that pure silica materials do not have any peaks in this region. The peak at 970 cm^{-1} is assigned to the symmetric stretching mode of the terminal W=O bond of the tetrahedrally coordinated tungsten oxide species, which are active sites for metathesis reaction [38, 50, 56]. The Raman peak at about 900 cm^{-1} is related to the incorporation of the transition metal ions in the silica framework as reported in literature [56]. It is also a typical evidence for the isomorphous substitution of silicon by tungsten in the tungsten incorporated SBA-15 samples. High intensity crystalline peaks were observed for the impregnated samples with 10% WO_3 loadings compared to WO_3-SBA-15 materials. This clearly shows that more octahedral tungsten species were observed in impregnated samples. This indicating the formation of a very poorly dispersed tungsten oxides. On the other hand, WO_3-SBA-15 materials shows less intense crystalline peaks with tetrahedrally coordinated tungsten species.

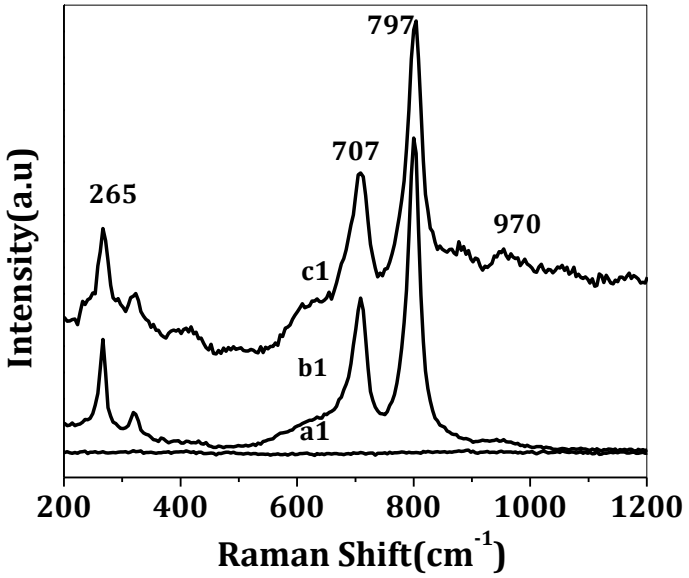

Figure 5.4 Raman spectra of different samples (a1) SBA-15, (b1) WO_3/SBA-15(35) and (c1) WO_3-SBA-15(30).

5.1.1.5 UV vis-DRS

Diffuse reflectance spectra of tungsten supported samples in the region of 200-600 nm are shown in Figure 5.5. This method is very sensitive for distinguishing the species between incorporated metal and extra-framework metal oxides in different heteroatomic mesostructures. The spectrum of sodium tungstate presents a spinal structure at 230 nm which mainly implies the presence of ligand to metal charge transfer involving isolated transition metal sites and considered direct proof of the framework tungsten oxide species in tetrahedral co-ordination [56, 57]. For, pure SBA-15, there is no evidence of the band (not in the figure). The samples tungsten incorporated into the framework, WO_3-SBA-15(30), show similar band at 230 nm can be attributed more presence of isolated $[WO_4]^{2-}$ tetrahedral species into the support. On the other hand, the spectrum of impregnated samples, WO_3/SBA-15(35) is not showing this band significantly, which implies less presence of tetrahedral species. The second band at 263 nm may be attributed to isolated tungsten species or low-condensed oligomeric tungsten oxide species. For the sample ammonium metatungstate, a broad band at 350-400 nm is observed showing mainly extra-framework bulk WO_3 particles or clusters in the sample.

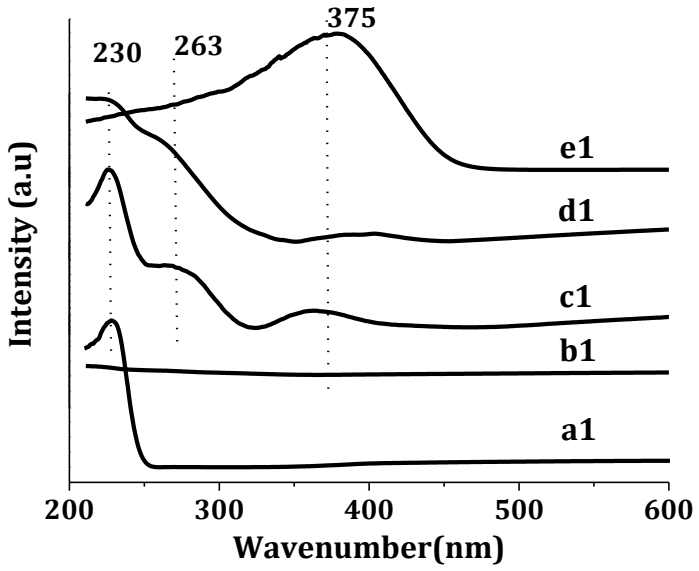

Figure 5.5 UV-vis diffuse reflectance spectra of various samples (a1) $Na_2.WO_4.2H_20$, (b1) SBA-15, (c1) WO_3-SBA-15(30, (d1) WO_3/SBA-15(35) and (e1) ammonium metatungstate.

5.1.1.6 Temperature programmed reduction

TPR profile of tungsten supported SBA-15 samples and bulk WO_3 are presented in Figure 5.6 at the temperature range of 100 to 975°C. The pure SBA-15 shows no reduction peaks in this range whereas three reduction peaks were detected for bulk WO_3. This is occurs for the three stepwise reduction of WO_3 to W(0) [56]. The higher temperatures reduction peaks at 840 and 975 °C are assigned for the reduction of W(VI) species in the tetrahedral co-ordinations. The lower temperature peak at 710 °C is associated with the reduction of bulk WO_3. The impregnated samples WO_3/SBA-15(35) shows three similar reduction peaks of WO_3 but great shift of temperature has been observed. De Lucas et al. (1998) reported that the aggregation of tungsten oxide increases significant reducibility of tungsten based silica catalysts as the interaction of metal oxide with the support decreases [58]. Tungsten incorporated in framework sample WO_3-SBA-15(30) exhibits two reduction peaks with less reduction at lower temperature which implies stronger interaction of metal oxide with the support. Therefore, it can be concluded that WO_3-SBA-15(30) has much stronger interaction in between metal oxide and support SBA-15 compared to the impregnated $W0_3$/SBA-15(35).

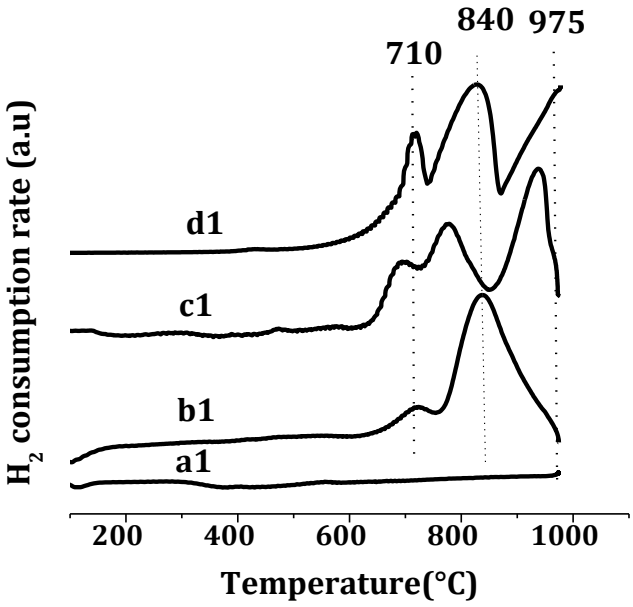

Figure 5.6 H_2-TPR profiles of different samples (a1) SBA-15, (b1) WO_3-SBA-15 (30), (c1) WO_3/SBA-15 (35) and (d1) ammonium metatungstate.

5.1.1.7 Temperature programmed desorption of ammonia

NH_3 TPD patterns for the supports and catalysts are shown in Figure 5.7 and the total acidity results are presented in Table 5.2. After Gaussian de-convolution, the peaks corresponding to weak (100–300°C) and medium (300–500°C) sites were obtained. As shown in Figure 5.7, a week ammonia desorption peak was observed at 180 °C for SBA-15. With increasing tungsten amount in the framework, the intensity of ammonia desorption peak at 180 °C was increased along with some medium acid site peaks observed above 350-400 °C. The total acidity of WO_3-SBA-15(30) was slightly higher than that of WO_3-SBA-15(60). In case of impregnated samples, the presence of WO_3 on the external surface of the catalyst was observed and it creates Lewis acid centers of bulky WO_3 as reported in literature [55]. Impregnated samples have very small amount of tungsten species deposited on the inner surface of the pores. However, higher acidity of WO_3-SBA-15(30) due to the presence of more Si-O-W bonds leading to high dispersion of tungsten species as observed in XRD.

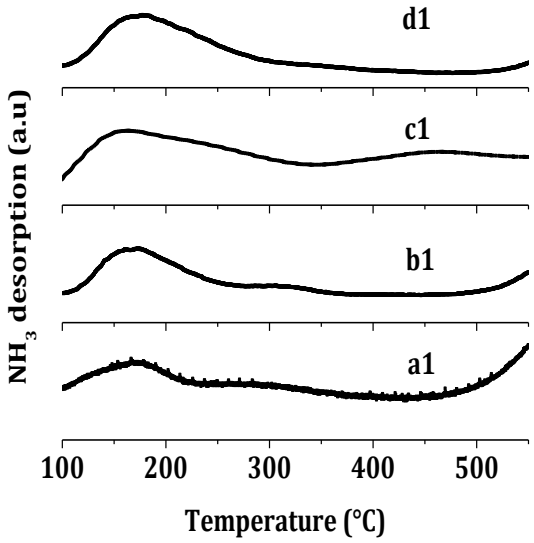

Figure 5.7 NH_3-TPD profiles of different samples (a1) SBA-15, (b1) WO_3-SBA-15(60), (c1) WO_3-SBA-15(30) and (e1) WO_3/SBA-15(35).

5.1.1.8 Pyridine adsorption by FT-IR

Pyridine adsorption measured by IR spectroscopy was carried out to evaluate the strength and types of acid sites present in the tungsten impregnated and framework samples. Figure 5.8 shows the FT-IR spectra of the SBA-15, WO_3-SBA-15 (60), WO_3-SBA-15 (30) and WO_3/SBA-15 (35) samples recorded after the adsorption of pyridine and subsequent evacuation at 150°C. The Py-FT-IR spectrum recorded after adsorption of pyridine at room temperature on the bare SBA-15 shows two major peaks at 1595 and 1445 cm^{-1}, ascribed to pyridine coordinately bonded to weak surface Lewis acid sites, which disappeared almost completely after outgassing at 350°C. In addition to bands at 1595 and 1445 cm^{-1}, the spectrum recorded for the WO_3-SBA-15 samples shows bands at 1485, 1545, and 1635 cm^{-1} due to protonated pyridine bonded to surface Brønsted acid sites, indicating that the presence of tungsten-doped species leads to the development of surface Brønsted acid sites [56, 59]. The intensities of all of these bands decrease after outgassing at increasing temperatures, but they are still recorded even after outgassing at 350 °C, illustrating that both types of acid sites are rather strong and are related to tungsten oxide incorporation (Figure 5.9 (A)). Similar spectra are recorded for tungsten impregnated samples of SBA-15, the number of the Lewis and Brønsted acid sites decreased after outgassing at 350 °C which is presented in Figure 5.9(B). The decrease in Lewis and Brønsted acid sites related to uneven distribution of WO_3 present in the samples. The amounts of Lewis and Brønsted acid sites is more for WO_3-SBA-15(30) compared to WO_3-SBA-15(60) due to increase in the framework tungsten oxide species covering more silica surface. The amount of Lewis and Brønsted acid sites at 150°C and 250°C are presented in Table 5.2. From pyridine adsorption FT-IR, it can be concluded

that the presence of Brønsted acid sites in the tungsten containing SBA-15 samples are related to amount tungsten oxide incorporated in the framework.

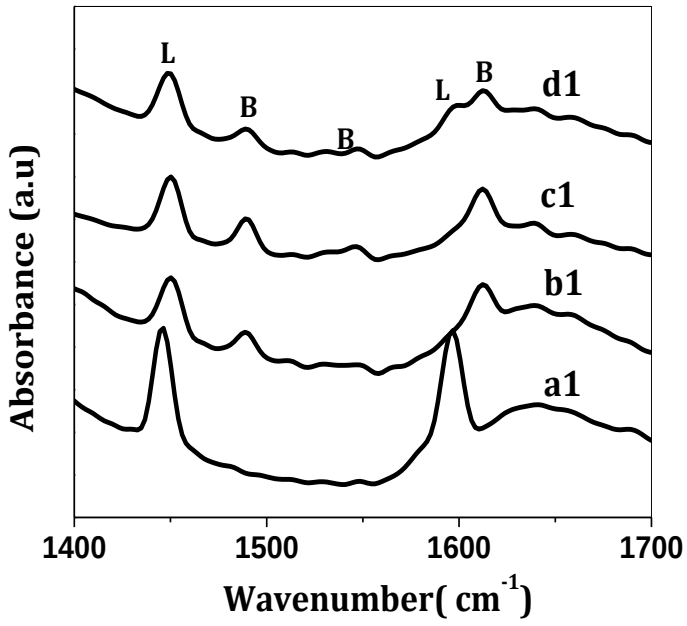

Figure 5.8 FTIR spectra of pyridine adsorbed on different samples at 150 °C, SBA-15 based catalysts (a1) SBA-15, (b1) WO_3-SBA-15(60), (c1) WO_3-SBA-15(60) and (d1) WO_3/SBA-15 (35).

L=Lewis acid site

B= Brønsted acid site

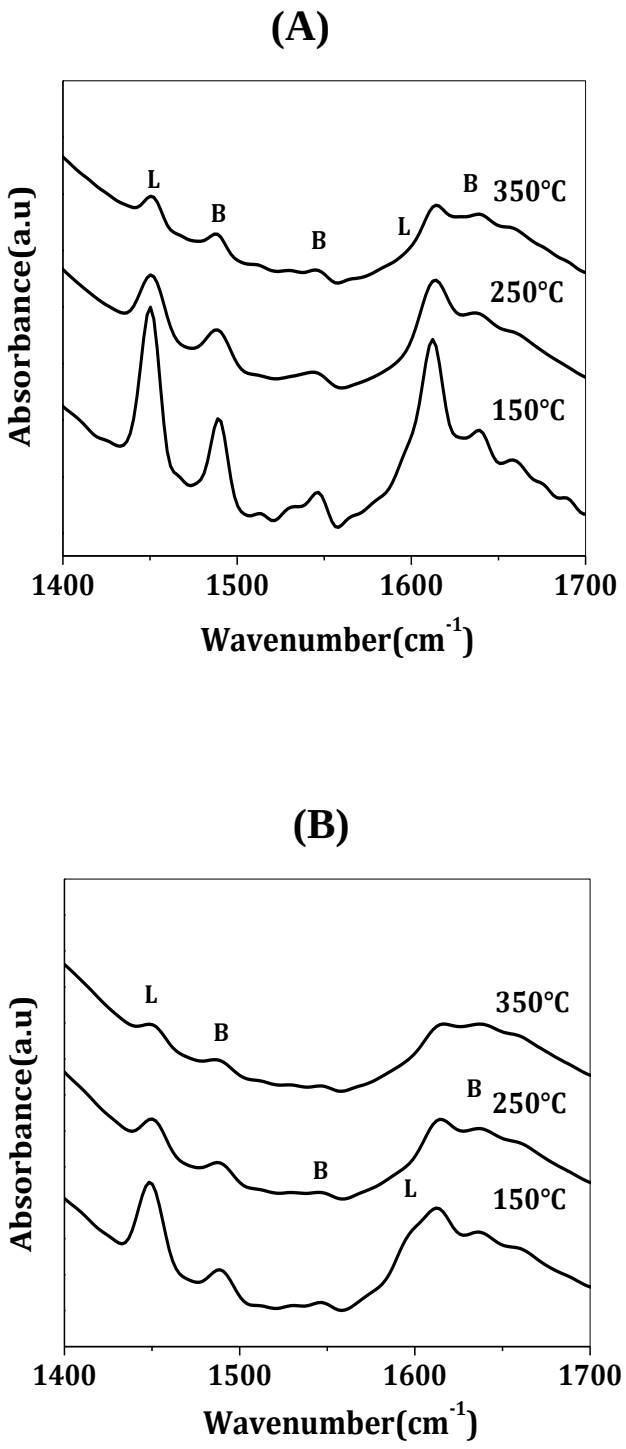

Figure 5.9 FTIR spectra of pyridine adsorbed on different samples at 150 °C, 250 °C and 350 °C (A) WO_3-SBA-15(30) and (B) WO_3/SBA-15 (35).

Table 5.2 Acid sites characteristics of tungsten incorporated and impregnated SBA-15 catalysts.

Samples	NH_3 TPD($mmolg^{-1}$)*			FT-IR chemisorbed pyridine ($mmolg^{-1}$)			
	TA	L.T <300°C	H.T 300-550°C	B 150°C	L 150°C	B 250°C	L 250°C
SBA-15	0.035	0.035	0.00	0.0265	0.3818	0.0056	0.1397
WO_3/SBA-15(35)	0.108	0.096	0.013	0.0347	0.1715	0.0152	0.0667
WO_3-SBA-15(30)	0.458	0.270	0.188	0.1086	0.3521	0.0539	0.1555
WO_3-SBA-15(60)	0.357	0.180	0.177	0.0433	0.1979	0.0208	0.0952

5.1.2 Catalytic activity on SBA-15

A systematic study of metathesis reactions of 2-butene over tungsten oxide supported mesoporous molecular sieves SBA-15 was performed. The main products from the metathesis reactions are ethylene, propylene, pentenes, hexenes and 1-butene. For major product of the carbon atoms, 2-pentene is considered as whole C_5= components and 3-hexene is considered as whole C_6= components. 2-butene can undergo a series of different reactions e.g. isomerization, metathesis, oligomerization, cracking etc. [60, 61]. All possible reactions of 2-butene are presented in Scheme 1. Metathesis reaction between 2-butene and 1-butene to produce propylene and 2-pentene is termed as Metathesis I. Apart from Metathesis I, propylene can also be produced by metathesis between 2-butene and ethylene (Metathesis II), as well as 2-butene with isobutylene (Metathesis III). Metathesis IV is a reaction between isomerized products 1-butene and isobutylene to produce ethylene with 3-hexene. 1-butene can also undergo self-metathesis to produce ethylene and 3-hexene, presented as metathesis V.

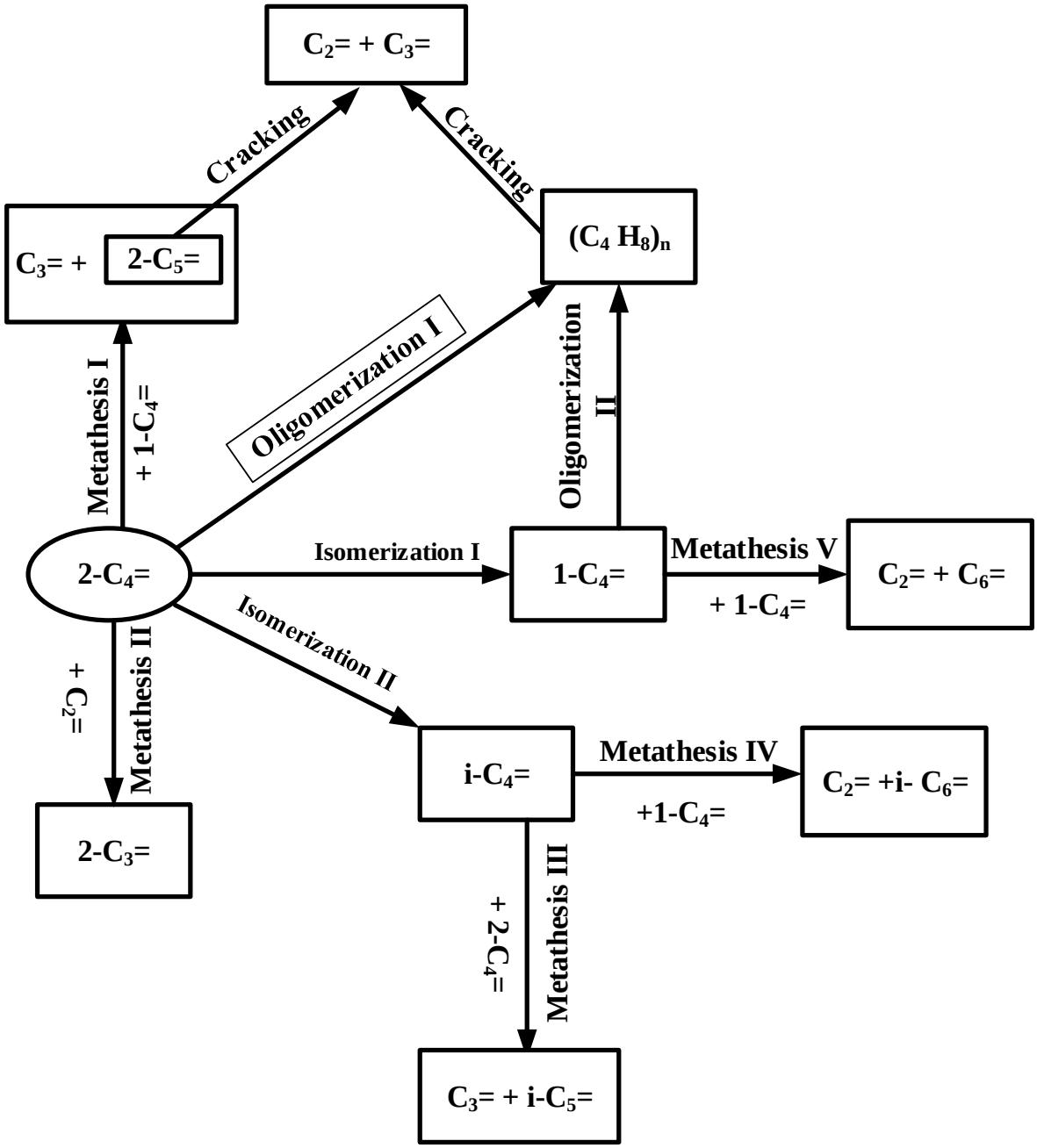

Scheme 1 Possible reaction pathways for 2-butene metathesis over W-based heterogeneous catalyst [61].

5.1.2.1 Effect of synthesis method

The tungsten oxide supported SBA-15 catalysts were prepared following two different methods. In the first method, two catalysts having tungsten oxide with Si/W ratio of 35 and 73 were prepared following wet incipient impregnation method while in the second method two catalysts having Si/W ratio of 30 and 60 were synthesized following hydrothermal crystallization procedure. The results of the metathesis reaction of 2-butene at 550 °C over tungsten oxide supported SBA-15 catalysts are presented in Figure 5.10 and Table 5.3. A significant increase in conversion of 2-butene was observed after incorporation of tungsten oxide. The catalytic conversion of 2-butene increased with an increase in the amount of tungsten oxide in both types of catalysts. The WO_3-SBA-15 with Si/W ratio of 30 resulted in high 2-butene conversion of 86.7 %. Similarly propylene and ethylene yields were observed to increase with an increase in the amount of tungsten oxide. Pure SBA-15 exhibited 1 mole % of propylene yield and 0 mole % of ethylene yield. The WO_3-SBA-15(30) depicted the highest yield of 37.1 mole %, and 16.7 mole % of propylene and ethylene, respectively. It was noticed that $C3^{=}/C5^{=}$ ratio also increased with an increase in the amount of tungsten oxide. The WO_3/SBA-15(73) resulted in a low ratio of $C3^{=}/C5^{=}$ (1.3) indicating metathesis I reaction was taking place predominately, whereas in the case of WO_3-SBA-15(30), $C3^{=}/C5^{=}$ ratio was 2.3 indicating the possibility of other reactions apart from metathesis I.

It was noticed that catalysts based on hydrothermal synthesis exhibited higher conversion and propylene yield as compared to that of impregnated ones, indicating the vital role of framework tungsten oxide sites in the metathesis reaction. The total acidity of WO_3-SBA-15(30) was higher than WO_3/SBA-15(35). Higher acidity of WO_3-SBA-15(30) enhanced

the isomerization of 2-butene to 1-butene and thus provide more availability of 1-butene for metathesis reaction with 2-butene. The higher acidity and availability of more tetrahedrally coordinated tungsten species are responsible for superior metathesis activity of WO_3-SBA-15(30) as compared to that of WO_3/SBA-15(35). The reproducibility of results were test by three different runs at 550 °C using WO_3-SBA-15(30) as catalyst showing 2-butene conversion with standard deviation of 0.96. The standard deviation of propylene and ethylene selectivity was found to be 0.69 and 1.17 respectively.

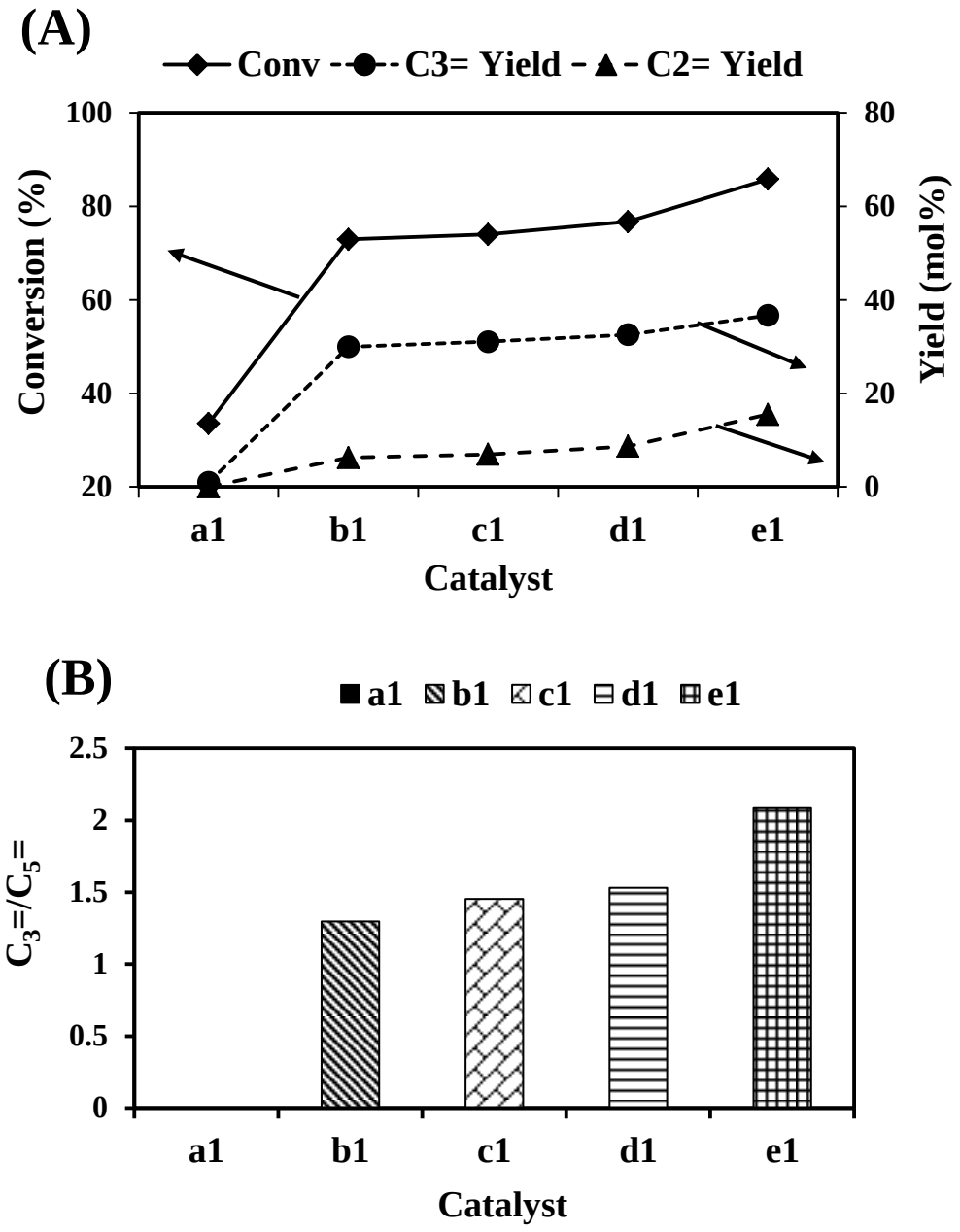

Figure 5.10 Results of metathesis reaction of 2-butene over (a1)SBA-15, (b1)WO_3/SBA-15(73), (c1)WO_3/SBA-15(35), (d1) WO_3-SBA-15(60), (e1) WO_3-SBA-15(30) catalysts at 2h (A) conversion of 2-butene, Propylene yield (mole %), ethylene yield (mole %) and (B) ratio of propylene to pentene (reaction temperature: 550 °C, pressure:1 atm, GHSV:900 h^{-1}).

Table 5.3 Product distribution (mole %) for metathesis reaction of 2-butene at 550 ºC over tungsten in the frame work and impregnated SBA-15 catalysts.

Time (hrs)	Conv.	C2=	C3=	1-C4=	*i*-C4=	2-C4=	C5=	C6+
SBA-15 1hr	31.5	0.0	1.1	28.6	1.9	68.5	0.0	0.0
2	33.6	0.0	1.0	30.8	1.8	66.4	0.0	0.0
3	33.9	0.0	1.0	31.3	1.6	66.1	0.0	0.0
4	33.9	0.0	1.0	31.4	1.6	66.1	0.0	0.0
5	34.0	0.0	1.0	31.6	1.5	66	0.0	0.0
WO_3/ SBA-15(73)-1hr	67.2	5.7	27.6	10.7	1.8	32.8	21.0	0.4
2	73.0	6.3	30.0	10.9	1.8	27.1	23.1	0.9
3	73.8	6.4	30.5	10.9	1.7	26.1	23.5	0.9
4	74.3	6.4	30.7	10.8	1.7	25.7	23.8	1.0
5	74.8	6.6	31.1	10.5	1.7	25.2	23.9	1.0
WO_3/SBA-15(35)1hr	69.0	5.1	26.9	14.3	2.1	31	20.3	0.4
2	74.0	7.0	31.1	12.0	2.1	26	21.4	0.6
3	75.9	7.6	32.0	11.1	2.1	24	22.4	0.9
4	76.8	8.0	32.6	10.7	2.0	23.2	22.1	1.1
5	77.0	8.4	33.3	10.6	2.0	23	21.3	1.2
WO_3-SBA-15(60) 1hr	70.5	8.4	31.5	9.6	4.5	29.5	16.2	0.3
2	76.7	8.7	32.5	9.6	4.2	23.2	21.3	0.4
3	77.4	8.7	32.9	9.7	3.9	22.6	21.4	0.7
4	77.5	8.6	33.1	9.7	3.7	22.5	21.8	0.8
5	77.6	8.4	32.7	9.7	3.4	22.3	22.7	0.8
WO_3-SBA-15(30) 1hr	86.7	16.7	37.2	6.2	9.0	13.4	16.4	1.2
2	85.8	15.5	36.7	6.6	8.4	14.3	17.6	1.1
3	85.2	14.4	36.0	6.8	7.7	14.8	19.2	1.2
4	84.8	13.9	35.9	7.0	7.2	15.2	19.6	1.3
5	84.2	13.1	35.5	7.2	6.6	15.7	20.5	1.3

5.1.2.2 Effect of tungsten loading

In wet impregnation method, four catalysts were synthesized changing the loading 5, 10, 15 and 20 wt% WO_3 supported on SBA-15. Figure 5.11 shows catalytic performances of these catalysts. Conversion of 2-butene increased up to 15 wt% of WO_3 loading and then became stable at 20 wt % loading. Propylene and ethylene yield showed same trend of catalytic performances. In direct hydrothermal method, three catalysts were synthesized changing the Si/W ratio 20, 30 and 60**.** Figure 5.12 shows the catalytic performances of these three catalysts. Conversion of 2-butene and ethylene and propylene yield increased up to Si/W ratio 30. After that, with the increase of tungsten amount the catalytic performance decreased steadily. WO_3-SBA-15 (30) shows the best catalytic performance among the catalyst synthesized by hydrothermal method. However, 20 wt% WO_3 loading shows the best catalytic performances among the impregnated catalyst.

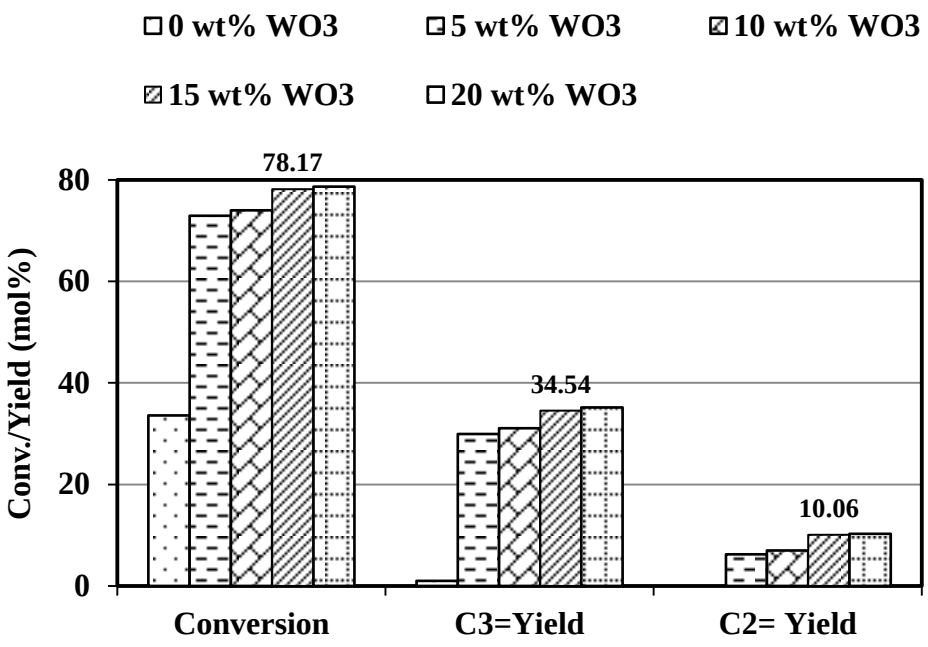

Figure 5.11 Conversion of 2-butene, Propylene yield (mol %), ethylene yield (mol %) of 2-butene metathesis reaction over SBA-15 and 5,10,15 and 20 wt% WO_3 catalysts supported on SBA-15 at 2hr (reaction temperature: 550 °C, pressure:1 atm, GHSV:900 h^{-1}).

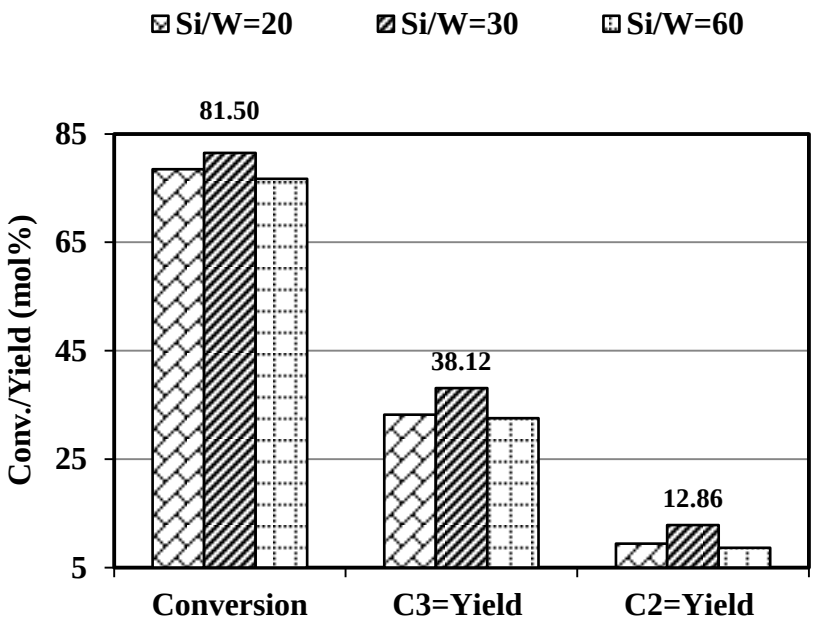

Figure 5.12 Conversion of 2-butene, Propylene yield (mol %), ethylene yield (mol %) of 2-butene metathesis reaction over WO_3-SBA-15 catalyst with Si/W ratio (20, 30 and 60) at 2hr 550 ° C (reaction temperature: 550 °C, pressure:1 atm, GHSV:900 h^{-1}).

5.1.2.3 Effect of reaction temperature

We investigated the influence of reaction temperature on 2-butene metathesis reaction over WO_3-SBA-15(30) catalyst at five different temperatures from 350-550 °C and at constant 900h^{-1} GHSV, atmospheric pressure. It is clear from the result that temperature has significant effect on the catalytic performance of WO_3-SBA-15(30). Several reactions are involved during this wide range temperature changes: isomerization, primary cross metathesis, self-metathesis, secondary cross metathesis and cracking. The effect of reaction temperature on activity is presented in Figure 5.13. As expected, 2-butene conversion was increasing with the increment of temperature. It is instructive to concentrate first on the temperature range below 400 °C where the 2-butene conversion was low and the selectivity of 1-butene was significant on overall product distribution. There was no appreciable formation of ethylene, propylene, 2-pentene and 3-hexene at the temperature below 400°C. It is thus evident that, at lower temperature 2 butene is isomerized to 1-butene which made the main role for the formation of other products at higher temperature. As can be seen Figure 5.13, 2-butene conversion increased rapidly from to 35.8 to 72.4 % and 1-butene selectivity suddenly dropped from 58 to 13.5 mole% between 400 to 450 °C. The selectivity of the propylene and 2-pentene increased to 41.3 and 25.9 mole% respectively which are the main two products at 450°C. The selectivity of ethylene and 3-hexene was also 7 and 6.9 mole% at 450°C. From the product distribution gathered so far, the reaction network can be drawn the following sequence of reaction products:

$$2-\text{Butene} \leftrightarrow 1-\text{Butene (up to 400°C)}$$

$$2-\text{Butene}+1-\text{Butene}\ \leftrightarrow \text{Propylene}+2-\text{Pentene}(\text{ between 400 to 450°C})$$

$$1-\text{Butene}\leftrightarrow \text{Ethylene}+3-\text{Hexene}(\text{ between 400 to 450°C})$$

According to the above reactions, the molar ratio of propylene and pentene should be 1:1. But it assume that due to some secondary metathesis reactions propylene selectivity was 15% more than 2-pentene at 450°C. 2-Butene conversions at 500 and 550 °C were still increasing while the selectivity of propylene and ethylene increased but the selectivity of 2-pentene and 3-hexene were in decline. This is because, acid catalyzed reactions of cracking are favorable at higher temperature and hence more propylene and ethylene were produce by cracking of 2-butene and 2-pentene at 500 and 550 °C. The effect of cracking at higher temperature were presented in Figure 5.14 with the comparison of $C_3=/C_5=$ and $C_2=/C_6=$ ratios at different temperature. It was noticed that, at 450 °C $C_2=/C_6=$ ratio was 1.02 which increased to 1.69 and 2.74 at 500 and 550 ° C respectively. In the same way, $C_3=/C_5=$ ratio was 1.62 at 450 ° which increased to 1.89 and 2.36 at 500 and 550 °C. These increments of ratios with temperature are the clear evidence of 2-butene and 2-pentene cracking for the formation of ethylene and propylene at higher temperature. In summary, based on the product distribution from 350 to 550 °C it was confirmed that at lower temperature 2-butene was isomerized to 1- butene, all the metathesis reactions started above 400°C and at higher temperature cracking of 2-butene and 2-pentene are involving.

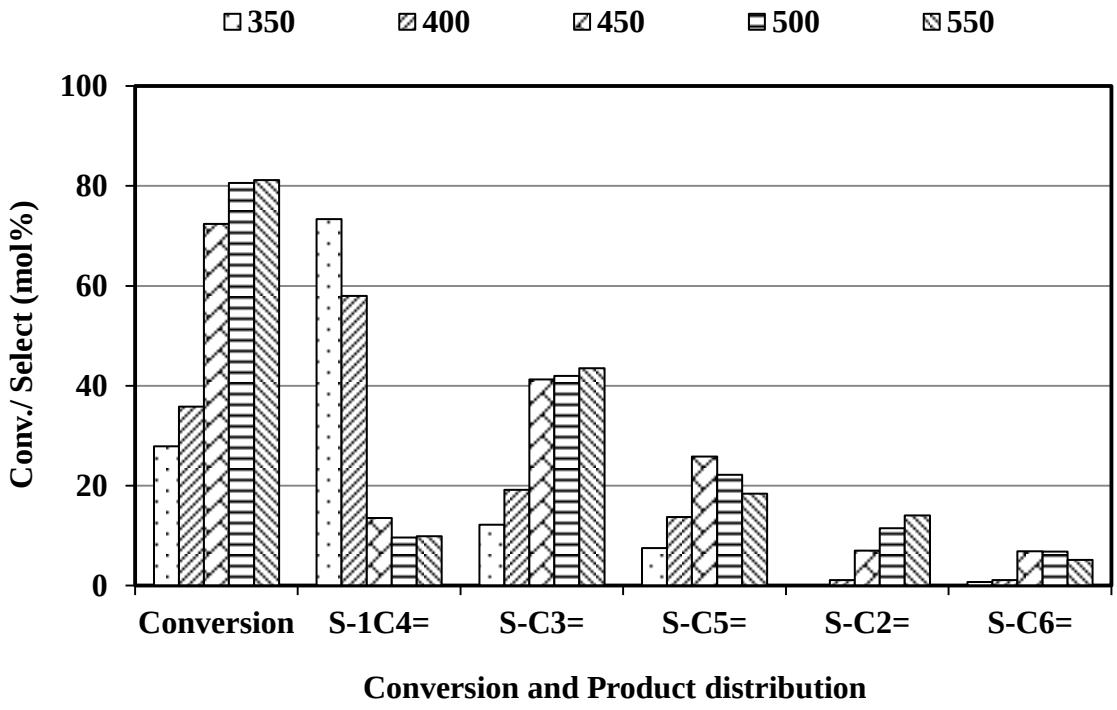

Figure 5.13 2-Butene Conversion and Selectivity of product over WO_3-SBA-15(30) catalyst from 350-550 ° C temperature at 24s contact time.

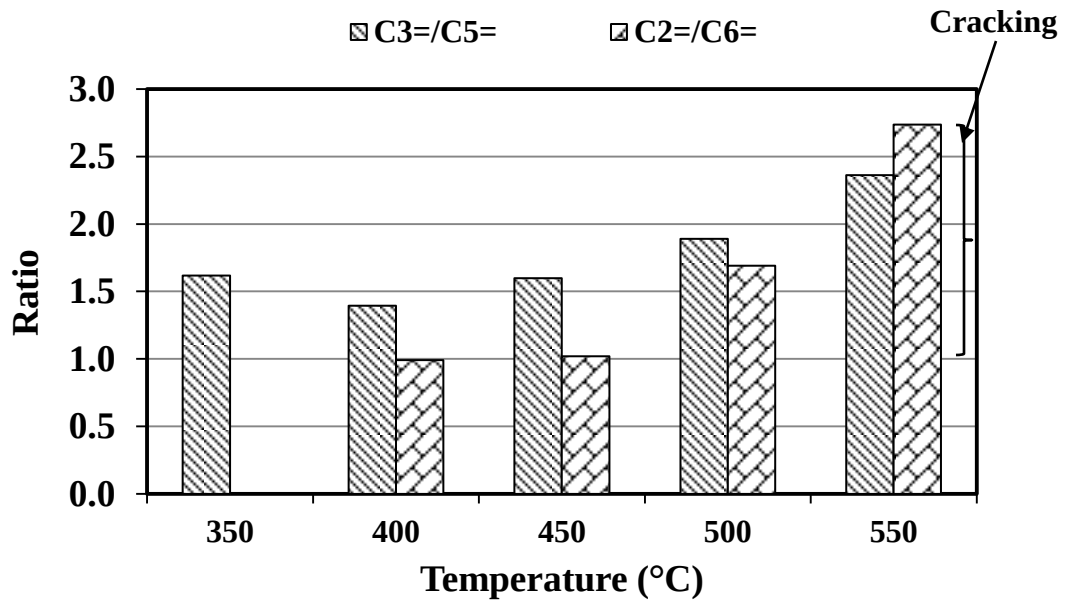

Figure 5.14 Ratio of Propylene to Pentene and Ethylene to Hexene over WO_3-SBA-15(30) catalyst from 350-550 ° C temperature at 24s contact time.

5.1.2.4 Effect of residence time

We studied the effect of residence time changing form 24s to 8s at 350-550 °C atmospheric pressure. Experimental results of 550 °C are shown in Figure 5.15. With the increasing of contact time, reactant 2-butene yield decreased from 58.4 to 18.8 mole% at 8 to 24s contact time. However, propylene yield was increasing with the increase of residence time. The same trend was following to other products also. The involvement of secondary metathesis and cracking of 2-butene could be explained with the comparison of $C_3=/C_5=$ ratios at different temperature and different residence time which are presented at Figure 5.16. The ratio of $C_3=/C_5=$ decreased more at 550°C than 450 °C with the decreasing of residence time. From this trend, it is assumed that residence time influenced more on cracking than the secondary metathesis reactions for the production of propylene. The ratio of $C_2=/C_6$ at different residence time and temperature is presented at Figure 5.17. The ratio of $C_2=/C_6$ decreased with the decreasing of residence time and there was no formation of ethylene and 3-hexene at 450°C after 9s residence time. From this result, it is confirmed that self-metathesis of 1-butene for the production of ethylene and 3-hexene is highly influenced by the residence time.

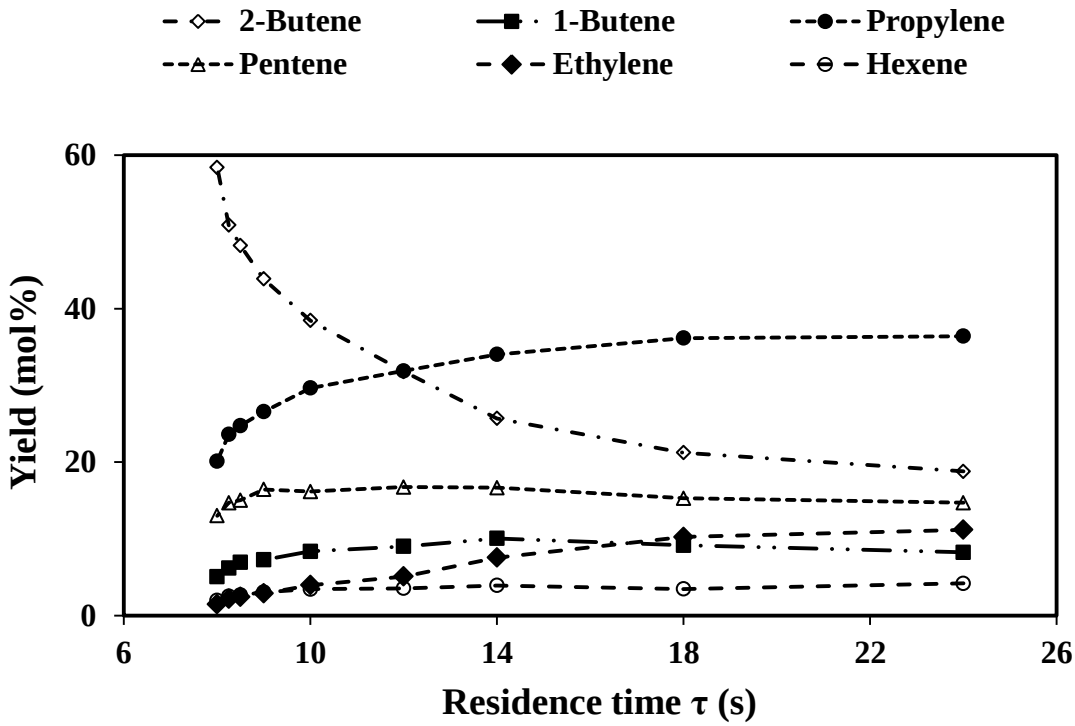

Figure 5.15 Product distribution from 8 to 24s contact time over WO_3-SBA-15(30) catalyst at 550 °C.

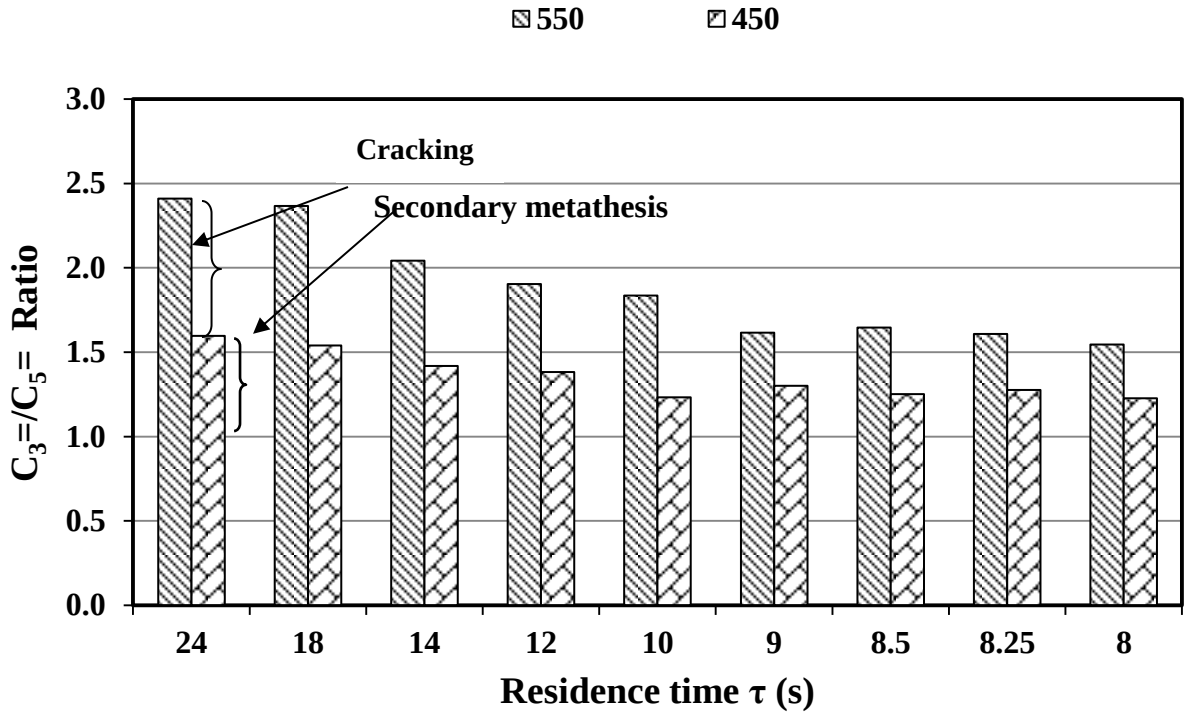

Figure 5.16 Ratio of Propylene to Pentene over WO_3-SBA-15(30) catalyst from 8 to 24s contact time at 450 and 550° C temperature.

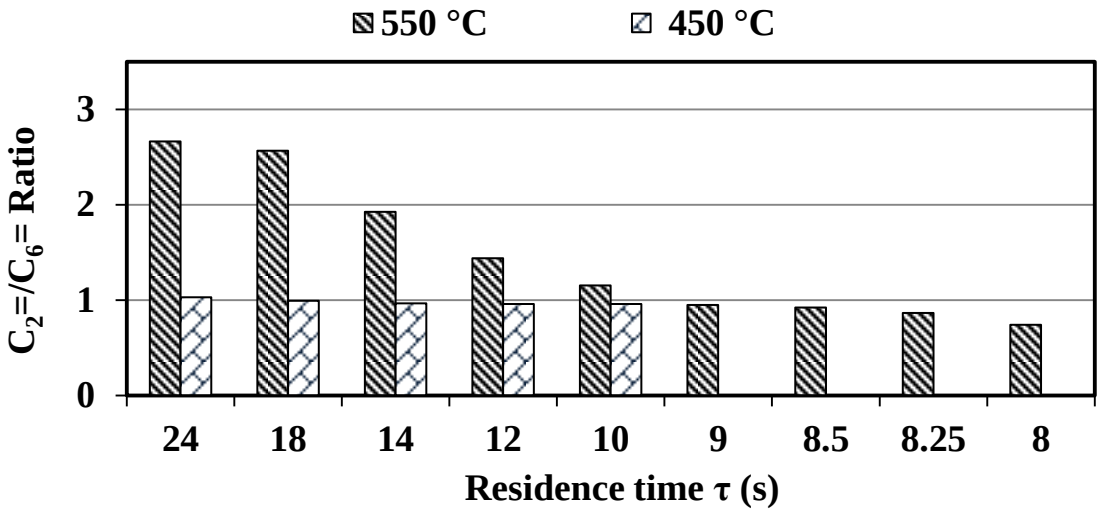

Figure 5.17 Ratio of Ethylene and Hexene to 1-Butene over WO_3-SBA-15(30) catalyst from 8 to 24s contact time at 450 and 550 °C.

5.1.3 Catalytic Stability

The catalytic stability of WO_3-SBA-15(30) catalyst was investigated at 550 ºC for 16 hours of stream. The results are displayed in Figure 5.18. The conversion of 2-butene, yield of propylene and ethylene were initially 81.1%, 37.5 mole% and 12.11 mole % respectively. After 16 hours, catalyst has almost same metathesis activity with 2-butene conversion 80.2 %, propylene yield 35.7 mole% and ethylene yield 10.5 mole% respectively. There was little coke formation after 16 h operation. Furthermore, the opportunity of pore blocking is low due to the large pore diameter and intercrossed connection of the channels.

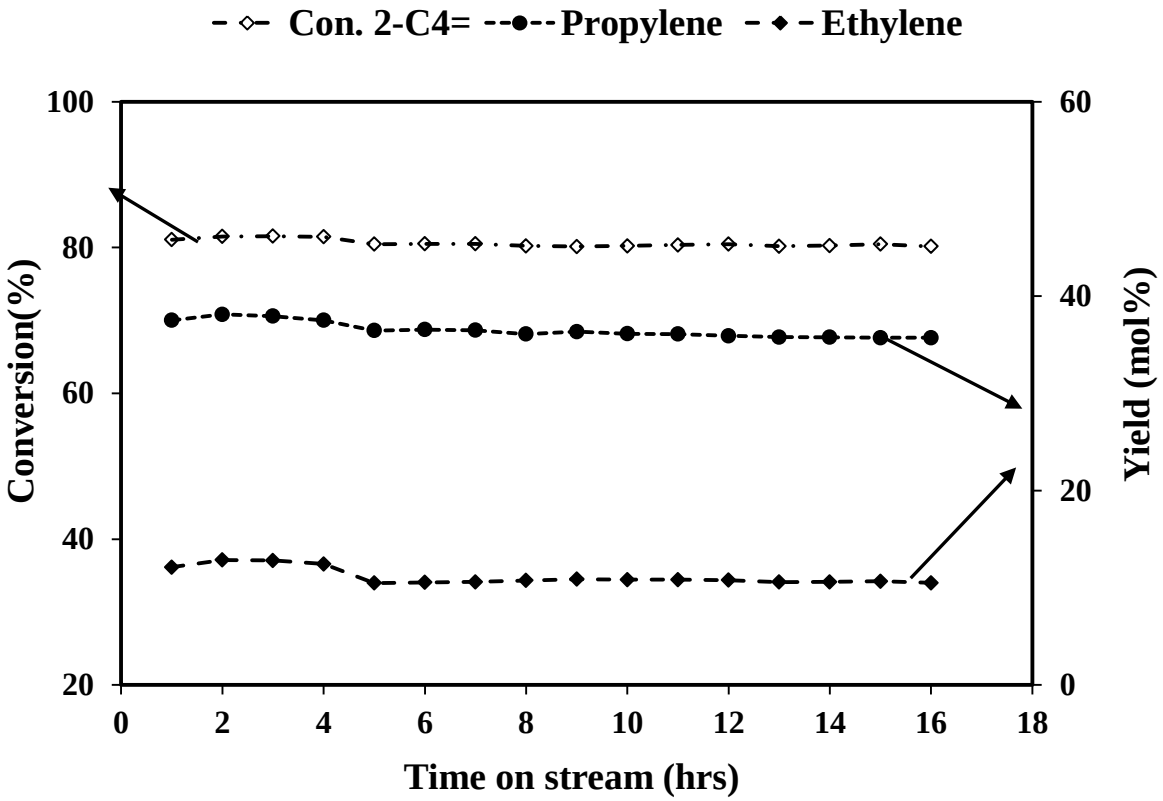

Figure 5.18 Results of 2-butene metathesis reaction over WO_3-SBA-15(30) catalyst at 16 h operation.

Table 5.4 Product distribution (mol%) for metathesis reaction of 2-butene at 350-550 ºC and 8 to 24 s contact time over WO_3-SBA-15 (30) catalyst.

Temp	C. Time	Conv.	2-C4=	1-C4=	C3=	*2-C5=*	C2=	6-C3=
550	24	81.2	18.8	8.2	36.4	14.7	11.2	4.2
	18	78.8	21.2	9.2	36.2	15.3	10.2	3.5
	14	74.3	25.7	10.0	34.0	16.7	7.6	3.9
	12	66.2	31.8	9.0	31.9	16.7	5.1	3.5
	10	61.6	38.4	8.4	29.7	16.2	4.0	3.4
	9	56.1	43.9	7.3	26.6	16.4	2.9	3.0
	8.5	51.8	48.2	6.9	24.8	15.0	2.4	2.7
	8.25	49.1	50.9	6.2	23.6	14.7	2.2	2.5
	8	41.6	58.4	5.1	20.1	13.0	1.5	2.0
500	24	80.6	19.38	7.77	33.83	17.83	9.22	5.48
	18	76.6	23.38	9.24	33.21	18.35	7.51	5.18
	14	72.4	27.61	10.02	31.37	18.36	5.77	4.67
	12	64.0	35.96	8.30	30.02	18.00	4.03	3.69
	10	57.8	42.16	7.77	26.53	17.50	2.75	3.29
	9	44.4	55.60	7.65	19.23	14.15	1.38	1.99
	8.5	42.2	57.85	7.51	18.80	13.99	1.18	1.90
	8.25	38.8	61.22	7.10	17.23	12.95	1.08	1.04
	8	30.6	69.39	4.94	14.16	10.62	0.00	0.88
450	24	72.7	27.29	9.62	29.97	18.77	5.15	5.00
	18	65.0	34.99	12.45	26.14	16.98	3.79	3.82
	14	56.3	43.73	14.67	21.50	15.15	2.43	2.52
	12	53.2	46.79	11.19	21.91	15.84	1.97	2.31
	10	42.2	57.83	13.36	14.83	12.04	0.95	0.99
	9	29.8	70.22	16.29	5.93	4.56	0.00	0.00
	8.5	26.6	73.37	13.08	9.20	7.35	0.00	0.00
	8.25	26.5	73.50	10.13	9.17	7.19	0.00	0.00
	8	18.7	81.34	11.20	4.11	3.35	0.00	0.00
400	24	35.4	64.60	20.90	6.87	4.98	0.39	0.20
	18	32.1	67.92	21.95	5.11	3.74	0.00	0.00
	14	26.6	73.39	23.97	1.99	0.65	0.00	0.00
	12	24.0	76.05	22.84	1.12	0.00	0.00	0.00
	10	21.3	78.72	21.28	0.00	0.00	0.00	0.00
	9	17.9	82.07	17.93	0.00	0.00	0.00	0.00
	8.5	16.4	83.60	16.90	0.96	0.00	0.00	0.00
	8.25	15.5	84.52	15.48	0.00	0.00	0.00	0.00
	8	12.0	88.03	11.97	0.00	0.00	0.00	0.00
350	24	27.5	72.51	20.48	3.26	2.03	0.00	0.00
	18	24.7	75.34	21.23	1.72	0.63	0.00	0.00
	14	22.6	77.45	21.73	0.82	0.00	0.00	0.00
	12	20.0	80.03	19.97	0.00	0.00	0.00	0.00
	10	17.7	82.30	17.70	0.00	0.00	0.00	0.00
	9	15.6	84.36	15.64	0.00	0.00	0.00	0.00
	8.5	14.9	85.12	14.88	0.00	0.00	0.00	0.00
	8.25	13.1	86.92	13.08	0.00	0.00	0.00	0.00
	8	9.5	90.48	9.52	0.00	0.00	0.00	0.00

5.2 Metathesis of 2-butene over WO_3 contained on MCM-41

5.2.1 Physicochemical properties

5.2.1.1 X-ray powder diffraction

The results of low angle powder X-ray diffraction (XRD) patterns for all samples based on MCM-41 are presented in Figure 5.19. The peak at 2θ ranging from 1.5° to 2.5° is indicative of MCM-41 structure. The intense peak at 1.8° is due to [1 0 0] reflection and the weak broad signals between 2.5° and 4° (2θ) are due to [1 1 0], [2 0 0] and [2 1 0] reflections. The d-spacing values of these samples are presented in Table 5.5. These peaks were indexed by Beck et al. [62] for the hexagonal unit. These XRD patterns coincide with the data already reported in the literature [63]. Incorporation of tungsten into the MCM-41 framework resulted in reduction of [1 0 0] reflection intensity for WO_3-MCM-41(30) and WO_3-MCM-41(50) samples due to the change in electron density of the tungsten incorporated materials [63]. In the case of impregnated samples, apart from the reduction in peak intensity, a small shift in the [1 0 0] reflection was also observed. The intensity of the [1 0 0] reflection decreased drastically and the [1 1 0] and [2 0 0] reflections are disappeared completely due to the impregnation of WO_3 oxide. The d spacing values of 4.32 nm and 4.07 nm were observed for WO_3-MCM-41(30) and WO_3-MCM-41(50), respectively. In the case of the WO_3/MCM-41(35), d spacing value was smaller than parent material. Very small peaks at 22-30° (2θ) corresponding to the crystalline phase of WO_3 were observed for the WO_3-MCM-41(30), whereas no peak was

observed for WO_3-MCM-41(50). In the case of impregnated samples, strong peaks of crystalline WO_3 were observed in the range 25° to 35° (2θ). The intensity of crystalline WO_3 peaks was increased with an increase in W loading.

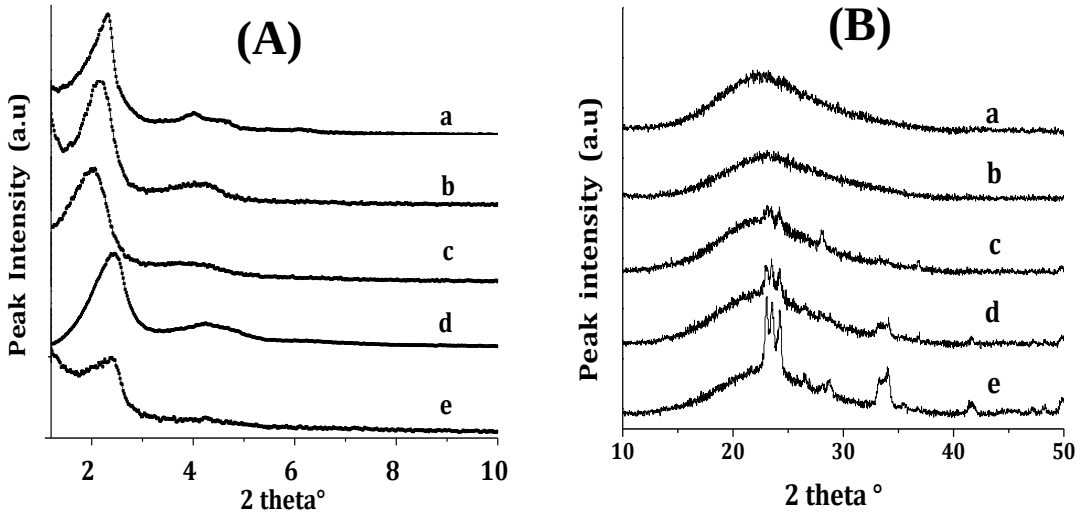

Figure 5.19 XRD patterns of different samples (a) MCM-41, (b) WO_3-MCM-41(50), (c) WO_3-MCM-41(30), (d) WO_3/MCM-41(73) and (e) WO_3/MCM-41(35) at (A) low angle and (B) wide angle.

5.2.1.2 N_2 adsorption isotherm

Table 5.5 summarizes the textural properties of the supports and catalysts calculated from nitrogen adsorption studies. The isotherms of nitrogen adsorption for the calcined MCM-41 materials are shown in Figure 5.20. The isotherm shows three well-defined stages and they coincide with those already reported in the literature [64]. All MCM-41 samples show a typical type IV adsorption isotherm with steps of capillary condensation in the primary mesopores. It is evident from these isotherms that high mesostructural ordering and narrow pore size distribution were attained. The surface areas of the catalysts decreased in the order; WO_3/MCM-41(35) < WO_3-MCM-41(30) < WO_3-MCM-41(50) < Si-MCM-41. The pore volumes also decreased in the same order due to the presence of textural mesoporosity. The surface area of WO_3/MCM-41(35) is lower than that of other catalysts probably due to the sintering of tungsten metal itself and/or tungsten metal and silica support [65].

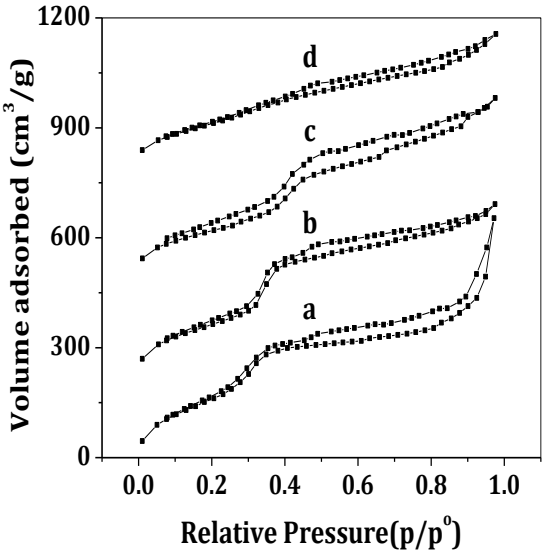

Figure 5.20 N_2 adsorption isotherms of different samples (a) MCM-41, (b) WO_3-MCM-41(50), (c) WO_3-MCM-41(30), (d) WO_3/MCM-41(35).

Table 5.5 Physicochemical properties of WO_3 loaded MCM-41 catalysts.

Samples	$d_{spacing}$ (nm)	% of WO_3 (ICP-AES)	Surface Area (m^2/g)	Pore Diameter (nm)	Total Pore Volume (cc/g)
MCM-41	3.75	-	1056	4.4	1.169
WO_3/MCM-41(35)	3.61	10	419	4.2	0.453
WO_3-MCM-41(30)	4.315	7.43	680	4.9	0.785
WO_3-MCM-41(50)	4.07	4.91	714	4.7	0.82

5.2.1.3 Scanning Electron Microscopy

The SEM images of the MCM-41 samples are shown in Figure 5.21 (A) and (B). It is clear from the images that particles have a distorted sphere shape and agglomerated in a space with a uniform size of 0.3-0.5 μm, smaller than that of the extracted silica (50 μm) about 100 order of magnitude [66,67]. This is because the well-organized assembly of silicate ions reacted with the cationic template in adequate crystallization.

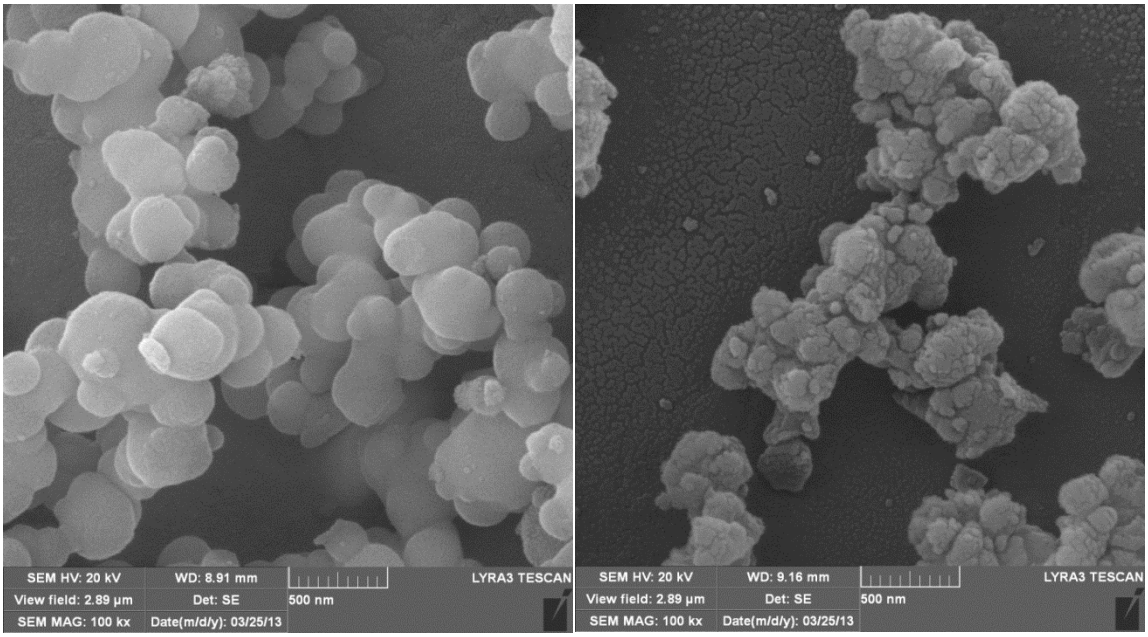

(A) **(B)**

Figure 5.21 SEM images of (A) MCM-41 and (B) WO_3-MCM-41(30)

5.2.1.4 Raman Spectroscopy

Raman spectra of the supports and catalysts are shown in Figure 5.22. For all the catalysts except the support materials, three strong peaks were observed at 265, 707 and 797 cm^{-1}. These crystalline WO_3 peaks were assigned to the symmetric stretching mode of W-O, bending mode of W-O and the deformation mode of W-O-W, respectively [55]. It is obvious that pure silica materials do not possess any peaks in this region. A small peak at 970 cm^{-1} could be assigned to the symmetric stretching mode of the terminal W=O bond of the tetrahedrally coordinated tungsten oxide specie, which are considered as active sites for metathesis reactions [38, 56, 63, 68]. Another peak at about 900 cm^{-1} could be related to the incorporation of the transition metal ions in the silica framework [56]. It is also a typical evidence for the isomorphous substitution of silicon by tungsten in the WO_3-MCM-41 catalysts. High intensity crystalline peaks were observed for the impregnated samples with 10% WO_3 loadings compared to WO_3-MCM-41 framework catalysts. This clearly shows that more octahedral tungsten species were observed in impregnated samples due to poor dispersion of tungsten oxides. On the other hand, WO_3-MCM-41 materials shows less intense crystalline peaks with tetrahedrally coordinated tungsten species.

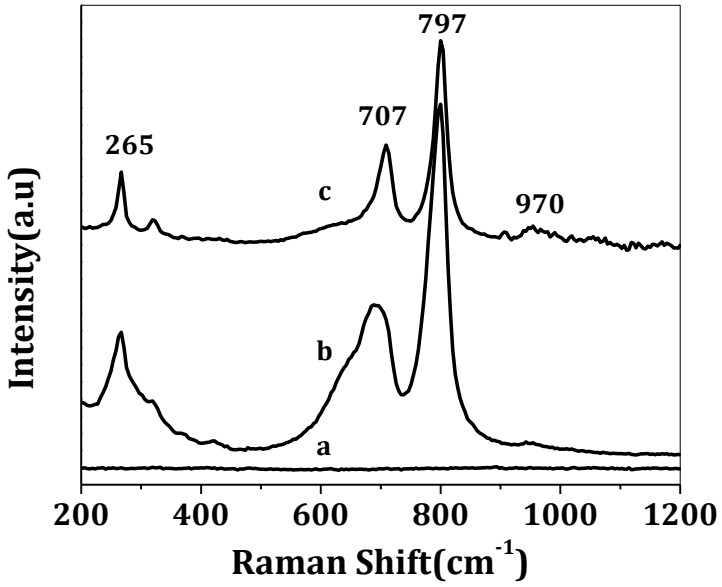

Figure 5.22 Raman spectra of different samples (a) MCM-41, (b) WO_3/MCM-41(35) and (c) WO_3-MCM-41(30)

5.2.1.5 UV vis DRS

Diffuse reflectance spectra of tungsten supported samples in the region of 200-600 nm are shown in Figure 5.23. This method is very sensitive for distinguishing the species between incorporated metal and extra-framework metal oxides in different heteroatmic mesostructures. The spectrum of sodium tungstate presents a spinel structure at 230 nm which mainly implies the presence of ligand to metal charge transfer involving isolated transition metal sites and considered a direct proof for the presence of framework tungsten oxide species in tetrahedral co-ordination [63]. This band was not observed in case of pure MCM-41. The WO_3-MCM-41(30) exhibit a similar band at 230 nm, which could be attributed to the presence of isolated $[WO_4]^{2-}$ tetrahedral species in the catalysts. On the other hand, the spectra of impregnated sample, WO_3/MCM-41(35) have a less intense band at 230 nm, indicating small concentration tetrahedral tungsten oxide species. The second band at 263 nm may be attributed to isolated tungsten species or low-condensed oligomeric tungsten oxide species. For ammonium metatungstate, a broad band at 350-400 nm is observed showing mainly crystalline tungsten oxide species present in the sample. The peak at 375 nm was observed for WO_3/SBA-15(35), WO_3/MCM-41(35) and WO_3-SBA-15(30) catalysts shows the presence of crystalline tungsten oxide species. This band was not observed for WO_3-MCM-41(30) catalyst shows more tetrahedral tungsten species present in the catalyst.

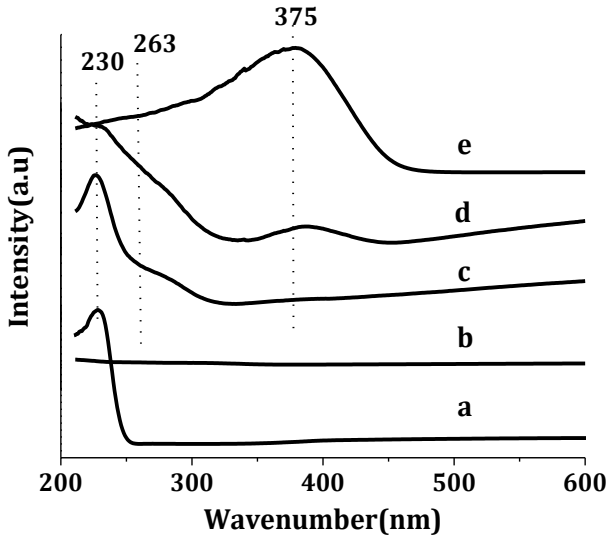

Figure 5.23 UV-vis diffuse reflectance spectra of various samples (a) $Na_2.WO_4.2H_20$, (b) MCM-41, (c) WO_3-MCM-41(30), (d) WO_3/MCM-41(35), (e) ammonium metatungstate.

5.2.1.6 Temperature programmed desorption of ammonia

NH_3 TPD patterns for the supports and catalysts are shown in Figure 5.24 and the total acidity results are presented in Table 5.6. After Gaussian de-convolution, the peaks corresponding to weak (100–300°C) and medium (300–500°C) sites were obtained. As shown in Figure 5.24, a week ammonia desorption peak was observed at 140 °C for MCM-41. With increasing tungsten amount in the framework, the intensity of ammonia desorption peak at 140 °C was increased along with some medium acid site peaks observed above 350-400 °C. In case of impregnated samples, the presence of WO_3 on the external surface of the catalyst was observed and it creates Lewis acid centers of bulky WO_3 as reported in literature [55]. Impregnated samples have very small amount of tungsten species deposited on the inner surface of the pores. However, higher acidity of W-MCM-41(30) due to the presence of more Si-O-W bonds leading to high dispersion of tungsten species as observed in XRD.

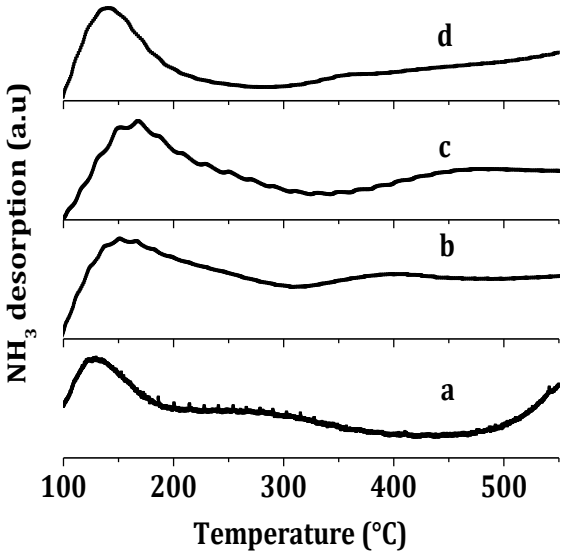

Figure 5.24 NH_3-TPD profiles of different samples (a) MCM-41, (b) WO_3-MCM-41(50), (c) WO_3-MCM-41(30), (d) WO_3/MCM-41(35).

5.2.1.7 Pyridine adsorption by FT-IR

Pyridine adsorption measured by IR spectroscopy was carried out to evaluate the strength and types of acid sites present in the tungsten impregnated and framework samples. Figure 5.25 shows the FT-IR spectra of the all the catalysts recorded after the adsorption of pyridine and subsequent evacuation at 150 °C. The Py-FT-IR spectrum recorded after adsorption of pyridine at room temperature on the pure MCM-41 shows two major peaks at 1595 and 1445 cm^{-1}, ascribed to pyridine coordinately bonded to weak surface Lewis acid sites. These peaks disappeared after outgassing at 450 °C. In case of WO_3-MCM-41 samples three additional peaks at 1485, 1545, and 1635 cm^{-1} were also observed due to protonated pyridine bonded to surface Brønsted acid sites, indicating the presence of tungsten-incorporated species [56, 59]. The intensities of all of these bands were decreased after outgassing at 350 °C. This observation was indicated that both type of acid sites are rather strong and are related to tungsten oxide incorporation. Similar spectra are recorded for tungsten impregnated samples of MCM-41, the number of the Lewis and Brønsted acid sites decreased after outgassing at 250 °C, as presented in Figure 5.26. The amount of Lewis and Brønsted acid sites was higher for WO_3-MCM-41(30) as compared to WO_3-MCM-41(50) due to increase in the tetrahedrally co-ordinated tungsten oxide species **(**Table 5.6**)**. This observation is a good evidence for better catalytic activity of WO_3-MCM-41(30) compared to WO_3-MCM-41(50). It can be concluded that the presence of Brønsted acid sites in the tungsten containing MCM-41 samples are related to the presence of tetrahedrally co-ordinated tungsten oxide species.

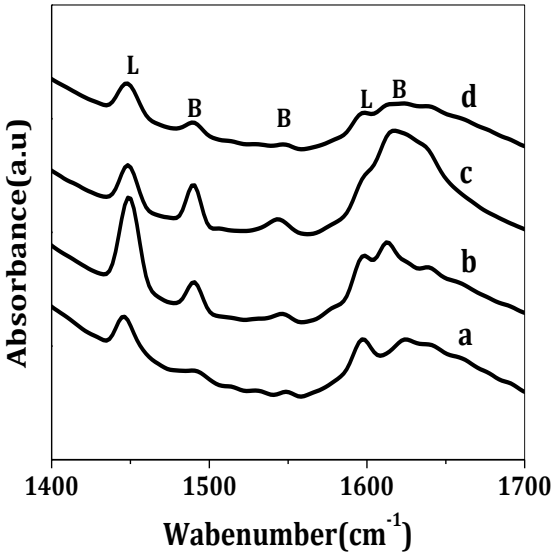

Figure 5.25 FT-IR spectra of pyridine adsorbed on different samples at 150 °C, MCM-41 based catalysts (a) MCM-41, (b) WO_3-MCM-41(50), (c) WO_3-MCM-41(30) and (d) WO_3/MCM-41(35).

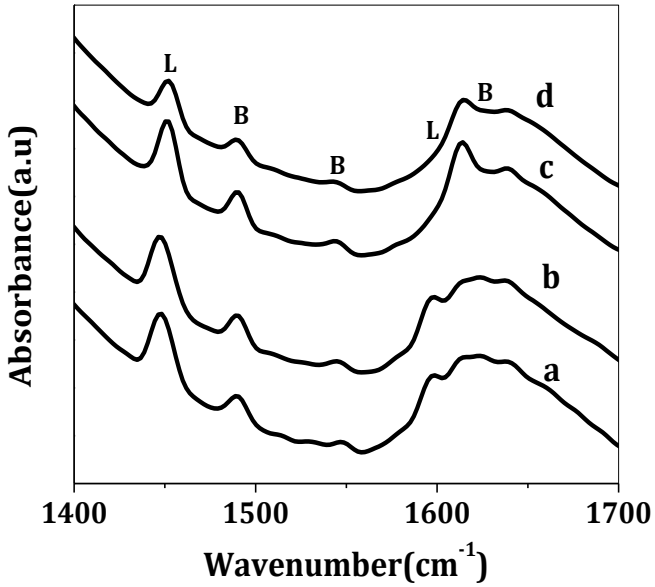

Figure 5.26 FTIR spectra of pyridine adsorbed on the sample recorded at different temperature (a) WO_3-MCM-41(30) at 150 °C, (b) WO_3-MCM-41 (30) at 250 °C, (c) WO_3/MCM-41(35) at 150°C and (d) WO_3/MCM-41(35) at 250°C.

Table 5.6 Acid sites characteristics of tungsten incorporated and impregnated MCM-41 catalysts.

Samples	NH_3 TPD($mmolg^{-1}$)*			FT-IR chemisorbed pyridine ($mmolg^{-1}$)			
	TA	L.T <300°C	H.T 300-550°C	B 150°C	L 150°C	B 250°C	L 250°C
MCM-41	0.039	0.039	0.00	0.0233	0.3611	0.0033	0.1155
WO_3/MCM-41(35)	0.160	0.080	0.080	0.0318	0.1889	0.0205	0.0709
WO_3-MCM-41(30)	0.391	0.210	0.181	0.1527	0.2581	0.0484	0.1685
WO_3-MCM-41(50)	0.325	0.140	0.185	0.0608	0.2410	0.0241	0.1036

Calculated from the areas of Gaussian deconvolution bands; TA = total acidity; L.T = low temperature; H.T = high temperature; B = Bronsted acidity; L = Lewis acidity.

5.2.2 Catalytic activity on MCM-41

5.2.2.1 Effect of synthesis method

The MCM-41 supported tungsten oxide catalysts were also prepared following two different methods. In first case, tungsten was impregnated using wet incipient impregnation method, whereas in second case, tungsten was incorporated into the framework of mesoporous MCM-41 support using hydrothermal crystallization procedure. The catalytic activity of MCM-41 supported tungsten oxide catalysts for 2-butene metathesis at 550 °C are presented in Figure 5.27 and Table 5.7. A significant increase in conversion of 2-butene was observed after incorporation of tungsten oxide into MCM-41. The catalytic conversion of butene was increased with an increase in the amount of tungsten oxide in both types of catalysts. The WO_3-MCM-41(30) exhibited the highest conversion of 86.7%. Pure MCM-41 exhibited 5 and 2 mole % yield of propylene and ethylene, respectively, whereas WO_3-MCM-41(30) depicted highest yield of 36.3 and 16.5 mole % of propylene and ethylene, respectively. It was noticed that $C3^{=}/C5^{=}$ ratio was greater than 1.5 over all four catalysts. The higher activity of WO_3-MCM-41(30) compared to other catalysts could be related to its higher acidity as well as larger amount of tetrahedrally co-ordinated tungsten species as observed from Pyridine-FT-IR, XRD and Raman spectroscopy. The lower activity of impregnated MCM-41 samples was probably due to less availability of tetrahedral tungsten species and higher intensity of extra framework octahedral WO_3 species.

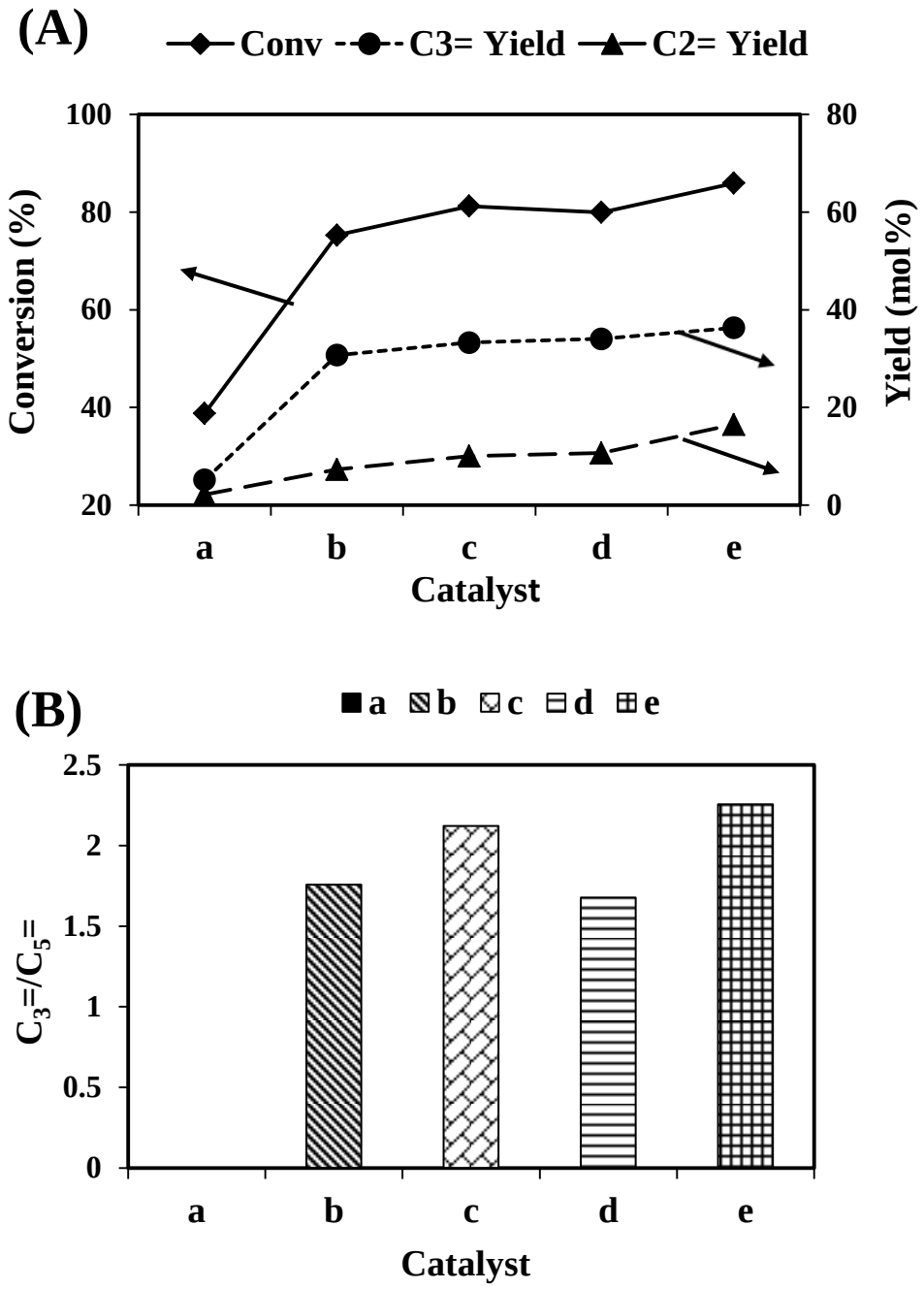

Figure 5.27 Results of metathesis reaction of 2-butene over (a)MCM-41, (b)WO_3/MCM-41(73), (c) WO_3/MCM-41(35), (d)WO_3-MCM-41(50), (e) WO_3-MCM-41(30) catalysts at 2h (A) conversion of 2-butene, propylene yield (mole %), ethylene yield (mole %) and (B) ratio of propylene to pentene (reaction temperature: 550 °C, pressure: 1 atm, GHSV:900 h^{-1}).

5.2.2.2 Effect of WO_3 loading

In wet impregnation method, four catalysts were synthesized changing the loading 5,10,15 and 20 wt% WO_3 supported on MCM-41. Figure 5.28 shows catalytic performances of these catalysts. Conversion of 2-butene increased up to 10 wt% of WO_3 loading and then decreased at 15 and 20 wt % loading. Propylene and ethylene yield showed same trend of catalytic performances. In direct hydrothermal method, three catalysts were synthesized changing the Si/W ratio 10, 30 and 50. Figure 5.29 shows the catalytic performances of these three catalysts. Conversion of 2-butene and ethylene and propylene yield increased up to Si/W ratio 30. After that, with the increase of tungsten amount the catalytic performance decreased steadily. WO_3-MCM-41 (30) shows the best catalytic performance among the catalyst synthesized by hydrothermal method. However, 10 wt% WO_3 loading shows the best catalytic performances among the impregnated catalyst.

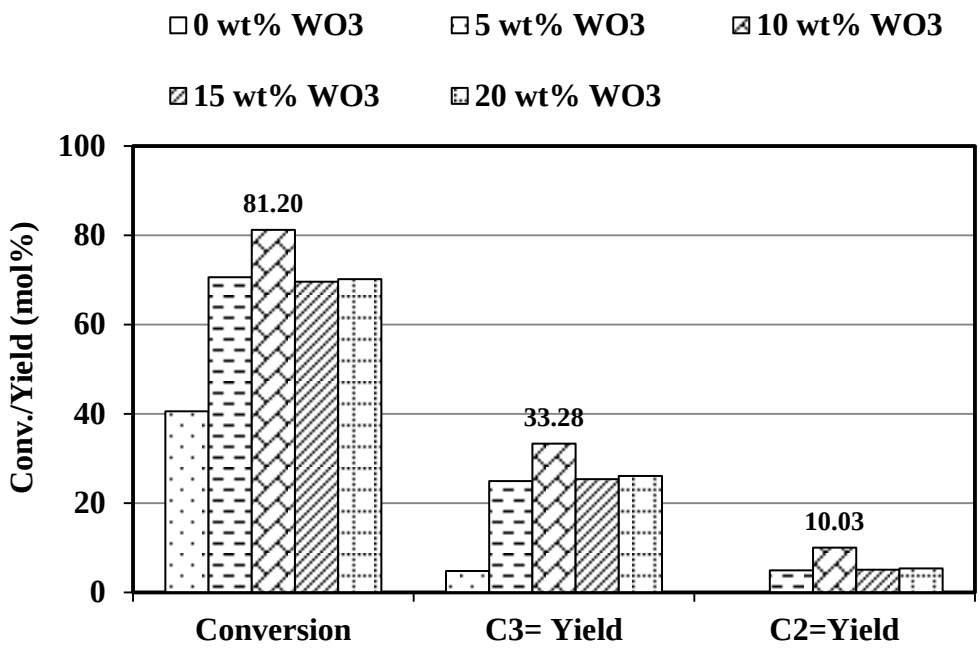

Figure 5.28 Conversion of 2-butene, Propylene yield (mol %), ethylene yield (mol %) of 2-butene metathesis reaction over 5,10,15 and 20 wt% WO_3 catalysts supported on MCM-41 at 2hr.

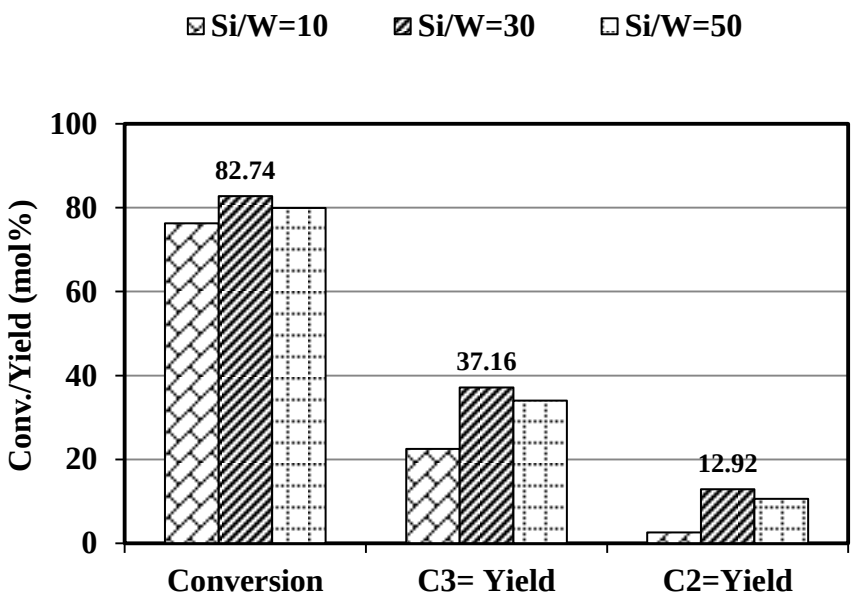

Figure 5.29 Conversion of 2-butene, Propylene yield (mol %), ethylene yield (mol %) of 2-butene metathesis reaction over WO_3-MCM-41 catalyst with Si/W ratio (10, 30 and 60) at 550 ° C 2hr run.

Table 5.7 Product distribution (mole %) for metathesis reaction of 2-butene at 550 ºC over tungsten in the frame work and impregnated MCM-41 catalysts.

Time (hrs)	Conv.	C2=	C3=	1-C4=	*i*-C4=	*2*-C4=	C5=	C6+
MCM-41 1hr	38.8	2.1	5.2	25.2	5.1	61.1	0.3	0.9
2	40.5	1.8	4.8	27.4	5.3	59.5	0.3	0.8
3	40.1	1.6	4.3	28.2	5.3	59.9	0.3	0.4
4	39.7	1.4	3.9	28.6	5.2	60.0	0.3	0.3
5	39.1	1.2	3.5	29.0	5.1	60.0	0.3	0.0
WO_3/MCM-41(73)1hr	70.6	4.9	24.9	14	7.2	29.4	17.1	2.5
2	75.3	7.3	30.7	11.7	8.1	24.7	17.5	0
3	74.7	6.3	28.5	12	6	25.3	20.1	1.7
4	75.4	6.5	29	11.7	5.4	24.6	21.2	1.5
5	75.4	6.5	29.1	11.7	5	24.6	21.6	1.6
WO_3/MCM-41(35)1hr	81.7	11	34.1	8.6	12.5	18.4	12.5	1.9
2	81.2	10	33.3	8.8	10.8	18.7	15.7	2.1
3	80.7	9.3	32.4	9.1	9.8	19.3	17.1	2.6
4	80.7	9.2	32.2	9.1	9	19.3	18.5	2.7
5	80.2	8.8	31.8	9.4	8.5	19.8	19.2	2.5
W-MCM-41(50) 1hr	74.3	9.8	31.7	8.1	3.4	25.7	20.4	0.9
2	79.9	10.7	34	8.5	3.5	20.0	20.3	1.5
3	81.1	10.9	34.3	8.4	3.4	18.8	20.6	1.8
4	81.1	11.2	35.2	8.6	3.4	18.8	19.7	1.3
5	81.9	10.9	34.3	8.4	3.2	18.1	21.5	2.1
W-MCM-41(30) 1hr	86.7	18.7	38.9	6.2	8.4	13.2	13.7	0.9
2	85.9	16.5	36.3	6.5	7.1	14.1	16.1	1.8
3	85.0	14.7	34.9	6.9	6.1	15	18.5	2.3
4	84.6	14.5	34.9	7.1	5.7	15.4	18.4	2.4
5	84.2	14.2	34.8	7.2	5.3	15.7	18.5	2.5

5.2.2.3 Effect of reaction temperature

We investigated the influence of reaction temperature on 2-butene metathesis reaction at five different temperatures from 350-550 °C and at constant 900 GHSV over tungsten based MCM-41 catalysts. WO_3-MCM-41 catalyst shows the same trend of temperature effect like WO_3-SBA-15 (30). The effect of reaction temperature on activity is shown in Figure 5.30. When the temperature was 350 °C, the 2-butene conversion was only 27.2 %. With the increment of reaction temperature, the conversion increased to 37.2, 75.5, 77.7 and 82.2 % at 400,450,500 and 550 °C respectively. At lower reaction temperature at 350 °C and 400 °C, the selectivity's of 1-butene were 75.2 and 54.5 mole%. Thereafter, when the temperature reached at 450 °C, 1-butene selectivity dropped rapidly at 11.9 mole% and at 550 °C it decreased to 10.0 mole%. The selectivity's of propylene was only 12.3 and 21.6 mole% at 350 °C and 400°C respectively and increased to 43.7, 44.6 and 46.2 mole% at 450, 500 and 550° C respectively. The selectivity of pentene followed the same trend like propylene. From the activity of 2-butene conversion, 1-butene selectivity, propylene, pentene selectivity, it is evident that 2-butene was first isomerized to 1-butene at lower temperature range at 350 °C and 400°C. Thereafter, 2-butene and 1-butene was involved in a cross metathesis reaction resulting in the formation of propylene and 2-pentene. At lower temperature range at 350 and 400 °C, ethylene and 3-hexene selectivity's were negligible that suggests 1-butene is not going for self-metathesis under lower reaction temperature. At the higher temperatures of 500 and 550 °C, 2-pentene was involved in cracking resulting ethylene and propylene. From the Figure 5.31, it was noticed that the ratios of $C_3=/C_5=$ and $C_2=/C_6=$ were increased with the increase of temperature. At 450 °C $C_3=/C_5=$ ratio was 1.87 which increased to

2.2 and 2.8 at 500 and 550 °C. At the same way, $C_2=/C_6=$ ratio was 1.08 which increased to 2.5 and 5.2 at 500 and 550 ° C. Self-metathesis and secondary cross metathesis of ethylene and hexene have the same influence in the temperature range of 450-550 °C.

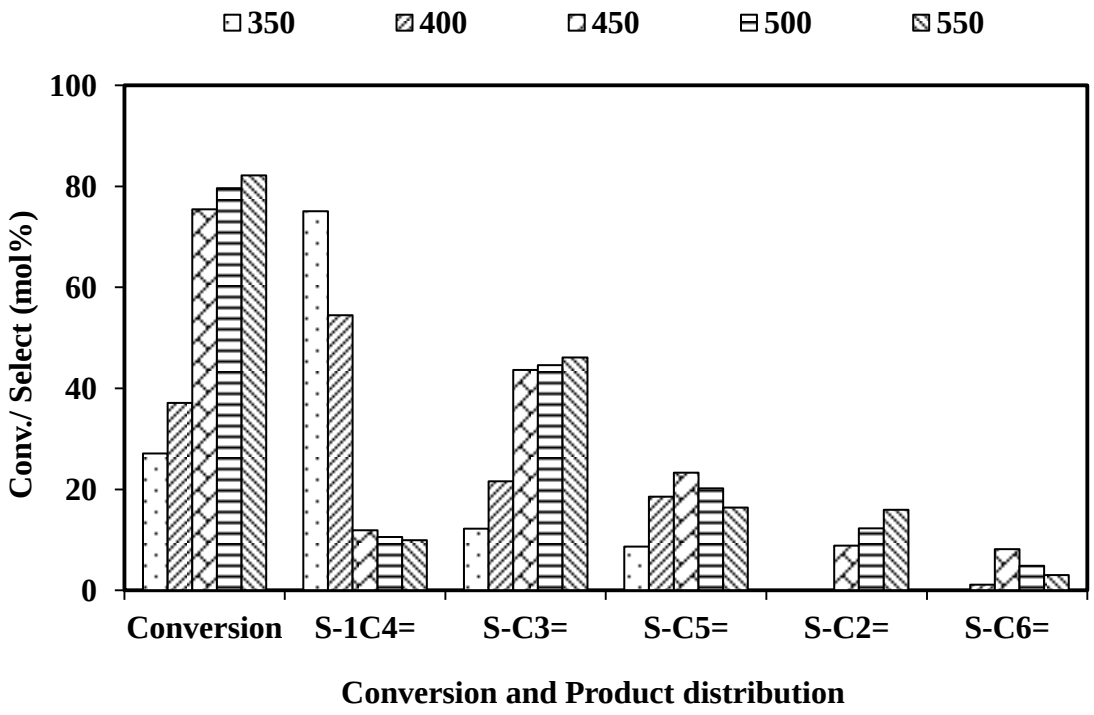

Figure 5.30 2-Butene Conversion and Selectivity of product over WO_3-MCM-41(30) catalyst from 350-550 ° C temperature at 24s contact time.

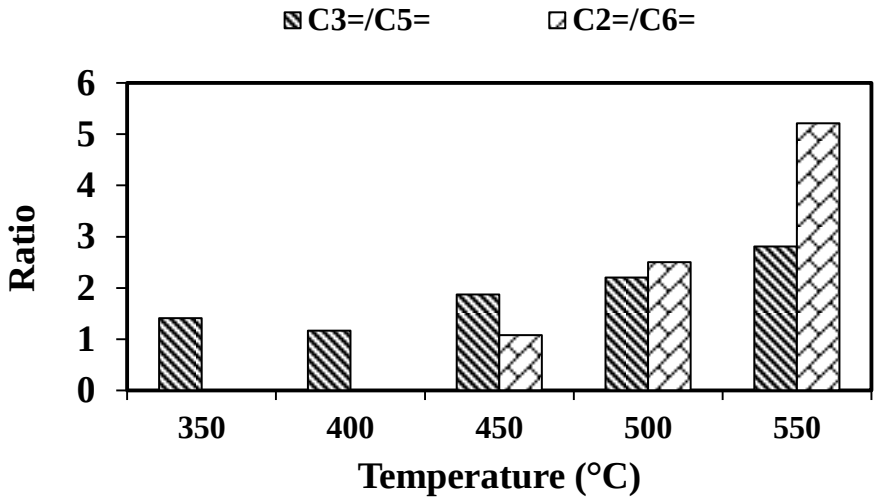

Figure 5.31 Ratio of Propylene to Pentene over WO_3-MCM-41 (30) catalyst from 350-550 °C.

5.2.2.5 Effect of residence time

The activity of catalyst is significantly depending on the contact time of reaction. We studied the effect of contact time verifying form 24s to 8s at 350-550 °C atmospheric pressure. Experimental results of 550 °C are shown in Figure 5.32. With the increasing of contact time, reactant 2-butene yield decreased from 42.8 to 17.8 mole% at 8 to 24s contact time. However, propylene yield was increasing with the increase of contact time. The same sequence was following to other products also. The involvement of secondary cross metathesis of ethylene and 2-butene and cracking of 2-pentene could be explained by the contact time influence. Figure 5.33 shows, at 550°C 24s contact time the ratio of $C_3=/C_5=$ was 2.8 which decreased to 1.8 at 8s contact time. At 450° C 24s contact time $C_3=/C_5=$ ratio was 1.8 which decrease to 1.2 at 8s contact time. Contact time influenced more on cracking reaction than the secondary metathesis of ethylene and 2-butene reaction. From Figure 5.34, it was evident that contact time is influencing the self-metathesis of 1-butene reaction. At 550 °C, 24s contact the ratio of $C_2=/C_6=$ was 2.9 which decreased to 0.7 at 8s contact time. Same phenomena are going on 450°C also.

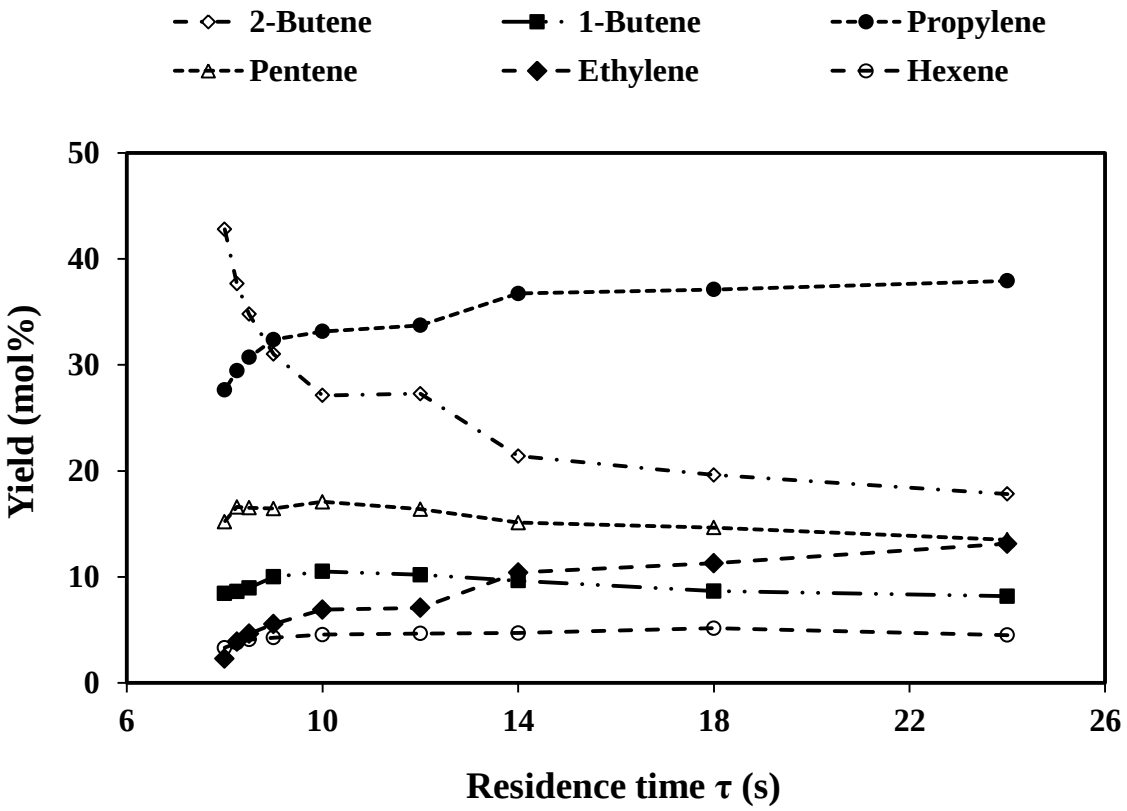

Figure 5.32 Product distribution from 8 to 24s contact time over WO_3-MCM-41(30) catalyst at 550 °C.

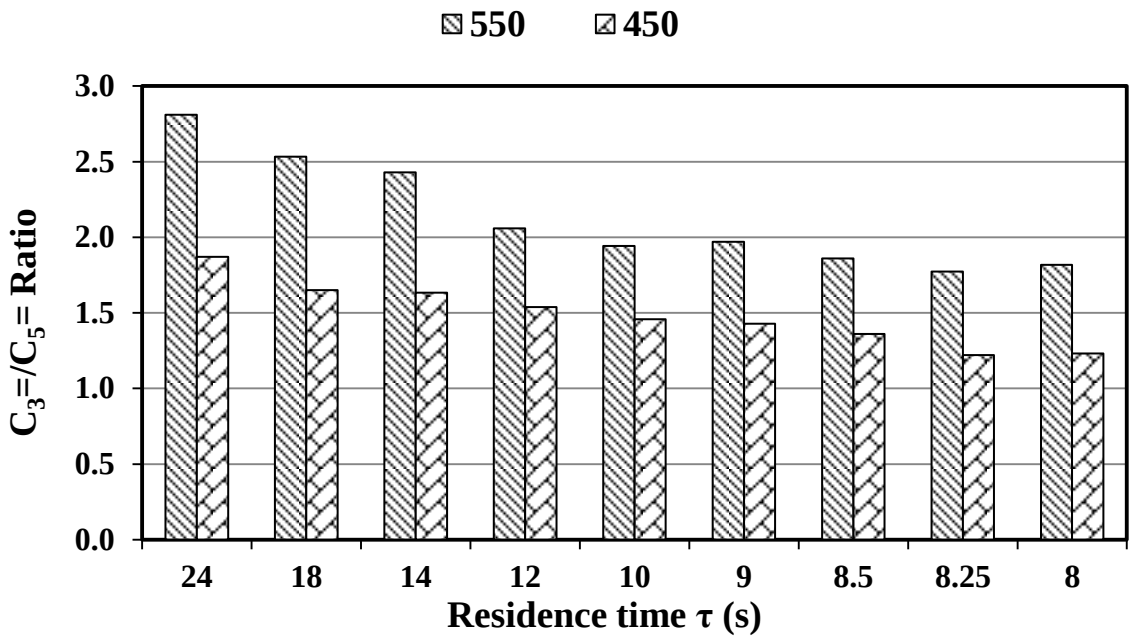

Figure 5.33 Ratio of Propylene to Pentene over WO_3-MCM-41(30) catalyst from 8 to 24s contact time at 450 and 550° C temperature.

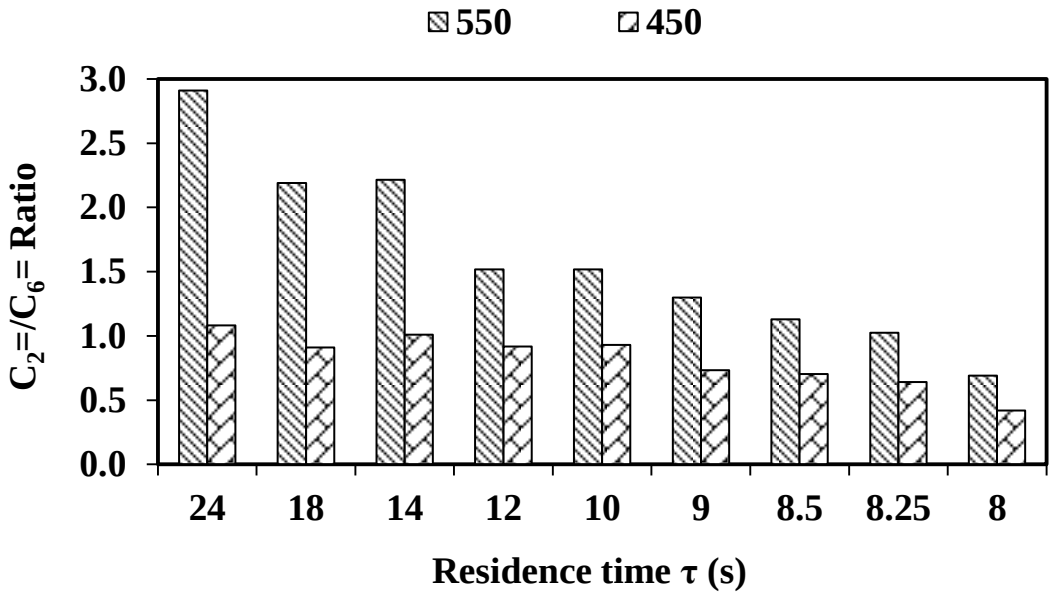

Figure 5.34 Ratio of Ethylene to Hexene over WO_3-MCM-41(30) catalyst from 8 to 24s contact time at 450 and 550° C temperature.

5.2.3 Catalytic Stability

Figure 5.35 shows the metathesis activity of WO_3-MCM-41(30) catalysts at 550 ℃ for 16 hours of stream. The conversion of 2-butene, yield of propylene and ethylene were initially 83.0%, 37.2 and 13.0 mole % respectively. After 16 hours, catalyst has almost same metathesis activity of 2-butene conversion 81.4 %, propylene yield 36.8 mole% and ethylene yield 11.8 mole%. There was no coke formation after 16 hrs of 2-butene stream.

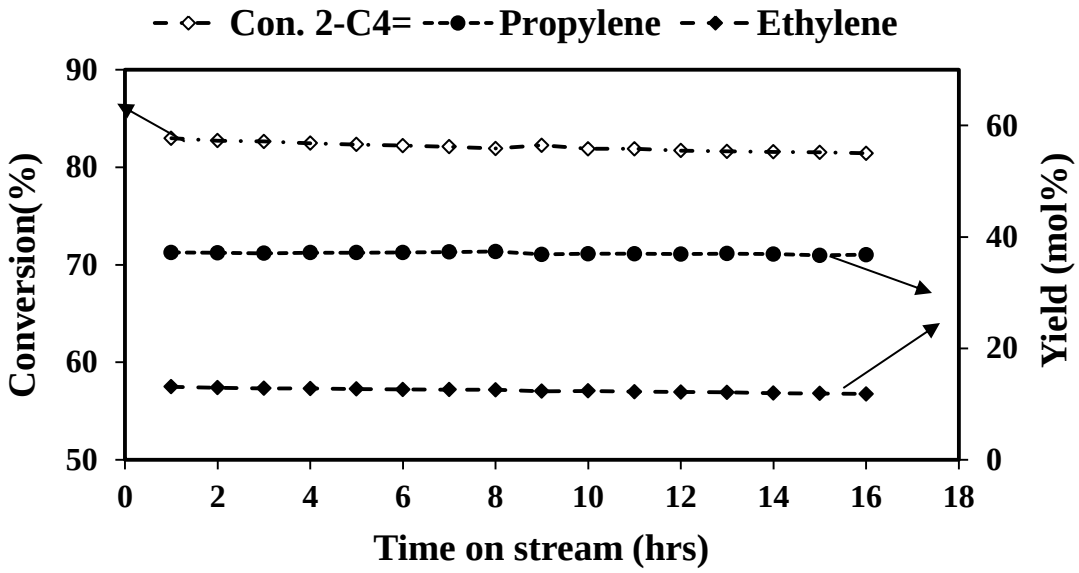

Figure 5.35 Results of 2-butene metathesis reaction over WO_3-MCM-41(30) catalyst at 16 h operation.

Table 5.8 Product distribution (mol%) for metathesis reaction of 2-butene at 350-550 ºC and 8 to 24 s contact time over WO_3-MCM-41 (30) catalyst.

Temp	C. Time	Conv.	2-C4=	1-C4=	C3=	*2-C5=*	C2=	6-C3=
550	24	82.2	17.8	8.2	37.9	13.5	13.1	4.5
	18	80.4	19.6	8.7	37.1	14.7	11.3	5.2
	14	78.6	21.4	9.6	36.7	15.1	10.4	4.7
	12	72.7	27.3	10.2	33.7	16.4	7.1	4.7
	10	72.9	27.1	10.5	33.2	17.1	6.9	4.6
	9	69.0	31.0	10.0	32.4	16.4	5.6	4.3
	8.5	65.2	34.8	9.0	30.7	16.5	4.6	4.1
	8.25	62.3	37.7	8.6	29.5	16.6	3.9	3.8
	8	57.2	42.8	8.5	27.6	15.2	2.3	3.3
500	24	79.7	20.3	8.5	35.5	16.1	9.8	3.90
	18	78.5	21.5	8.5	34.6	16.8	8.7	6.05
	14	75.9	24.2	9.3	33.3	16.6	8.2	5.82
	12	69.9	30.1	10.0	31.5	17.4	5.5	4.87
	10	70.3	29.7	10.2	30.9	17.9	5.5	5.21
	9	66.9	33.1	9.5	30.0	17.6	4.3	4.53
	8.5	62.4	37.6	8.5	28.2	17.0	3.5	4.58
	8.25	58.9	41.2	8.2	26.4	16.8	3.1	4.42
	8	56.6	43.5	8.4	25.5	16.1	1.9	4.07
450	24	75.5	24.5	9.0	33.0	17.6	6.7	6.2
	18	69.3	30.7	10.7	29.3	17.8	5.5	6.1
	14	69.6	30.4	10.1	29.0	17.7	5.5	5.4
	12	60.0	40.0	12.0	25.3	16.4	3.0	3.3
	10	60.2	39.8	12.4	25.0	17.1	2.7	3.0
	9	55.1	44.9	12.2	22.3	15.6	2.1	2.9
	8.5	49.0	51.0	11.9	19.2	14.1	1.9	2.7
	8.25	47.4	52.6	10.5	18.0	14.8	1.6	2.4
	8	43.4	56.6	10.5	16.3	13.3	1.0	2.4
400	24	38.1	61.9	20.2	9.1	6.9	0.0	0.4
	18	36.9	63.1	19.6	8.5	7.1	0.0	0.3
	14	36.7	63.3	20.9	7.3	7.7	0.0	0.8
	12	29.7	70.3	21.5	4.7	3.4	0.0	0.0
	10	28.6	71.5	22.6	3.5	2.5	0.0	0.0
	9	26.6	73.5	22.1	2.5	2.0	0.0	0.0
	8.5	23.8	76.2	21.0	1.9	1.0	0.0	0.0
	8.25	22.3	77.7	19.9	1.5	0.9	0.0	0.0
	8	22.2	77.8	20.3	1.1	0.8	0.0	0.0
350	24	27.1	72.9	20.4	3.3	2.4	0.0	0.0
	18	23.5	76.5	20.5	1.3	0.4	0.0	0.0
	14	22.7	77.3	21.8	0.9	0.0	0.0	0.0
	12	21.5	78.6	21.5	0.0	0.0	0.0	0.0
	10	21.7	78.3	21.7	0.0	0.0	0.0	0.0
	9	21.0	79.0	21.0	0.0	0.0	0.0	0.0
	8.5	19.3	80.7	19.3	0.0	0.0	0.0	0.0
	8.25	19.1	81.0	19.1	0.0	0.0	0.0	0.0
	8	20.7	79.3	20.7	0.0	0.0	0.0	0.0

CHAPTER 6

KINETIC MODELING

6.1 Reactions for 2-Butene metathesis over WO_3-SBA-15 (30) catalyst

In this section, a comprehensive kinetic model for metathesis of 2-butene over W-based mesoporous SBA-15 catalysts was developed by applying power law. Following reactions are involved for the production of propylene and other side products during 2-butene metathesis reaction.

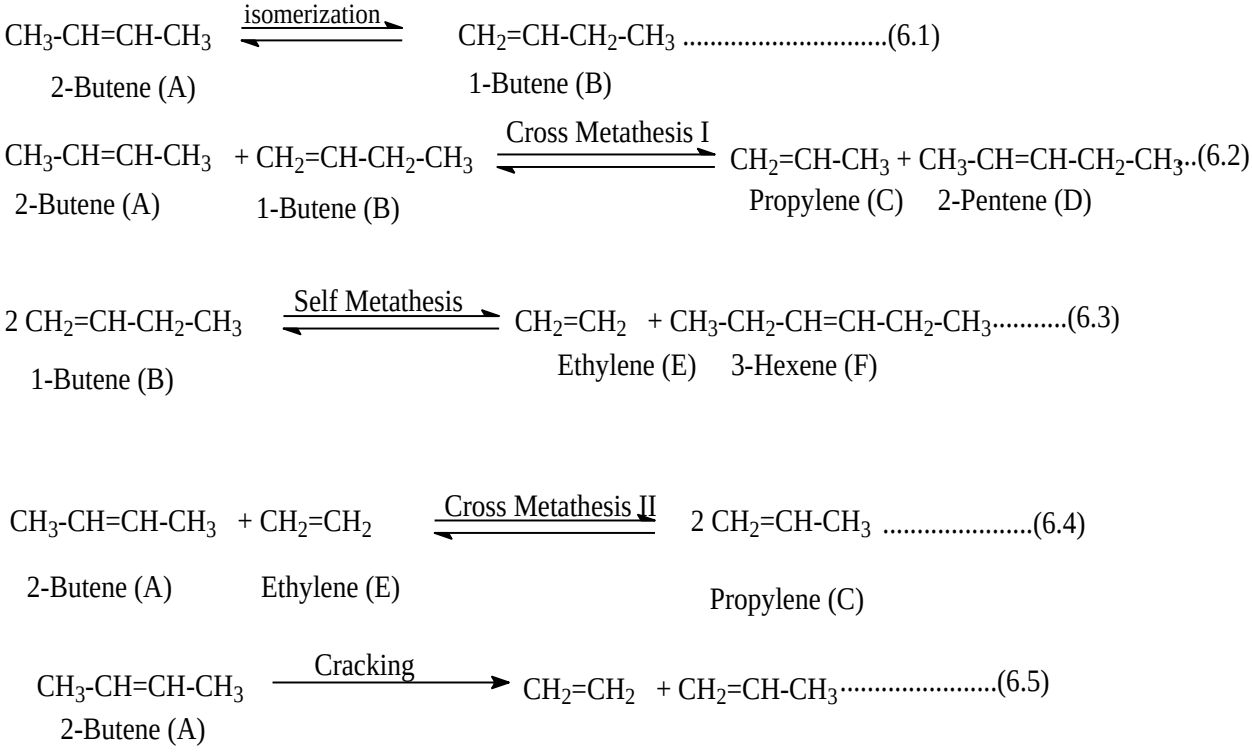

6.2 Proposed scheme for model development

Base on the discussion of previous chapter during the metathesis of 2-butene over WO_3-SBA-15(30) catalyst one can consider Scheme 2 for the possible reaction pathways. In this scheme all the pentene isomers lumped as C_5= while hexane isomers combined as C_6=. According to Scheme 2, the desired product, propylene is produced via three alternative routes: (i) cross metathesis of 1-butene and 2-butene, (ii) secondary metathesis of ethylene and 2-butene and (iii) by cracking of 2-butene. Due to low concentration of ethylene (by product) the secondary metathesis as source of propylene is considered to be negligible. Although the contributions of each of the pathways widely depend on the characteristics of the catalysts material, it is important to recognize that the 1-butene required in cross metathesis comes via the isomerization of 2-butene. On the other hand, 1-butene also undergoes self- metathesis to form ethylene and 3-hexene. An excessive isomerization of 2-butene will promote the 1-butene self-metathesis. Therefore, a balance of 2-butene isomerization is crucial here to maximize propylene production by cross metathesis and to minimize side products.

It is well known that metathesis performances of W- based catalyst are influenced by nature of supports. From BET surface area measurement it is found that catalyst WO_3-SBA-15(30) has high surface area creates more chance of presence active sites. At the same time, high pore diameter allows high diffusion rate of reactant 2-butene into the pore of catalyst [51]. Based on XRD results, it is clear that catalyst WO_3-SBA-15 (30) has low amount of crystallite WO_3. The tungsten oxide species present into the catalyst is

highly dispersed into the SBA-15 surface and account for the activity of metathesis [50]. Furthermore, Raman spectroscopy and UV-vis DRS experiments reveal that this catalyst has more tetrahedral coordinated tungsten oxide species which works as an active site of the catalyst for metathesis reaction [38, 69]. The FTIR pyridine adsorption experiment confirms the presence of Brønsted and Lewis acid sites on incorporating tungsten oxide species into the SBA-15 materials, enhancing the metathesis performance [56]. On the other hand, a weak acid site by the Si–OH group of SBA-15 worked as an active site in the positional isomerisation of 2-butene to 1-butene [70]. Brønsted acid sites of the catalyst WO_3-SBA-15(30) enhances the cracking of 2-butene at higher temperature [71].

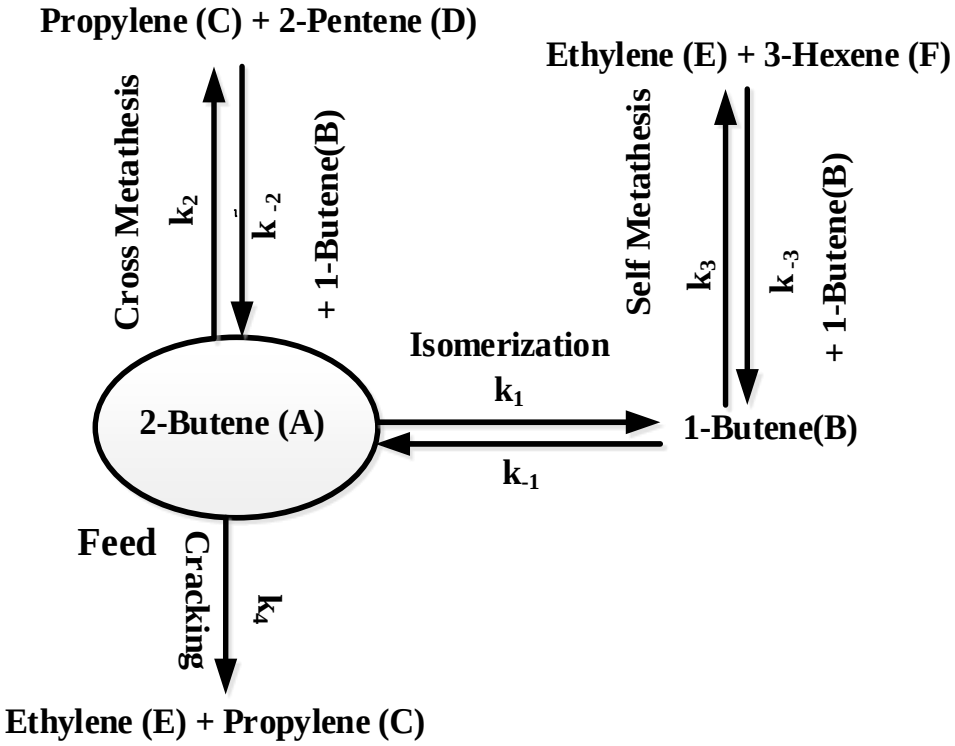

Scheme 2

Scheme 2 Possible reaction scheme of 2-butene metathesis reaction along with isomerization and cracking reactions over WO_3-SBA-15(30) catalyst.

6.3 Mass transfer limitations

The overall reaction rate for metathesis of 2-butene over WO_3-SBA-15(30) catalyst involves diffusion, adsorption and intrinsic reaction steps. In the context of the present study, the possibilities of both the external and internal diffusions were examined by evaluating the mass transfer limiting criterions using experimental data.

The possibility of external mass transfer (bulk fluid to catalyst surface) limitations of the reactants and products is assessed using the Sherwood number with Froessling's dimensionless correlations evaluated at the experimental conditions [72, 73].

$$Sh = 2 + 0.6\,Sc^{0.33}Re^{0.66}(Fröessling\ correlation) \qquad (6.6)$$

$$k_c = \frac{ShD_{AB}}{d_P} \qquad (6.7)$$

$$\left(C_{AB,b} - C_{AB,s}\right)_{film} = \Delta C_{film} = \frac{\left(-r''_{AB(obs)}\right)}{k_c} \qquad (6.8)$$

$$D_{AB} = \frac{1 \times 10^{-3} T^{1.75} \left(\frac{1}{M_A} + \frac{1}{M_B}\right)^{1/2}}{P_{atm}\left(\sum v_A^{1/3} + \sum v_B^{1/3}\right)^2} \qquad (6.9)$$

where, *Sh*, *Sc* and *Re* are Sherwood, Schmidt and Reynolds numbers, respectively. k_c is the external mass transfer co-efficient (m/s), subscript A is using for 2-butene and B is using for nitrogen, D_{AB} molecular diffusivity of 2-butene in carrier gas nitrogen (m^2/s), d_p is the particle diameter (m), $-r''_{AB(obs)}$ is the observed reaction rate (mol/m^2 s), $C_{AB,b}$ is the bulk concentration of gaseous reactant and $C_{AB,s}$ is the surface concentration of

gaseous reactant(mol/m^3). The diffusivity for 2-butene in nitrogen (D_{AB}) was estimated using the Fuller, Schettler, and Giddings correlation (Eq.6.9) [74].

Frössling correlation was evaluated by considering the fluid surrounding the particles is almost stagnant which corresponds to possible highest gas film resistances. The observed reaction rate (mol/m^2 s) in the fixed bed reactor can be expressed as:

$$-r''_{AB(obs)} = \frac{F_{A0}}{S_{ex}} \times \frac{X_A}{W} \qquad (6.10)$$

where, F_{A0} is the molar flow rate of reactant 2-butene , X_A is the conversion of 2-butene and S_{ex} is the external surface area per gram of sample and W is the weight of the catalyst.

The calculated ΔC_{film} (using Eq. 6.8) values are listed in Table 6.1. One can easily notice that at calculated values of ΔC_{film} at various reaction conditions are very small as compared to the bulk 2-butene concentration. The small values of ΔC_{film} suggest that in the context of the present study the external mass transfer limitation is not significant.

Table 6.1 Parameter used to calculate the effects of external mass transfer limitations.

Temp. (°C)	D_{AB} (m^2/s)	k_c (m/s)	Residence time(τ),s	r''_{AB}(obs) (μ mol/m^2s)	$C_{AB,b}$(mole/m^3)	ΔC_{film} (mmole/m^3)[a]
350	3.7×10^{-5}	0.12	24	98.3	43.0	0.80
400	4.2×10^{-5}	0.14	24	122.8	43.0	0.87
450	4.8×10^{-5}	0.16	24	256.2	43.0	1.60
500	5.4×10^{-5}	0.18	24	284.3	43.0	1.58
550	6.1×10^{-5}	0.20	24	287.8	43.0	1.43

The influence of intra-particle mass transfer (diffusion) is examined by evaluating the Weisz‑Prater criterion [72]. According to the Weisz‑Prater criterion the diffusion mass transfer can be considered negligible if the following inequality satisfies:

$$C_{WP} = \frac{-r'_{AB(obs)}\rho_P R_P^2}{D_{eff}C_{AB,s}} \ll 1 \qquad (6.11)$$

where, $-r'_{AB(obs)}$is the observed reaction rate (mol/kg s), ρ_P is the particle density (kg/m^3), R_p is the particle radius (m), D_{eff} is the effective diffusivity (m^2/s) and $C_{AB,S}$ is the concentration of gaseous reactant at the surface of solid particles (mol/m^3). The effective diffusivity (D_{eff}) is estimated as [73]:

$$D_{eff} = 0.1 D_{AB} \qquad (6.12)$$

The concentration of 2-butene at the surface of the catalyst is taken as the initial concentration of 2-butene. This ensures the evaluation of Weisz–Prater criterion at conditions where the possibility of diffusion limitations is highest. Table 6.2 reports the calculated Weisz–Prater parameters and the other variables used to for this evaluation. It is clear for Table 6.2 that even at worst case scenarios the values of C_{WP} was much smaller than 1 (one). Thus, the concentration gradient within the catalyst carrier pellet is expected to be negligible. Thus, it can be concluded that in overall and for the catalyst particles of the present study, the chemical reaction is the limiting resistance for all the runs developed in the fixed bed reactor.

Table 6.2 Parameter used to calculate the effects of internal mass transfer limitations.

Temp. (°C)	D_{eff} (m^2/s)	Residence time(τ),s	$r'_{AB}(obs)$ (mmol/kg s)	$C_{AB,s}$(mole/m^3)	C_{WP}[a]
350	3.7×10^{-6}	24	3.34	43.0	5.7×10^{-4}
400	4.2×10^{-6}	24	4.18	43.0	6.2×10^{-4}
450	4.8×10^{-6}	24	8.71	43.0	1.1×10^{-3}
500	5.4×10^{-6}	24	9.67	43.0	1.1×10^{-3}
550	6.1×10^{-6}	24	9.79	43.0	1.0×10^{-3}

6.4 Model development

The mathematical models representing the rates of chemical reactions are developed based on Scheme 1 which considers (i) isomerization of 2-butene to 1-butene (ii) cross metathesis of 2-butene and 1-butene, (iii) self-metathesis of 1-butene and (iv) cracking of 1-butene. As previously discussed, all these reactions are greatly influenced by temperature and residence time. In formulation of the kinetic model the following assumptions have been considered:

i. Isomerization, cross metathesis and self-metathesis reactions is reversible while 2-butene cracking is irreversible.
ii. The pentene isomers are considered as 2-pentene and the hexene isomers as 3-hexene.
iii. All paraffin, isobutene and aromatic products are negligible.
iv. Contribution of secondary metathesis in propylene production is insignificant.

From the design equation of Fixed Bed Tubular Reactor

$$\frac{dF_A}{dW} = -r'_A \qquad (6.13)$$

$$F_A = C_A \vartheta_o \qquad (6.14)$$

$$\vartheta_o \ \frac{dC_A}{dW} = -r'_A \qquad (6.15)$$

$$\frac{dC_A}{d\tau'} = -r'_A \qquad (6.16)$$

$$\tau' = \frac{W}{\vartheta_0} = \frac{\rho_b V}{\vartheta_0} = \rho_b \tau \qquad (6.17)$$

From the reactions, the following rate equations have been developed

$$r_1' = k_1\left(C_A - \frac{1}{K_{1e}}C_B\right) \qquad (6.18)$$

$$r_2' = k_2(C_A C_B - \frac{1}{K_{2e}}C_C C_D \qquad (6.19)$$

$$r_3' = k_3\left(C_B^2 - \frac{1}{K_{3e}}C_E C_F\right) \qquad (6.20)$$

$$r_4' = k_4 C_A \qquad (6.21)$$

From the reaction network in scheme and the assumptions, the following species balances and catalytic reactions can be written

Disappearance of 2-butene, r_A

$$-\mathrm{r_A} = \frac{\mathrm{dC_A}}{\mathrm{d\tau'}} = -\mathrm{r_1'} - \mathrm{r_2'} - \mathrm{r_4'}$$

$$\frac{dC_A}{d\tau'} = -k_1\left(C_A - \frac{1}{K_{1e}}C_B\right) - k_2\left(C_A C_B - \frac{1}{K_{2e}}C_C C_D\right) - 2k_4 C_4^2 \qquad (6.22)$$

Formation of 1-butene, r_B

$$-\mathrm{r_B} = \frac{\mathrm{dC_B}}{\mathrm{d\tau'}} = -\mathrm{r_1'} + \mathrm{r_2'} - 2\mathrm{r_3'}$$

$$\frac{dC_B}{d\tau'} = k_1\left(C_A - \frac{1}{K_{1e}}C_B\right) - k_2\left(C_A C_B - \frac{1}{K_{2e}}C_C C_D\right) - 2k_3\left(C_B^2 - \frac{1}{K_{3e}}C_E C_F\right) \qquad (6.23)$$

Formation of Propylene, r_C

$$-\mathrm{r_C} = \frac{\mathrm{dC_C}}{\mathrm{d\tau'}} = \mathrm{r_2'} + \mathrm{r_4'}$$

$$\frac{dC_C}{d\tau'} = k_2\left(C_A C_B - \frac{1}{K_{2e}}C_C C_D\right) + k_4 C_A^2 \qquad (6.24)$$

Formation 2-Pentene, r_D

$$-\mathrm{r_D} = \frac{\mathrm{dC_D}}{\mathrm{d\tau'}} = \mathrm{r_2'}$$

$$\frac{dC_D}{d\tau'} = k_2\left(C_A C_B - \frac{1}{K_{2e}} C_C C_D\right) \qquad (6.25)$$

Formation of Ethylene, r_E

$$-\mathrm{r_E} = \frac{\mathrm{dC_E}}{\mathrm{d\tau'}} = \mathrm{r_3'} + \mathrm{r_4'}$$

$$\frac{dC_E}{d\tau'} = k_3\left(C_B - \frac{1}{K_{3e}} C_E C_F\right) + k_4 C_A^2 \qquad (6.26)$$

Formation of 3-Hexene, r_F

$$-\mathrm{r_F} = \frac{\mathrm{dC_F}}{\mathrm{d\tau'}} = \mathrm{r_3'}$$

$$\frac{dC_F}{d\tau'} = k_3\left(C_B^2 - \frac{1}{K_{3e}} C_E C_F\right) \qquad (6.27)$$

By definition, C_A can be written in terms of mass fraction of 2-butene (y_A) according to the following equation

$$C_A = \frac{y_A F_{TM}}{MW_A \vartheta} \qquad (6.28)$$

For gas phase the volumetric flow rate will be

$$\vartheta = \vartheta_0(1 + \varepsilon X) \times \frac{P_0}{P} \times \frac{T}{T_0} \qquad (6.29)$$

$$where, \varepsilon X = y_{A0}\delta X = y_{A0}\left(\frac{n_{Total} - n_{A0}}{n_{A0}\, X_A}\right) X = y_{A0}\frac{n_{Total} - n_{A0}}{n_{A0}} \qquad (6.30)$$

By substituting the equation, we get the following equation of reactant

$$\frac{dy_A}{d\tau'} = -k_1\left(y_A - \frac{1}{K_{1e}}y_B\right) - k_2(y_A y_B - \frac{1}{K_{2e}}y_C y_D) \qquad (6.31)$$

The activation energy E_i and temperature dependent rate constants k_i related to the temperature dependent rate constants K_i according to the Arrhenius equation

$$k_i = A_i e^{\left(-\frac{E_i}{RT}\right)} \qquad (6.32)$$

For reducing the parameter interaction, pre-exponential factor A_i could be replaced by the K_{oi} and the expression of k_i is given below

$$k_i = k_{0i} e^{\left(-\frac{E_i}{R}\left(\frac{1}{T}-\frac{1}{T_a}\right)\right)} \qquad (6.33)$$

Since the experimental runs were performed at 350, 400, 450, 550 and 550 °C, T_a was calculated as 450 °C.

$$k_1 = k_{01} e^{\left(-\frac{E_1}{R}\left(\frac{1}{T}-\frac{1}{T_a}\right)\right)} \qquad (6.34)$$

$$k_2 = k_{02} e^{\left(-\frac{E_2}{R}\left(\frac{1}{T}-\frac{1}{T_a}\right)\right)} \qquad (6.35)$$

$$k_3 = k_{03} e^{\left(-\frac{E_3}{R}\left(\frac{1}{T}-\frac{1}{T_a}\right)\right)} \qquad (6.36)$$

$$k_4 = k_{04} e^{\left(-\frac{E_4}{R}\left(\frac{1}{T}-\frac{1}{T_a}\right)\right)} \qquad (6.37)$$

For the thermodynamic consistency of the reaction, the temperature dependent equilibrium constant of the reversible reaction expressed as

$$K_{ie} = \frac{k_i}{k_{-i}} \qquad (6.38)$$

Which were calculated from the below equations of heat formation and Gibbs energy of formation of pure species

$$ln(\frac{K_{T2}}{K_{298}}) = -\frac{\Delta H^0_{rxn(298)}}{R}\left(\frac{1}{T_2} - \frac{1}{298}\right) \qquad (6.39)$$

$$\Delta H^0_{rxn,298} = \sum \vartheta_i (\Delta H^0_{form,298})_i \qquad (6.40)$$

$$K_{298} = e^{(-\frac{\Delta G^0_{Rxn}}{R \times 298})} \qquad (6.41)$$

$$\Delta G^0_{rxn,298} = \sum \vartheta_i (\Delta G^0_{form,298})_i \qquad (6.42)$$

The following three temperature dependent equilibrium constant were calculated for isomerization, cross metathesis I and self-metathesis reaction

$$K_{1e} = 21.45\, e^{\left((-\frac{9600}{R})\times(\frac{1}{T}-\frac{1}{298})\right)} \qquad (6.43)$$

$$K_{2e} = 196.5\, e^{\left((-\frac{1200}{R})\times(\frac{1}{T}-\frac{1}{298})\right)} \qquad (6.44)$$

$$K_{3e} = 181.8\, e^{\left((-\frac{26100}{R})\times(\frac{1}{T}-\frac{1}{298})\right)} \qquad (6.45)$$

6.5 Parameter estimation and kinetics evaluation

To estimate the parameters and evaluate the developed models, the temperature dependent specific reaction rate constants (Eqs. 6.34-6.37) and temperature dependent equilibrium constants (Eq. 6.43-6.45) were first combined with the kinetics model equations (Eqs. 6.22-6.27). The concentrations of various species were expressed in terms of mass fraction according Eq. 6.28. The resulting differential equations were then

numerically solved in conjunction with a least square fitting of the experimental 2-butene metathesis data to be obtained from the fixed bed reactor. In solving the differential equation MATLAB ODE 45 subroutine (Runge-Kutta-Gill method) was employed while the parameters were estimated using LSQCURVEFIT subroutine (Modified Marquad method).

In order to ensure reliable model parameter estimation, the catalytic 2-butene metathesis experiments were conducted at wide range of reaction temperatures (350 to 550 °C) and various residence times (8 to 24 sec). In this fashion total two hundred and seventy (270) data points were obtained and used in parameter estimation. Therefore, eight kinetics parameters were determined with a degree of freedom of 262 (degree of freedom = No of experimental data points – No of model parameters). The sufficient numbers of experimental data points obtained/used in parameter estimation provides reliability of the model parameter.

The following model evaluation criteria are considered:

(i) All the kinetics parameters (specific reaction rates and activation energies) should be consistent with physical principles.

(ii) Coefficient of determination (R^2).

(iii) Lower SSR (sum of the squares of the residuals).

(iv) Lower cross-correlation coefficient (γ).

(v) Smaller individual confidence intervals for the model parameters.

Figure 6.1 and 6.2 show the comparison between the experimental data and model predictions for the reaction scheme. We observed in these plots, model predictions compared favorably with experimental data for the reactions at 350,450 and 550°C. Some deviations are getting due to high conversion are predicted at 550 C and 24s contact time. Several reactions are involved in the reaction scheme and several products are producing. During the long range of contact time the model predicted higher conversion at higher temperature. The Arrhenius plots Figure 6.3 of the rate constants proved the validity of the Power Law model.

Table 6.3 lists the estimated kinetics parameters for different reaction paths displayed in scheme 2. From Table 6.3, it is noticed that the estimated activation energy of 2-butene isomerization forming 1-butene requires the least activation energy (39.4 kJ/mol) as compared to the other competing reactions. The estimated activation energies for cross metathesis of 2-butene and 1-butene is 71.3 kJ/mol, cracking of 2-butene is 73.1 kJ/mol.

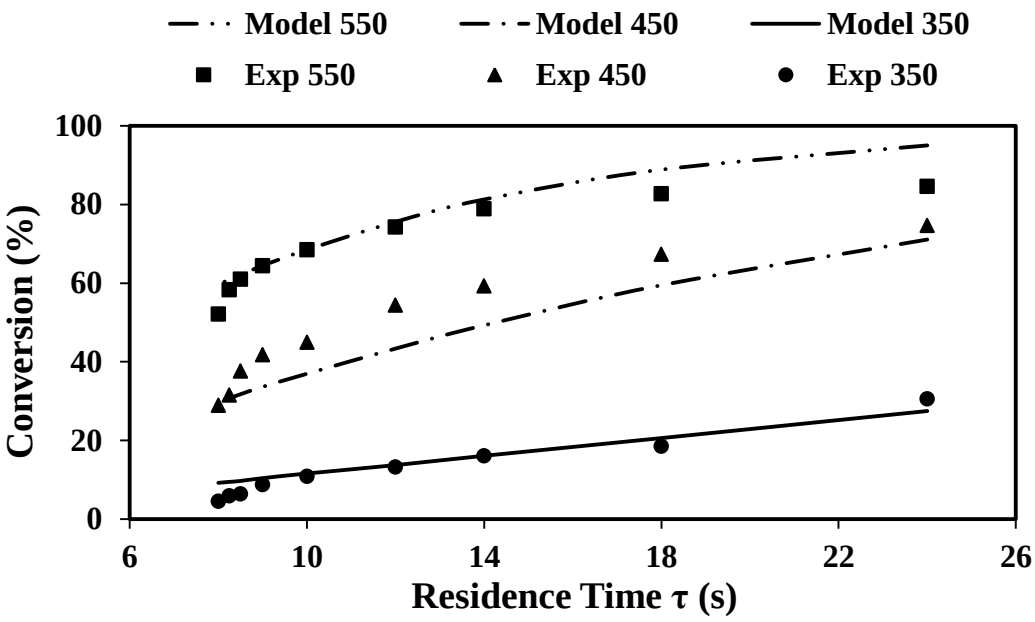

Figure 6.1 Comparison between experimental results and model predictions for 2-butene conversion at the reaction temperature at 350 °C, 450°C and 550°C.

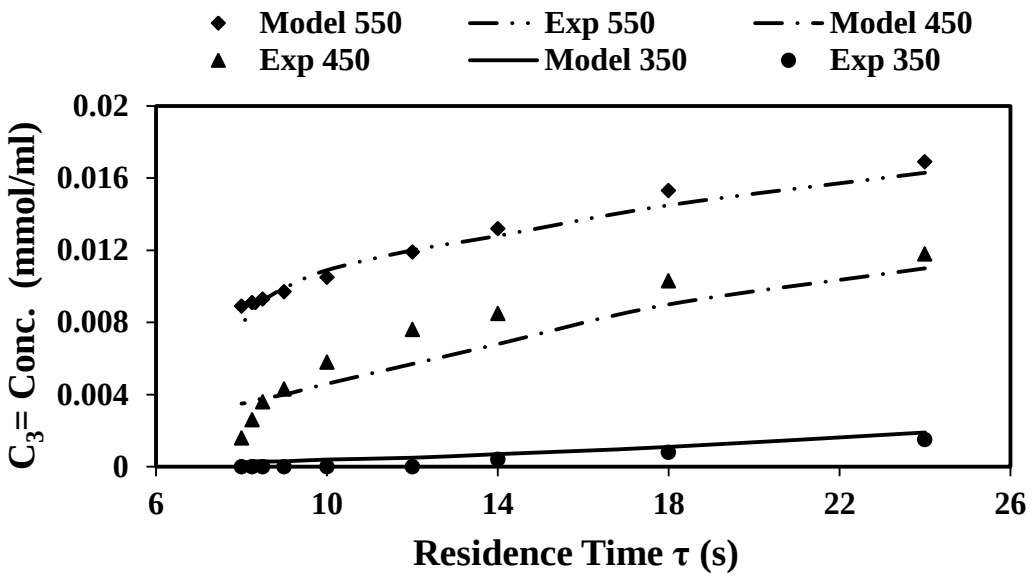

Figure 6.2 Comparison between experimental results and model predictions for propylene concentration at the reaction temperature at 350 °C, 450 °C and 550°C.

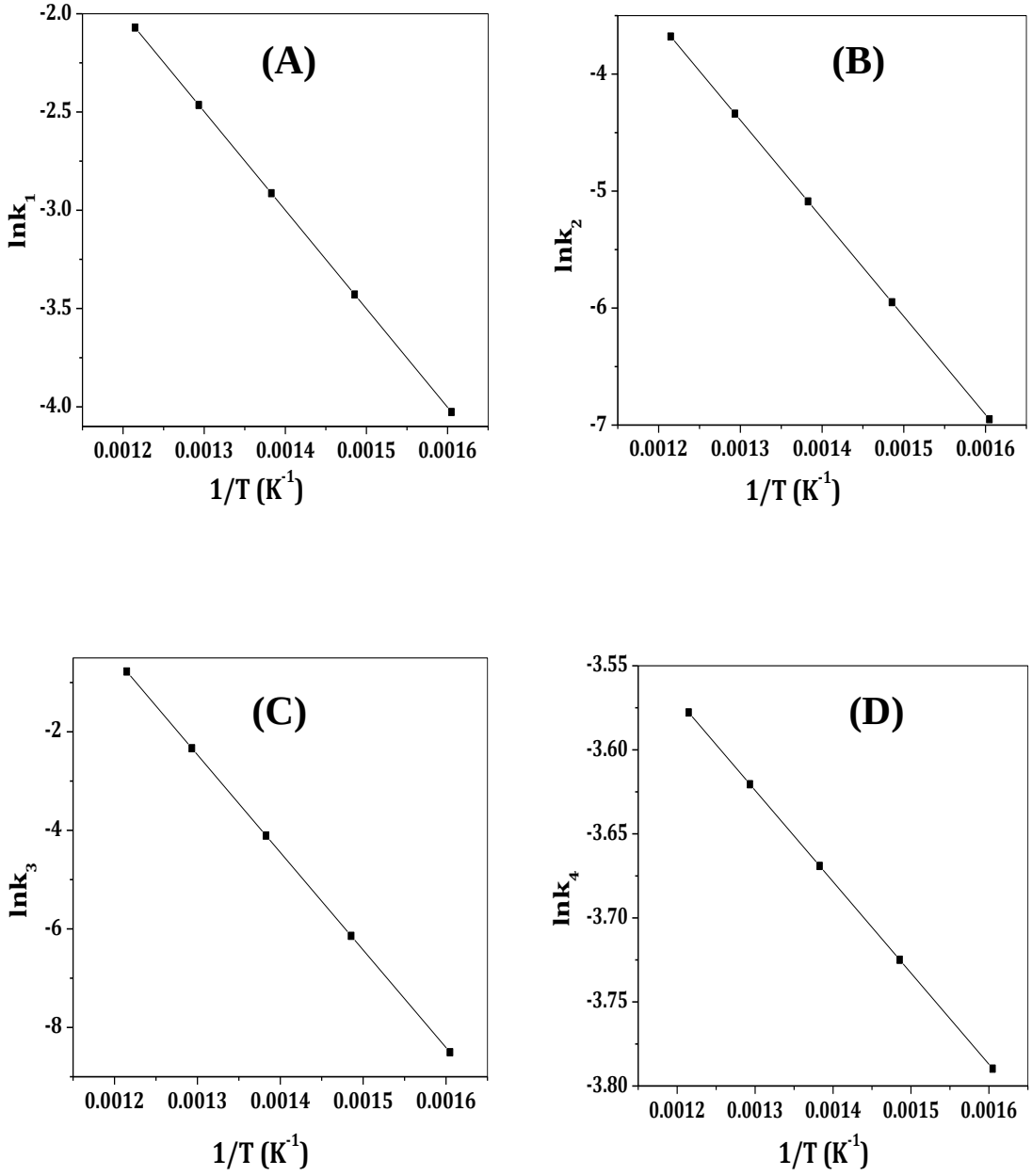

Figure 6.3 Arrhenius plots of different reactions rate constants obtained from Power Law Model (A) Isomerization reaction, (B) Cross metathesis of 1-butene an 2-butene, (C) Self-metathesis of 1-butene, (D) Cracking of 2-butene.

Unfortunately, in the open literature the activation energies for butene metathesis (either 1- and 2-butene cross metathesis or 1-butene self-metathesis) are not available for comparison. The value of activation energy for self- metathesis of 1-butene found to the highest (176.5 kJ/mol). The high activation energy for 1-butene self-metathesis is consistent to the experimental low selectivity 3-hexene as shown in Figure 5.13 and Table 5.4. On the other hand, the low value of activation energy of 2-butene isomerization is also reasonable given that the product 1-butene further reacts with 2-butene (cross metathesis) to give propylene. Therefore, isomerization of 2-butene to 1-butene is a pre-requirement of cross metathesis. The high selectivity of propylene as seen in Figure 5.13 and Table 5.4 confirms this explanation. One can argue that the origin of propylene might be the cracking of 2-butene. However, at low temperature (until 400 °C) the selectivity of the other cracking products ethylene is negligible while the selectivity of propylene is still high. This confirms the formation of propylene mainly via cross metathesis of 2-butne and 1-butene.

Table 6.3 Estimated values of the parameters, 95% confidence intervals and R^2

Parameter	**Estimated value**	**95% confidence interval**	**R^2**
$k_{01} \times 10^2 (m^3/kgs)$	4.72	0.17	0.9727
E_1 (kJ/mol)	39.4	1.92	
$k_{02} \times 10^2 (m^6/kgs)$	5.7	0.4	
E_2 (kJ/mol)	71.3	6.1	
$k_{03} \times 10^2 (m^6/kgs)$	1.64	0.48	
E_3 (kJ/mol)	176.9	36.8	
$k_{04} \times 10^2 (m^3/kgs)$	1.8	0.031	
E_4 (kJ/mol)	73.1	15.3	

Based on the kinetics analysis and catalyst characterizations on can consider the reaction mechanisms for cross metathesis (2-butene and 1-butene) and self-metathesis (1-butene) as shown in Scheme 3 and Scheme 4, respectively. First of all for both the cross and self-metathesis requires 1-butene which is originated from the skeleton isomerization of 2-butene over the silanol (Si-OH) group present on the SBA-15 support. In order to ascertain this the isomerization 2-butene experiments were conducted at 350 °C using only the support SBA-15 and WO_3-SBA-15(30) catalyst (after W loading) and results are reported in Table 6.4. One can notice form this Table that the 2-butene conversions and product selectivity were comparable with and without the presence of tungsten. This indicates that silanol (Si-OH) group of the mesoporous silica support (SBA-15) mainly responsible for the isomerization. Jeon and his co-workers (2007) reported that the formation of 1-butene through skeleton isomerization of 2-butene over mesoporous MCM-41 where H site of silanol (Si-OH) group working as an active site [70].

The terminal W=O bond of tetrahedrally coordinated tungsten species on SBA-15 is believed to be the active sites of WO_3-SBA-15(30) catalysts. The Raman spectra analysis WO_3-SBA-15(30) catalysts confirmed the evidence (the band of 970 cm^{-1}) of the active W=O bond. The UV-vis DRS results also demonstrate that WO_3-SBA-15(30) has tungsten oxide species in tetrahedrally coordinated into the support at 230 nm which works as an active site of metathesis reaction. In metathesis, the W=O interacts with the C=C of both 1-butene and 2-butene to form unstable carbene metal complex [19, 75, 76]. When the intermediate carbene metal complex formed from 1-butene it can react with both 2-butene and 1-butene. On the other hand the metal carbene complex originated

from 2-butene can only react with 1-butene [77]. Therefore, the probability of 1-butene and 2-butene cross metathesis is much higher than the 1-butene self-metathesis. In cross metathesis as shown in Scheme 3 and 4, the carbene metal complex reacts with 2-butene to give propylene and 2-pentene. While in self- metathesis (Scheme 5) the carbene complex reacts with 1-butene to produce ethylene and 3-hexene. Furthermore, at lower temperature 2-butene is thermodynamically more stable than 1-butene which reduces the possibility of 1-butene self- metathesis reaction [78]. Table 6.5 shows the reactivity of 1-butene and 2-butene separately used as only feed in a same operating condition and same catalyst. 1-Butene conversion is about 73% at 350°C while 2-butene conversion 35% and isomerization occurs at that temperature. These factors might have contributed to the lower activation energy of 1-butene and 2-butene cross metathesis (71.3 kJ/mol) than 1-butene self-metathesis (176.5 kJ/mol).

The estimated activation energy of 2-butene cracking is higher than the cross metathesis reaction. Due to the reactive nature of alkenes, at higher temperature 2-butene is forming intermediate carbenium ions and later propylene, ethylene produce from this carbenium ion. Low Brønsted acid sites of catalyst WO_3-SBA-15(30) which has calculated by Py-FTIR were hindered the formation of aromatics and alkanes from the carbenium ions by suppressing of alkene aromatization and hydrogen transfer reaction of propene [71].

$$C_4^= \rightarrow [C_8]^+ \rightarrow C_3^= + C_2^=$$

At higher temperature, 2-pentene and 2-hexene also cracked to form ethylene and propylene. Alkenes are highly reactive for involving secondary metathesis reactions which are producing some other alkenes. These reactions are not considered in the reaction scheme for which some deviation could be found. It can be conclude that, the estimated activation energies are fully consistent with experimental results.

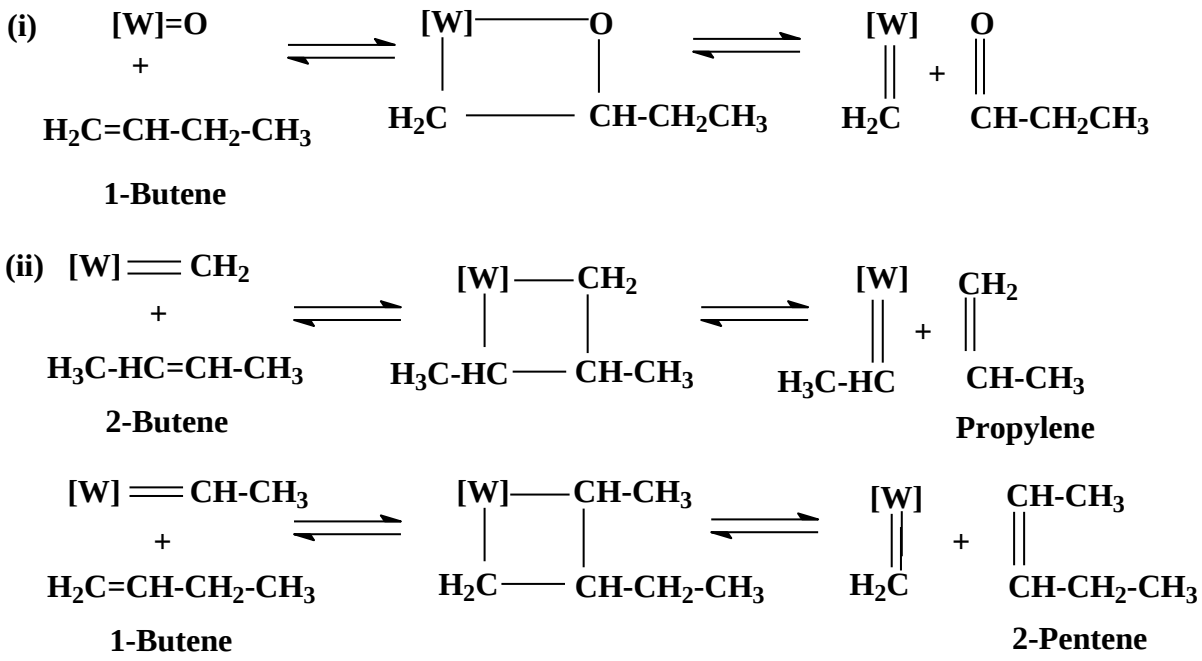

Scheme 3 Mechanism of cross metathesis of 1-butene and 2-butene to produce propylene and 2-pentene (Metal carbene complex originated from 1-butene)

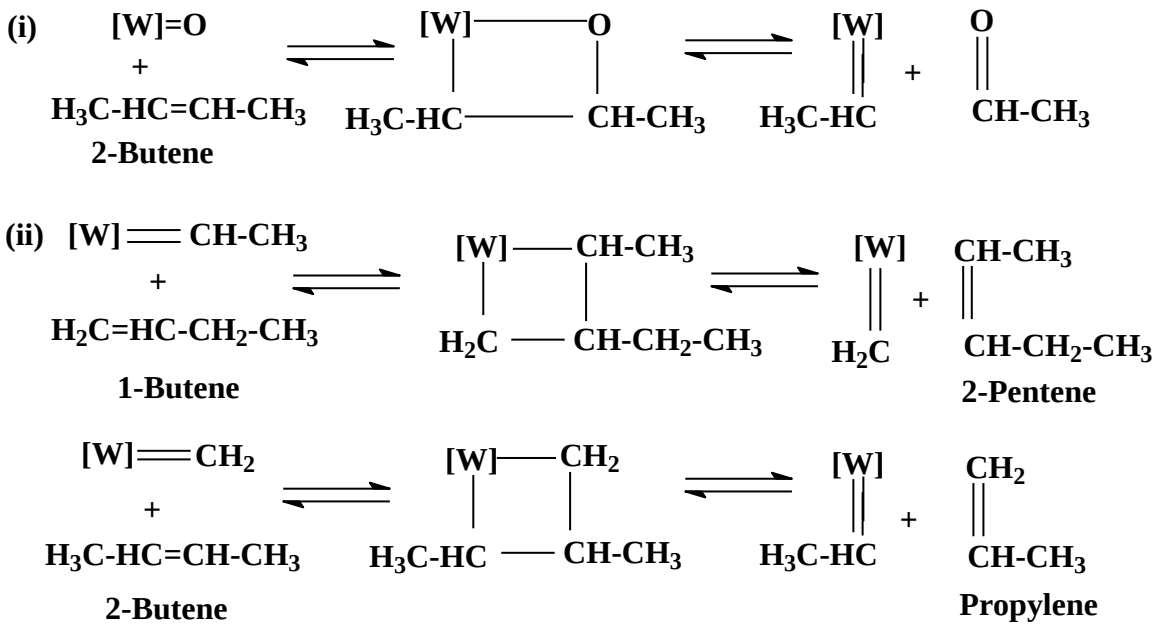

Scheme 4 Mechanism of cross metathesis of 1-butene and 2-butene to produce propylene and 2-pentene (Metal carbene complex originated from 2-butene)

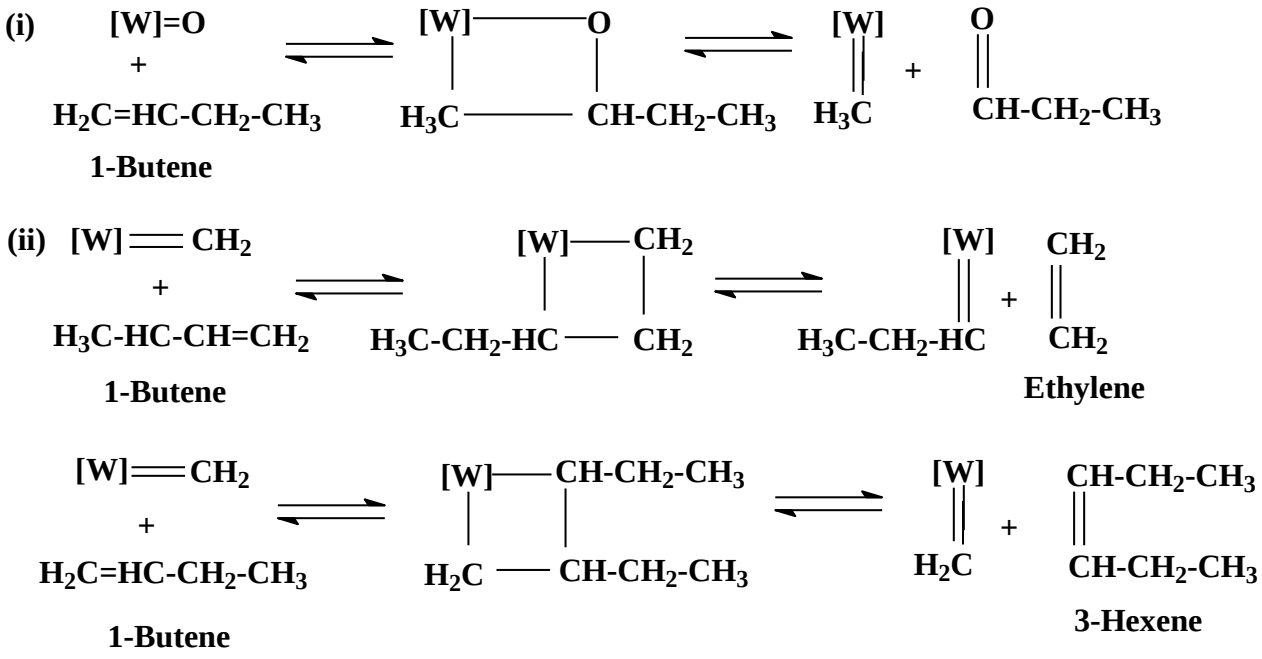

Scheme 5 Mechanism of self- metathesis of 1-butene to produce ethylene and 3-hexene (Metal carbene complex originated from 1-butene).

Table 6.4 Results of isomerization of 2-butene to 1-butene over support SBA-15 and catalyst WO_3-SBA-15(30) at 350°C.

Catalyst	**Conversion**	**S-1C_4=**	**S-C_3=**	**S-2C_5=**
SBA-15	26.4	80.2	9.5	5.9
WO_3-SBA-15(30)	27.7	73.4	12.1	7.5

Table 6.5 Conversions of 2-butene and 1-butene used as a feed alone over catalyst WO_3-SBA-15(30) from 350°C to 550°C.

Feed	**350 °C**	**400°C**	**450 °C**	**500°C**	**550°C**
2-Butene	27.8	35.8	72.4	80.6	81.2
1-Butene	75.7	75.2	90.7	90.4	90.2

CHAPTER 7

CONCLUSIONS AND RECOMMENDATIONS

7.1 Conclusions

The prime objective of the study was to evaluate the metathesis performance of tungsten oxide catalysts contained on SBA-15 and MCM-41. These catalysts were synthesized by different loading of WO_3 in impregnation method and different Si/W ratio in direct hydrothermal method. The conclusions of this study can be summarized as below:

- Catalysts having tungsten oxide in the framework of mesoporous silica exhibited the higher metathesis activity as compared to tungsten oxide impregnated catalysts.
- The lower activity of impregnated catalysts is due to abundance of crystalline WO_3, which are shown to be non-active for metathesis reactions.
- WO_3-MCM-41(30) and WO_3-SBA-15(30) catalyst showed comparable activity with highest propylene yield of 39 mol % and 37 mol %, respectively at 550 °C.
- The activity order of all catalysts at 450 °C was : WO_3-MCM-41(30) > WO_3/MCM-41(35) ~ WO_3-SBA-15(30) > WO_3/SBA-15(35), whereas at 550 °C the order was : WO_3-SBA-15(30) ~ WO_3-MCM-41(30) > WO_3/MCM-41(35) > WO_3/SBA-15(35).

- WO_3-MCM-41 catalysts exhibited much higher activity at low temperature (450 °C) as compared to that of WO_3-SBA-15.
- The synthesized WO_3-SBA-15(30) catalyst has tetrahedral tungsten oxide species as confirmed by Raman spectroscopy and UV-vis DRS. The tetrahedral tungsten oxide species acts as the active site for the metathesis reaction. Tungsten oxide effectively incorporated into the SBA-15 framework and highly dispersed into the lattice of the support as revealed by XRD analysis. The FT-IR pyridine adsorption experiment confirms the availability of both Lewis and Brønsted acid sites on the catalyst surface.
- The product selectivity was significantly influenced by the reaction temperature. Lower temperature favors the 2-butene isomerization to 1-butene. On the other hand, higher temperature was required for metathesis. However, high temperature was also responsible for undesired cracking reactions. Selectivity of propylene and ethylene were increased with the increasing of temperature, while pentene and hexene selectivities were decreased after 450°C.
- The reaction mechanisms suggested that metathesis reactions are initiated by the W-carbene complex formation. Under the studied reaction conditions both the cross metathesis of 2-butene and 1-butene and self-metathesis of 1-butene are possible. However, the probability of cross metathesis of 2-butne and 1-butene is much higher than the self- metathesis of 1-butene.
- The kinetics investigation showed that among the competing reactions, isomerization of 2-butene to 1-butene requires least amount of activation energy (39.4 kJ/mol) while the activation energy for self-metathesis of 1-butene was

highest (176.9 kJ/mol). The activation energy of cross metathesis of 2-butene and 1- butene, self-metathesis of 1-butene and 2-butene cracking are 71.3, 176.9 and 73.1 kJ/mol, respectively. These results are consistent to the proposed reaction mechanisms and the product selectivity data, which suggests that the isomerization of 2-butene gives 1-butene which further reacts (cross metathesis) with 2-butene to produce propylene.

- WO_3-MCM-41 is a better choice from industrial point of view due to lower cost of structure directing agent as compared to that of WO_3-SBA-15.

7.2 Recommendations

After sequential studies regarding the applicability of WO_3 catalyst on SBA-15 and MCM-41 catalyst for the 2-butene metathesis to propylene, the following recommendations can be advanced for future studies.

- The model developed by Power law didn't show the mechanism of surface reaction. This model showed the combined effect of (adsorption of reactant, surface reaction, desorption to product) a catalytic reaction. We need to develop a phenomenological kinetic model to understand the mechanism of the reaction.
- We consider only four main reactions for modeling. Several secondary metathesis reactions are involved in the reaction scheme. We should investigate the effects of secondary metathesis to the whole reaction scheme
- We should conduct a thorough study of isomerization, metathesis and cracking.

APPENDIX

Table A4.1 Retention time of different hydrocarbons in the GC.

Compounds	Retention time (min)
1.79	Methane
2.43	Ethane
2.83	Ethylene
4.91	Propane
7.60	Propylene
9.39	I-Butane
10.18	n-Butane
13.63	1-Butene
15.31	Isobutylene
15.55	t-2-butene
15.88	C-2-Butene
16.00	I-Pentane
16.69	n-Pentane
19.45	3-Methyl-1-Butene
20.50	1-pentene
21.06	t-2-Pentene
21.40	c-2-pentene
22.64	2-Methyl-1-Butene
23.05	1-hexene
23.35	2-Methyl-2-Butene
23.42	2,3 dimethyl1-butene
23.56	t-3-hexene
24.22	cis-3-hexene

Table A4.2 Retention time of different aromatics in the GC.

Compounds	Retention time (min)
4.71	Benzene
6.62	Toluene
8.65	Ethyl
8.85	m-Xylene
9.02	p-Xylene
9.83	o-Xylene
10.17	Isopropylbenzene
10.77	n-Propyl benzene
11.15	1-Methyl-3-ethylbenzene
11.21	1-Methyl-4-ethylbenzene
11.72	1,3,5-Trimethyl benzene
12.21	1-Methyl-2-ethylbenzene
12.78	1,2,4 trimethylbenzene
13.64	1,2,3 trimethylbenzene
13.72	Indan
14.34	1,4 diethylbenzene
14.59	n-Butylbenzene
15.66	1,2 diethylbenzene
17.02	1,2,4,5 tetramethylbenzene
17.29	1,2,3,5 tetramethylbenzene
21.57	Naphthalene
23.29	Pentamethylbenzene
24.94	1-Methylnaphthalene
25.46	2-Methylnaphthalene

Table A5.1 List of catalysts used in the metathesis reaction of 2-butene and their description

Catalysts Code	Description
SBA-15	Siliceous SBA-15 synthesized by hydrothermal method
WO_3-SBA-15(30)	W containing SBA-15 synthesized by hydrothermal method with Si/W molar ratio of 30
WO_3-SBA-15(60)	W containing SBA-15 synthesized by hydrothermal method with Si/W molar ratio of 60
WO_3/SBA-15(18)	20% WO_3 loaded SBA-15 synthesized by impregnation method
WO_3/SBA-15(27)	15% WO_3 loaded SBA-15 synthesized by impregnation method
WO_3/SBA-15(35)	10% WO_3 loaded SBA-15 synthesized by impregnation method
WO_3/SBA-15(73)	5% WO_3 loaded SBA-15 synthesized by impregnation method
MCM-41	Siliceous MCM-41 synthesized by hydrothermal method
WO_3-MCM-41(30)	W containing MCM-41 synthesized by hydrothermal method with Si/W molar ratio of 30
WO_3-MCM-41(50)	W containing MCM-41 synthesized by hydrothermal method with Si/W molar ratio of 50
WO_3/MCM-41(18)	20% WO_3 loaded MCM-41 synthesized by impregnation method
WO_3/MCM-41(27)	15% WO_3 loaded MCM-41 synthesized by impregnation method
WO_3/MCM-41(35)	10% WO_3 loaded MCM-41 synthesized by impregnation method
WO_3/MCM-41(73)	5% WO_3 loaded MCM-41 synthesized by impregnation method

NOMENCLATURE

C_i concentration of species i in the fixed bed reactor (mmol/cm^3)

CI confidence limit

E_i apparent activation energy of the i^{th} reaction (kJ/mol)

k_i apparent rate constant for the i^{th} reaction (1/s)

k_{oi} pre-exponential factor for the ith reaction after reaction paramerization

E_i apparent activation energy of the ith reaction (kJ/mol)

K_c equilibrium constant

MW_i molecular weight of the species

r_i rate constant of the species

v_o entering volumetric flow rate of the,

τ the residence time.

y_i mass fraction of species i in the reactor

F_{TM} total mass flow rate

To average temperature of the experiment

V volume of the reactor

Wc mass of the catalyst

Symbols

A 2-Butene
B 1-Butene
C Propylene
D 2-Pentene
E Ethylene
F 3-Hexene

REFERENCES

[1] Nexant, Propylene Technology-The Next Generation, 2009.

[2] A. M. Aitani , Propylene production, Encyclopedia of Chemical Processing, DOI: 10.1081/E-ECHP-120037901.

[3] J.S. Plotkin, The changing dynamics of olefin supply/demand, Catal. Today 106 (2005) 10-14.

[4] J.P. Dath, W. Vermeiren, K. Herrenbout, Production of Olefins, WO 00/78894 (to Fina Oil and Chemical Corporation).

[5] X.X. Zhu, X.J. Li, S.J. Xie, , S.L. Liu, , G.L. Xu, W.J. Xin, S.J. Huang, L.Y. Xu, Two new on purpose process enhances propene production: Catalytic cracking of C4 alkenes to propene and Metathesis of ethene and 2-butene to propene, Catal. Surv. Asia 13 (2009) 1-8.

[6] L.D. Johnson , E.K. Nariman , A.R. Ware, Catalytic production of light olefins rich in propylene, US Patent 6222087 (to Mobil corporation), 2001.

[7] J.D. Pless, B.B. Bardin, H.S. Kim, D.G. Ko, M.T. Smith, R.R. Hammond, P.C. Stair, K.R. Poeppelmeier, Catalytic oxidative dehydrogenation of propane over Mg-V/Mo oxides, J. Catal. 223(2004) 419-431.

[8] F. Cavani, N. Ballarini, A. Cericola, Oxidative dehydrogenation of ethane and propane: how far from commercial implementation, Catal. Today 127(2007) 113-131.

[9] X.X. Zhu, S.L. Liu, Y.Q. Song, S.J. Xie, L.Y. Xu, Catalytic cracking of 1-butene to ethane and propene on MCM-22 zeolite, Appl. Catal. A 290 (2005) 191-199.

[10] G.L Zhao, J.W. Teng, Z.K. Xie, W.Q. Jin, W.M. Yang, Q.L. Chen, Y. Tang, Effect of phosphorous on HZSM-5 catalyst for C4 olefin cracking reactions to produce propylene J. Catal. 248 (2007) 29-37.

[11] J.M. Botha, M.M. Mbatha, B.S. Nkosi, A. Spamer, J. Swart, Production of propylene, US 6586649-B1, 2003.

[12] M. Stocker, Methanol to hydrocarbons: catalytic materials and their behavior, Micropor. Mesopor. Mater. 29 (1999) 3-48.

[13] L. Harmse, C. van Schalkwyk, E. van Steen, On the product formation in 1-butene metathesis over supported tungsten catalysts, Catal. Lett. 137 (2010) 123-131.

[14] Nexant, Alternative routes to Propylene, Chemsystems Prep Program

[15] Technology economic program, Propylene production via metathesis, 2011.

[16] http://www.mitsuichem.com/release/2010/2010_0125.htm

[17] L. Sang, S.L.Chen,Y. Guimei, M. Zheng, J. You, A. Chen, R. Li, L. Chen, Metathesis of 1-Butene and 2-Butene to propene over Re_2O_7 supported on macro-mesoporous γ-Al_2O_3 prepared via a dual template method, J. Nat. Gas. Chem. 21 (2012) 105-108.

[18] J.C Mol, Industrial applications of olefin metathesis, J. Mol. Catal. A. 213 (2004) 39–45.

[19] J.C. Mol, P.W.M. Leeuwen, Metathesis of alkenes, Handbook of Heterogeneous catalyst 8 (2008).

[20] P. A. Amigues, Y. Chauvin, D. Commereuc, C.C. Lai, Y.H. Liu, J.M. Pan, Hydrocarbon Process, 69 (1990) 79.

[21] J. Cosyns, J. Chodorge, D. Commereuc, B. Torck, Hydrocarbon Process, 77 (1998) 61.

[22] R.J. Gartside, B. Ramachandran, Integrated Propylene Production, US Patent 2010/041930 A1 (2010).

[23] S. J. Huang, S.L. Liu, W.J. Xin, Q.S. Wang, L.Y. Xu, Effect of temperature and pressure on the metathesis reaction between ethene and 2-butene to propene on WO_3/Al_2O_3 catalyst, J. Nat. Gas Chem. 15 (2009) 93.

[24] A. Andreni, X.D. Xu, J.C.Mol, Acidity of Re_2O_7/SiO_2-Al_2O_3 catalyst for propene metathesis and the influence of alkyltin promoters, Appl. Catal. 27 (1986) 31.

[25] A. Behr, U. Schller, K. Bauer, D. Maschmeyer, K.D. Wise, F. Nierlich, Investigations of the reasons of deactivations of rhenium oxide alumina catalysts on pentene-1 metathesis, Appl. Catal. A 357(2009) 34.

[26] P. Topka, H. Balcar, J. Rathousky, N. Zillkova, F. Verpoort, J. Cejka, Metathesis of 1-octene over MoO_3 supported on mesoporous molecular sieves: The influence of the support architecture. Micropor. Mesopor. Mater. 96 (2006) 44.

[27] J. Handzlik, J. Ogonowski, J. Stoch, M. Mikolajczyk, P. Michorczyk, Properties of metathesis activity of molybdena-alumina, molybdena-silica-alumina, molybdena-silica catalyst-a comparative study, Appl. Catal. A 312 (2006) 213-219

[28] H. Balcar, D. Mishra, E. Marceau, X. Carrier, N. Zilkova, Z. Bastl, Molybdenum oxide catalysts for metathesis of higher 1-alkenes via supporting MoO_2 (acetylacetonate)$_2$ and MoO_2 (glycolate)$_2$ on SBA-15 mesoporous molecular sieves, Appl. Catal. A 359 (2009) 129-135

[29] D.P. Debecker, M. Stoyanova, U. Rodemerck, A. Léonard, B.L. Su, E.M. Gaigneaux, Genesis of active and inactive species during the preparation of MoO_3/SiO_2-Al_2O_3 metathesis catalyst via wet impregnation method, Catal. Today 169 (2011) 60-68.

[30] D.P. Debecker, B. Schimmoeller, M. Stoyanova, C. Poleunis, P. Bertrand, U. Rodemerck, E.M. Gaigneaux, Flame-made MoO_3/SiO_2-Al_2O_3 metathesis catalyst with highly dispersed and highly active molybdate species, J. Catal. 277 (2011) 154-163.

[31] S.J. Huang, H.J. Liu, L. Zhang, S.L. Liu, W.J. Xin, X.J. Li, S.J. Xie, L.Y. Xu, Effect of acid leaching post treatment on the catalytic performance of MoO_3/ mordenite-alumina catalyst for 1-butene metathesis reaction, Appl. Catal. A 404 (2011) 113-119.

[32] X.J. Li, W.P. Zhang, S.L. Liu, L.Y. Xu, X.W. Han, X.H. Bao, The role of alumina in the supported MoO_3/HBeta-Al_2O_3 catalyts for olefin metathesis: a high resolution solid NMR and electron microscopy study, J. Catal. 250 (2007) 55-66.

[33] Y. Wang, C. Ercan, Hybrid Catalyst for Olefin Metathesis US Patent Application 20120289617 A1, 2012.

[34] A. Spamer, T.I. Dube, D.J. Moodley, C.van Schalkwyk, J.M. Botha, Application of a WO_3/SiO_2 catalyst in an industrial environment: part II, Appl. Catal. A: Gen. 255 (2003) 133-142.

[35] Q.F. Zhao, S.L. Chen, J.S. Gao, C.M. Xu, Effect of tungsten oxide loading on metathesis activity of ethene and 2-butene over WO_3/SiO_2 catalysts, Transit. Met. Chem.34 (2009) 621-627.

[36] S.J. Huang, F.C. Chen, S.L. Liu, Q.J. Zhu, X.X. Zhu, W.J. Xin, Z.C. Feng, C. Li, Q.X. Wang, L.Y. Xu. The influence of preparation procedures and tungsten loading on the metathesis activity of ethene and 2-butene over supported WO_3 catalysts J. Mol. Catal. A: Chem. 267 (2007) 224-233.

[37] S. Huang, S. Liu, W. Xin, J. Bai, S. Xie, Q. Wang, L. Xu, Metathesis of ethane and 2-butene to propene over W/Al_2O_3-HY support, J. Mol. Catal. A 226 (2005) 61-68

[38] D.R. Hua, S.L. Chen, G.M. Yuan, Y.L. Wang, L. Zhang, Metathesis of butane to propene on WO_3 supported on MTS-9 titanium-silica: effect of loading on selectivity and yield to propene, Transit. Met. Chem. 36 (2011) 245-248.

[39] J. C. Mol, Olefin metathesis over supported rhenium based catalysts, Catalysis Today 51 (1999) 289-299.

[40] A. Taguchi, F. Schuth, Ordered mesoporous materials in catalysis, Micropor. Mesopor. Mater. 77 (2005) 1–45.

[41] V. Chiola, J.E. Ritsko, C.D. Vanderpool, US Patent No. 3 556725, 1971.

[42] F. Di Renzo, H. Cambon, R. Dutartre, A 28-year-old synthesis of micelle-templated mesoporous silica, Micropor. Mater. 10 (1997) 283-286.

[43] J.S. Beck, C.T.W. Chu, I.D. Johnson, C.T. Kresge, M.E. Leonowicz, W.J. Roth, J.W. Vartuli, WO Patent 91/11390, 1991.

[44] C.T. Kresge, M.E. Leonowicz, W.J. Roth, J.C. Vartuli, J.S. Beck, Nature 359 (1992) 710-712.

[45] J.S. Beck, J.C. Vartuli, W.J. Roth, M.E. Leonowicz, C.T. Kresge, K.D. Schmitt, C.T.W. Chu, D.H. Olson, E.W. Sheppard,S.B. McCullen, J.B. Higgins, J.L. Schlenker, J. Am. Chem. Soc. 114 (1992) 10834.

[46] N. Rahmat, A.Z. Abdullah, A. R. Mohamed, A Review: Mesoporous Santa Barbara Amorphous-15, Types, Synthesis and Its Applications towards Biorefinery Production, Am. J. Appl. Sci. 7 (2010) 1579-1586.

[47] Suyanta, Narsito, E. T. Wahyuni, Triyono, Synthesis and characterization of mesoporous aluminosilicates Al-MCM-41 and investigation of its thermal, hydrothermal and acidity stability, Indo. J. Chem. 10 (2010) 41 – 45.

[48] F. Kleitz, T.W. Kim, R. Ryoo, Design of mesoporous silica at low acid concentrations in triblock copolymer-butanol-water systems, Bull. Korean Chem. Soc. 26 (2005) 1653-1668.

[49] M. Manzanoab, M. Vallet-Regi, New developments in ordered mesoporous materials for drug delivery, J. Mater. Chem. 20 (2010) 5593–5604.

[50] J. C. Hu, Y. D. Wang, L.F. Chen, R. Richards, W.M. Yang, Z.C. Liu, W. Xu, Synthesis and characterization of tungsten-substitute SBA-15: An enhanced catalyst for 1-butene metathesis, Micropor. Mesopor. Mater. 93 (2006) 158-163

[51] L.F. Chen, J.U. Hu, Y.D. Wang, K. Zhu, R. Richards, W.M. Yang, Z.C. Liu, W. Xu, Highly efficiently tungsten-substitute mesoporous SBA-15 catalyst for 1-butene metathesis, Mater. Lett. 60 (2006) 3059-2062.

[52] W.L. Dai, H. Chen, Y. Cao, H.I. Li, S.H. Xie, K.N. Fan, Novel economic and green approach to the synthesis of highly active W-MCM41 catalyst in oxidative cleavage of cyclopentene, Chem. Commun. (2003) 892–893.

[53] C.A. Emeis, Determination of molar extinction coefficients for infrared absorption bands of pyridine adsorbed on solid acid catalysts. J. Catal. 141 (1993) 347-354.

[54] J. E. Herrera, J. H. Kwak, J. Z. Hu, Y. Wang, C.H.F. Peden ,J. Macht, E. Iglesia, J. Catal. 239 (2006) 200-211.

[55] Y.D. Wang, Q.L. Chen, W. Yang, Z. Xie, W. Xu, D. Huang, Effect of support nature of WO3/SiO2 and butane-1 metathesis, Appl. Catal. A 250 (2003) 25-37.

[56] X.L.Yang, W.L. Dai, R.H. Gao, K.N. Fan, Characterization and catalytic behavior of highly active tungsten-doped SBA-15 catalyst in the synthesis of glutaraldehyde using an anhydrous approach. J. Catal. 249 (2007) 278-288.

[57] E. Briot, J.Y. Piquemal, M. Vennat, J.M. Bregeault, G. Chottard, J.M. Manoli, Aqueous acidic hydrogen peroxide as an effcient medium for tungsten insertion into MCM-41 mesoporous molecular sieves with high metal dispersion, J. Mater. Chem. 10 (2000) 953-958.

[58] A. de Lucas, J.L. Valverde, P. Canizares, L. Rodriguez, Partial oxidation of methane to formaldehyde over W/HZSM-5 catalysts, Appl. Catal. A: Gen.172 (1998) 165-176.

[59] C. Martin, P. Malet, G. Solana, V. Rives, Structural Analysis of Silica-Supported Tungstates, J. Phys. Chem. B 102 (1998) 2759-2768.

[60] H. Liu, L. Zhang, X. Li, S. Huang, S. Liu, W. Xin, S. Xie, L. Xu, Production of propene from1-butene metathesis reaction on tungsten based heterogeneous catalyst, J. Nat. Gas Chem. 18(2009) 331-336.

[61] D.H. Zhang, X.J. Li, S.L. Huang, X.X. Zhu , F.C. Chen, S.J. Xie, L.Y. Xu, Metathesis of C4 olefin over Mo-based heterogeneous catalysts: A novel route to propene and isopentene , Appl. Catal. A: Gen. 439-440 (2012) 171-178.

[62] C. T. Kresge, M. E. Leonowicz, W. J. Roth, J. C. Vartuli, J. S. Beck, Ordered mesoporous molecular sieves synthesized by liquid crystal template mechanism, Nature 359(1992) 710-712.

[63] Z.R. Zhang, J.H. Suo, X.M. Zhang, S.B. Li, Synthesis, characterization, and catalytic testing of W-MCM-41 mesoporous molecular sieves, Appl. Catal. A 177 (1999) 11-19.

[64] C.Y. Yang, Z. Lin, X.J. Shi, J.F. Kang , X.G. Wang, X.C. Zheng, Influence of the Preparation Processes on the Structure and Catalytic Properties of W-MCM-41 Mesoporous Materials, J. Disper. Sci. Technol. 32 (2011) 1497-1501.

[65] S. Chaemchuen, S. Phatanasri, F. Verpoort, N. Sae-ma, K. Suriye, The Structure–reactivity relationship for metathesis reaction between ethylene and 2-butene on WO_3/SiO_2 catalysts calcinated at different temperatures, Kinet. Catal. 53(2012) 247–252.

[66] C. Siriluk, S. Yuttapong, Structure of mesoporous MCM-41 prepared from rice husk ash, The 8th Asian Symposium on visualization, 2005.

[67] M. Teymouri , A.R.S. Maybodi , A. Vahid, A Rapid Method for the Synthesis of Highly Ordered MCM-41, Int. Nano Lett. 1 (2011) 34-37.

[68] H. Chen, W.L. Dai, J.F. Deng, K.G. Fan, Novel heterogeneous W-doped MCM-41 catalyst for highly selective oxidation of cyclopentene to glutaraldehyde by aqueous H_2O_2. Catal. Lett. 81(2002) 131-136.

[69] D.R. Hua, S.L. Chen, G.M. Yuan, Y.L. Wang, Q.F. Zhao, X.L. Wang, B. Fu, Micropor. Mesopor. Mater. 143 (2011) 320-325.

[70] J.K. Jeon, H.J. Lee, J.H. Yim, Y.S. Kim, S.J. Lee, Y.K. Park, J.K. Shon, J.M. Kim, Selective synthesis of 1-butene through positional isomerisation of 2-butene over mesoporous silica MCM-41, Catal. Lett.119 (2007) 179–184.

[71] X.X. Zhu, S.L. Liu, Y.Q. Song, L.G. Xu, Catalytic cracking of C4 alkenes to propene and ethene: Influences of zeolites pore structures and Si/Al_2 ratios, Applied Catalysis A: General 288 (2005) 134-142.

[72] H.S. Foglar, Elements of Chemical Reaction Engineering, forth ed. (2006), Princeton Hall International, New Jersey.

[73] M.M. Hossain, H.I. de Lasa, Reactivity and stability of Co-Ni/Al_2O_3 oxygen carrier in a multicycle CLC, AIChE J. 53 (2007) 1817-1829.

[74] J.R. Welty, C.E. Wicks, R.E. Wilson, G. Rorrer, Fundamentals of Momentum, Heat and Mass Transfer, fifth ed. John Wiley & Sons, Inc., New York (2006) , pp. 435R.E.

[75] Z. Cheng, C.S. Lo, Formation of active sites on WO_3 catalysts: A Density Functional Theory study of olefin metathesis, ACS Catal. 2 (2012) 341-349.

[76] X. Li, J. Guan, D.H. Zhou, G.H. Li, X.W. Han, W.P. Zhang, X.H. Bao, A DFT study of olefin metathesis over heterogeneous Mo/HBeta catalyst: The influence of Mo oxidation state, Comp. Theor. Chem. 913 (2009) 167–172.

[77] R.J. Gartside, M.I. Green, Q.J. Jones, Process producing propylene and hexene from C4 olefin streams, US Patent (2004) 6777582.

[78] K.G. Lee, J.K. Jeon, E.H. Hwang, Y.S. Ko, Y.K. Park, S.J. Lee, J.H. Lee, Selective positional isomerization of 2-butene over alumina and La-promoted alumina catalysts, J. Ind. Eng. Chem.13 (2007) 1062-1066.

VITAE

Name	Tazul Islam Bhuiyan
Nationality	Bangladeshi
Date of Birth	September 18, 1983
Email	tazul.bhuiyan@gmail.com tazul_805@yahoo.com
Address	6 no, Pandit Para Mymensingh, Bangladesh

Academic Background

B.Sc. in Chemical Engineering (1st Class)

Bangladesh University of Engineering and Technology

Dhaka, Bangladesh

January, 2008

M.Sc. in Chemical Engineering (Distinction)

King Fahd University of Petroleum and Minerals

Dhahran, Saudi Arabia

May, 2013